2012

Development of fluorescence-based methods to study the effect of cytoplasmic proteins, cholesterol, and extracellular ligand on integrin diffusion and clustering in single cells

Suzanne Mary Sander
Iowa State University

Development of fluorescence-based methods to study the effect of cytoplasmic proteins, cholesterol, and extracellular ligand on integrin diffusion and clustering in single cells

by

Suzanne Sander

A dissertation submitted to the graduate faculty

in partial fulfillment of the requirements for the degree of

DOCTOR OF PHILOSOPHY

Major: Analytical Chemistry

Program of Study Committee:
Emily A. Smith, Major Professor
Robert S. Houk
Mei Hong
Nicola L. Pohl
Amy Andreotti

Iowa State University

Ames, Iowa

2012

To my Family and Friends

TABLE OF CONTENTS

ACKNOWLEDGEMENTS

I would like to thank my Ph.D. advisor, Dr. Emily A. Smith, whose guidance, patience, and dedication to research has helped me expand my horizons. I would also like to thank my committee members: Dr. Smith, Dr. Houk, Dr. Hong, Dr. Pohl, and Dr. Andreotti. Their input and support has been and is very much appreciated. I would like to express my gratitude for the help and support of my lab mates, especially Cherry (Chien-Ju) Shih and Deepak Dibya, whose conversations and collaborations have helped my growth, both personally and professionally.

I would also like to express my appreciation to my friends and family whose support has been essential to my success in life and in graduate school. Thank you to Yan Yan Hu, for all your encouragement both in and out of the lab. Thank you to the women from the Women's Enrichment Group who's countless hours of discussion about life and learning has been of immeasurable support to me. Thank you to Ron and Marlene Black, Jack Smith, Kari Kraemer, and Michael Lawrinenko for your friendship and support. Thank you to my parents, Jan and Steve Sander, my grandparents, and my siblings, especially Jeff and Anna, whose love, encouragement and prayers have helped make me the person that I am. Thank you to my cousins, Dale Lenz and Matt Thatcher, and their families, for food and countless hours of entertainment, both of which helped keep me alive and levelheaded during my graduate studies.

"No one who achieves success does so without acknowledging the help of others. The wise and confident acknowledge this help with gratitude." *Unknown* I appreciate and thank all who have provided inspiration and encouragement during my journey towards achieving my Ph.D.

CHAPTER 1: GENERAL INTRODUCTION

Research Motivation and Goals

Communication pathways in cells are of fundamental importance to overall health. Components of the cell membrane play a critical role in these pathways and are often the target of various drug treatments. Cell membrane organization can provide insight into how cells respond to their environment and ultimately provide the knowledge needed to understand disease regulation. Membrane receptors are important intermediaries in the transmission of information across the cell membrane. Integrins are one of the main transmembrane proteins on animal cells that bind to extracellular matrix. These proteins integrate the extracellular matrix with the intracellular cytoskeleton. Individually, integrins bind to ligand with low affinity (μM^{-1} to mM^{-1}), but their ability to cluster within the cell membrane facilitates strong adherence to the extracellular matrix [1]. They are known to be involved in cell signaling, growth and differentiation [2]. Deviations in integrin signaling can cause disease ranging from metastasis to angiogenesis [3].

It is the goal of this work to measure integrin clustering and diffusion properties in the presence of altered extracellular, membrane, and cellular compositions in order to elucidate the molecular mechanisms of integrins. Changes in integrin diffusion and clustering are measured using select fluorescence microscopy techniques. FRET, fluorescence resonance energy transfer, is a technique that measures interactions on the 0 to 10 nanometer scale. While FRAP, fluorescence recovery after photobleaching, monitors the two-dimensional diffusion of fluorescent molecules into a previously photobleached area.

Cell Membrane

As the structural and functional unit of living organisms, cells perform a wide variety of functions, including energy conversion, molecule transport, and reproduction. The cell includes many organelles that are separated from the surrounding environment by the cell membrane. The dynamic nature of the cell is evidenced by its capacity to grow, reproduce, and become specialized; as well as by its ability to respond to stimuli and adapt to changes in its environment.

The membrane is a lipid bilyer with embedded proteins, carbohydrates and other small biomolecules (Figure 1). It is a semipermeable membrane and therefore able to regulate what passes into/out of the cell. Based on the fluid mosaic model [4], the membrane is seen as a two-dimensional liquid. However, biological details are more involved than this model and the large number of proteins present in the cell membrane provides structure and can inhibit Brownian diffusion [5]. In fact, the interconnectivity and spatial organization of networks of proteins are what sustain basic cellular function [6]. New data on membrane protein structures and interactions have transformed our understanding of membrane morphology [7,8].

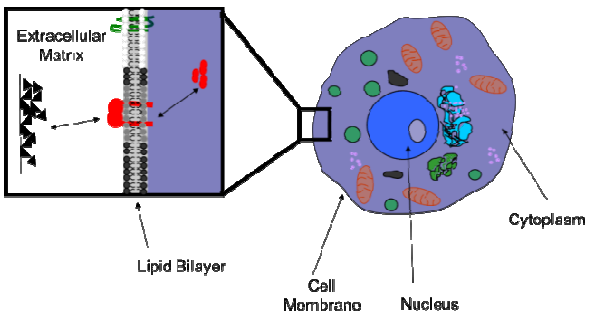

Figure 1: Schematic representation of a cell: The cell membrane is composed of proteins, lipids, carbohydrates, and other small biomolecules. Integrins are a class of proteins that span the membrane and are involved in cell signaling

Integrins

One process for transmitting information across the cell membrane is achieved via integrins, which are membrane proteins that are critical to many cellular processes including cell adhesion, growth, and differentiation [2]. Integrins are composed of an α and β subunit that are non-covalently associated and usually consist of a short cytoplasmic tail with a large extracellular ligand binding domain (Figure 2). The short cytoplasmic tail interacts with the actin cytoskeleton indirectly though a number of adapter proteins, such as vinculin, steamer duck, and paxillin. Integrin conformations exist in equilibrium within the cell, however, when this equilibrium shifts toward a greater number of the integrins' extracellular region being extended, there is an increase in ligand affinity [9]. Many probes are available to measure structural changes in receptors [10-12]. More recently studies have looked at the clustering properties of integrins [13,14].

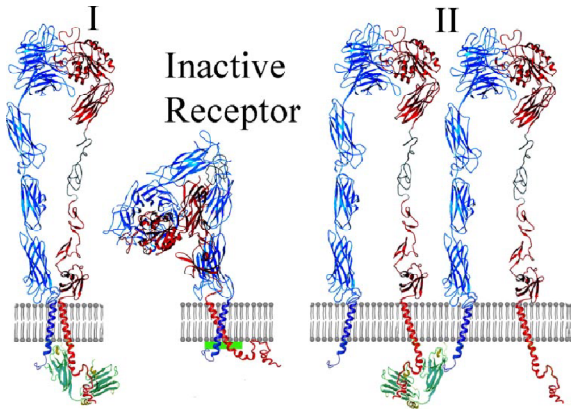

Figure 2: Integrins span the cell membrane and consist of a large extracellular domain, a transmembrane region, and a short cytoplasmic domain. Integrins in the bent conformation are considered to have a low extracellular ligand affinity. (Adapted from reference 15)

Fluorescence Microscopy

Fluorescence is the absorption of photons at a particular wavelength to promote electronic excitation and the subsequent emission of light with a lower energy (Figure 3) due to the loss of energy through heat or molecular vibration. This process is nearly simultaneous (less than 10^{-9}sec) due to the short time delay between photon absorption and emission. Fluorophores are identified on the basis of their excitation and emission properties.

Due to high sensitivity and specificity, florescence microscopy is commonly used in cell biology. The high sensitivity and specificity are the result of the discovery and cloning of the green fluorescent protein (GFP), which made it possible to express GFP fused to a particular protein of interest throughout a given cell or organism. This break-through resulted in the awarding of the Noble Prize in Chemistry to Osamu Shimomura, Martin Chalfie, and Roger Y. Tsien in 2008.

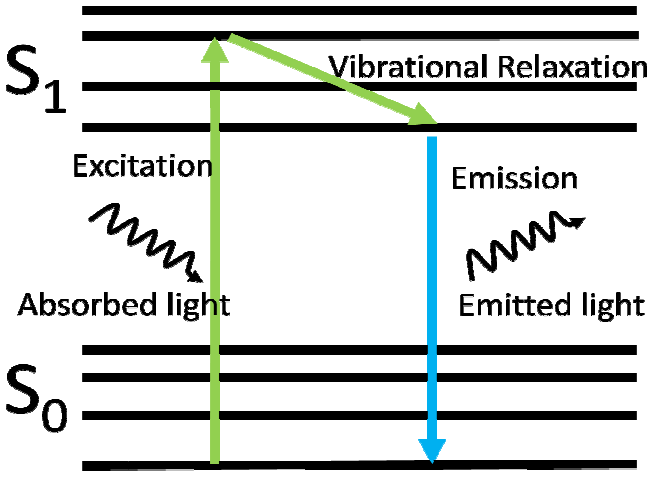

Figure 3: Jablonski Diagram: A fluorophore absorbs energy, loses a small amount of the energy through nonradiative decay and emits at a longer wavelength

Fluorescence Recovery after Photobleaching (FRAP)

FRAP quantifies the diffusion of fluorophores in the cell membrane by photobleaching a small region and monitoring the recovery of surrounding molecules back into the photobleached area. Assuming the bleaching beam has a Gaussian profile, Brownian diffusion (D) is modeled by the following equation (Eq. 1):

$$D = \frac{\omega^2}{4t_{1/2}} \qquad \text{(Eq. 1)}$$

where ω = radius of the photobleaching beam, and $t_{1/2}$= the time required for the bleach spot to recover to half its initial intensity [15].

The Saffman-Delbrück equation (Eq. 2) predicts diffusion in a two-dimensional membrane to be on the order of magnitude of 10^{-8} cm^2/s:

$$D_{calc} = \frac{kT}{4\pi\eta_m h}\left(ln\frac{\eta_m h}{\eta_w a} - 0.5572\right) \qquad \text{(Eq. 2)}$$

where D_{calc} = lateral diffusion, k = Boltzmann constant, T = temperature, a = radius of the diffusing object, h = membrane thickness, η_m = viscosity of membrane, and η_w = viscosity of surrounding aqueous medium. This value, however, is faster than the experimentally measured values of proteins in the membrane [16]. Multiple reasons exist for this slower than expected diffusion of membrane proteins: interactions with extracellular and cytoplasmic proteins, higher concentrations of membrane proteins, and/or the confinement of proteins to different sized domains within the membrane. These associations are studied in the following chapters.

Förester Resonance Energy Transfer (FRET)

FRET is the radiationless transfer of energy between two fluorophores. If appropriate spectral overlap exists between the FRET donor and acceptor and the two molecules are in close proximity (0-10 nm) to one another, instead of emitting a photon after light absorption, the donor molecule transfers its energy via a dipole-dipole interaction to the acceptor (Figure 4). The acceptor then emits the photon at a longer wavelength than that of the donor. The Förester distance (R_0) (Figure 5) is the distance between the donor and acceptor where the efficiency of energy transfer is 50%. This distance is dependent on several factors: the overlap of the donor emission spectrum with that of the acceptor absorption spectrum, the fluorophore molecular orientation, the donor quantum yield, and the index of refraction of the surrounding medium.

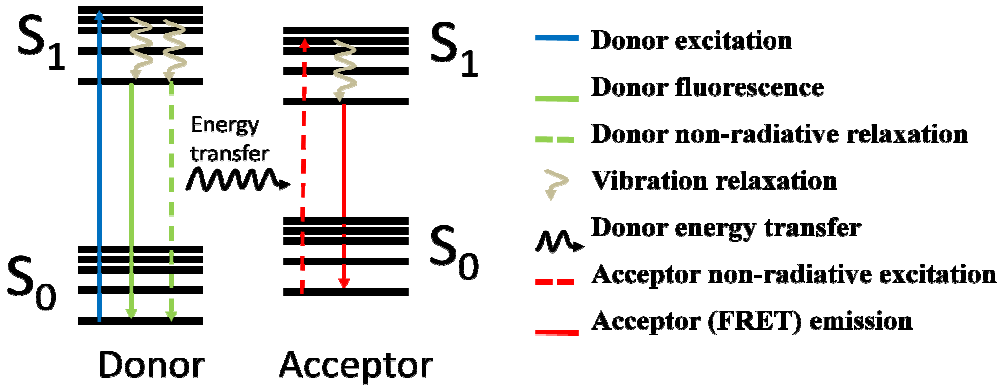

Figure 4: Jablonski diagram: Depiction of (FRET) (adapted from Nikon Inc.)

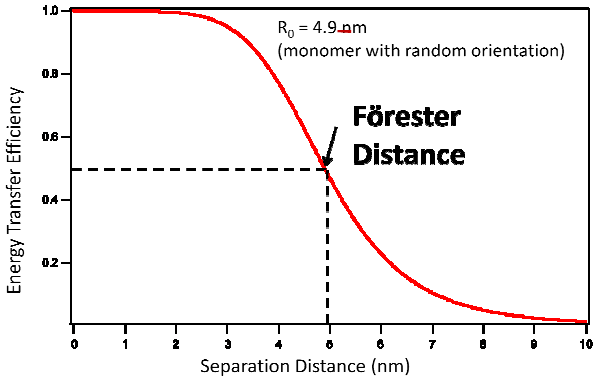

Figure 5: The Förester distance (R_0) in FRET measurements is the distance between the donor and acceptor where the efficiency of energy transfer is 50%.

Literature Review:

Text from this review will be incorporated into a review article on single cell analysis with multiple contributing authors

Donor-Acceptor Fluorescence Resonance Energy Transfer (FRET) Pairs

The sensitivity of fluorescence makes it a widely used technique for a broad range of applications. Among other purposes, fluorescence microscopy can be used to measure trajectory, speed and timing of molecular and cellular movements. One fluorescence technique, fluorescence resonance energy transfer (FRET), has become extensively used to measure biological interactions on the nanometer scale. Live cell FRET measurements use carefully chosen fluorescence proteins fused to the protein(s) of interest or small molecules that bind to specific targets.

There are several factors that need to be addressed when choosing a donor and acceptor including: (a) sufficient separation of donor and acceptor absorption spectra to obtain selective excitation of the fluorophores, (b) overlap of the emission spectrum of the donor and the excitation spectrum of the acceptor, (c) reasonable separation in emission spectra to allow independent measurement of the fluorescence of each fluorophore, (d)

extinction coefficients and (e) quantum yields of the fluorophores. The importance of several of the spectral factors discussed above (a, b, c) are shown in Figure 6, which depicts one of the most commonly used FRET pairs: cyan fluorescent protein as the donor and yellow fluorescent protein as the acceptor (CFP-YFP).

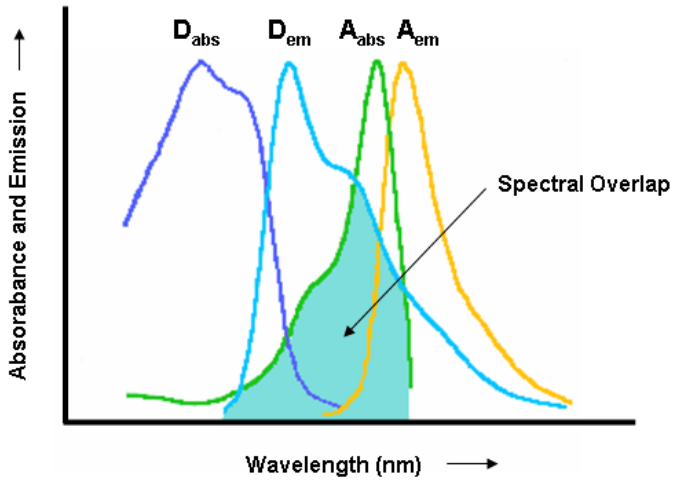

Figure 6: Excitation and emission spectra of a typical FRET pair D_{abs} = donor absorbance, D_{em} = donor emission, A_{abs} = acceptor absorbance, A_{abs} = acceptor emission. (adapted from reference 17).

Generally there are two main types of fluorophores used for live cell FRET: (i) autofluorescent proteins that are expressed using the cell's transcription and translation machinery and (ii) small organic fluorophores that are chemically synthesized. In addition to GFP, there are other fluorescent proteins, such as dsRED. These naturally occurring fluorescent proteins have been modified to produce an entire color palette of fluorescent proteins with suitable properties for FRET. Some popular fluorescent protein FRET pairs that have been used over the years include cyan fluorescent protein-yellow fluorescent protein (CFP-YFP), CFP-dsRED, and YFP-dsRED. There has also been development in small

molecule fluorophores which provides more options than just the available genetically encoded fluorophores. Additionally, their size is drastically smaller than that of fluorescent proteins (27 kDa) [17]. This literature review will cover the donor and acceptor probes from both groups that have been developed within the last five years for FRET measurements using one or two FRET pairs within a given system. This review will also discuss the use of quenchers, optical switches, and computational tools to expand the capabilities of FRET measurements.

Fluorescent Proteins

Currently known fluorescent protein pairs have different limitations and new pairs are constantly being sought that will provide an optimal combination of donor and acceptor to enable large dynamic range FRET measurements, fast maturation (i.e. protein folding), bright fluorescence, and reliable detection. Much research has been done to address these concerns and improve systems of measurement. Novel FRET pairs that have been identified include mutant green fluorescent protein (TagGFP)-mutant red fluorescent protein (TagRFP) and GFP^2 and DsRed2. While these FRET pairs have been tested in a particular biological context, they should be applicable to a whole range of systems.

Screens for high efficiency FRET pairs compared the amplitude of fluorescence before and after protein separation and identified TagGFP–TagRFP as a promising FRET pair. Further characterization showed the Förester radius for this FRET pair to be higher than GFP-mCherry, with high pH stability and an emission signal that can be separated in most imaging systems. This novel FRET pair was used in combination with caspase 3 to generate an effective apoptosis reporter [18].

Another advantageous FRET pair that was identified as potentially beneficial compared to the CFP-YFP is GFP^2 and DsRed2. Specifically, the quality of the probes was monitored by co-transfecting the fluorescent proteins into cells and monitoring their energy transfer. As a proof of concept, these fluorophores were connected via a peptide containing a cleavage motif for the enterovirus 2A protease. Energy transfer is measured until cleavage of the enterovirus occurs. Resulting FRET decay is monitored as a function of quantity and duration of the virus. This FRET system can be used in diagnostics and screening procedures [19].

In addition to creating new FRET pairs, another approach is to make modifications on a previously existing FRET pair, such as CFP-YFP. One group replaced YFP with a variant sREACh (super resonance energy accepting chromoprotein) which has low quantum efficiency and high absorbance [20]. Another group used sREACh and tested 3 possible replacements for CFP and found that using a two photon excitation microscope mTFP1 (monomeric teal fluorescent protein) had the highest gain on epidermal growth factor stimulation [21]. Using modified YFP-CFP maximizes parameters that are important to FRET pairs as discussed above.

Changes to where fluorophores are attached to proteins can also be made and was shown to improve spatiotemporal resolution. To study protein-protein interactions florescent proteins are often fused to one of the termini of the host protein. Efforts have to be made, however, to minimize disruption of protein folding as well as maximize FRET. One group engineered periplasmic binding proteins with increased separation between the YFP and CFP which were attached to both termini of periplasmic binding proteins. The resulting constructs showed a larger FRET dynamic range than their native forms [22].

Small Molecules

Specific labeling techniques for biomolecules, not directly encoded by the genome, have been limited. This is in part due to difficulties in selectively labeling the molecule of interest without affecting its molecular recognition in the cell, thus limiting the number of molecules available for cell-based studies. Accurate measurement of small molecules in cells using FRET contributes towards understanding different interactions of individual molecules in signaling networks, tracking metal ions in cells, and analyzing other important cell functions that can be studied without genetic manipulation, such as metabolic regulation [23]. Monitoring azides in cells was achieved by creating a fluorogenic phosphine reagent containing a FRET quencher that is activated upon reaction with azides [24].

A class of caged coumarin probes was developed that has a high FRET efficiency and promising chemistry for bioconjugation. Calcein was chosen as the acceptor due to its water solubility, long cytoplasmic retention time and the extensive spectral overlap of the excitation wavelength with coumarin's emission. Chemistries of iminodiacetates and dextrin amines were utilized to conjugate the caged FRET dye. This dye can be localized by exciting it near 490 nm prior to photolysis [25].

The development of a borondipyrromethanene (BODIPY)-rhodamine complex has good spectral overlap due to the presence of a biphenyl spacer that allowed for efficient energy transfer. Mercury acceptors were introduced into the complex and showed excellent sensitivity and selectivity as well as insensitivity to pH [26]. The 2'-carboxyl group of the rhodamine can be used to develop a molecular ruler for a wide range of transition-metal ions.

A probe that can be used to measure mechanical force in proteins via FRET was created. CFP and YFP were attached to two distant sites of single-stranded DNA of the

spectrin protein. Single-stranded DNA is floppy and causes minimal stress in the protein. However, once it binds to complementary DNA sequence the loop straightens, pushing the fluorophores apart and decreasing FRET over time. This probe is reliable, has high sensitivity, and doesn't create interference with protein function [27].

Dual FRET

Over the years there have been many genetically encoded sensors developed based on the concept of FRET as discussed above, which provide a means of monitoring a variety of interactions within the cell. The ability to simultaneously measure multiple interactions within the cell would help in the development of an understanding of different complex signaling networks. However, due to broad spectral signals, often significant fluorophore overlap is observed. Efforts to resolve this difficulty have included temporally separating the FRET signal using spectrally compatible sets of FRET pairs. In this strategy, the second donor is excited immediately after excitation of the first donor and the subsequent emission from the acceptors are collected. These sets include ECFP/Venus and TagRFP/mPlum [28], ECFP/YFP and pmOrange/mCherry [29], and mTFP1/mCitrine and mAmetrine/tdTomate [30]. One difficulty with sequential data collection, however, is the time lapse between the collected data, making it impractical for interactions that are occurring on a faster time scale.

To address the poor time resolution in dual FRET measurements, a single-excitation dual-FRET method was developed. A single excitation wavelength is used with subsequent linear unmixing to identify between fluorescent proteins. One group used sapphire/red fluorescent protein FRET sensor in combination with CFP/YFP. Both sapphire and CFP were excited simultaneously at 405 nm (Figure 7) and resulting signal was comparable to single FRET measurements. This method can be used in a variety of cell samples [31]. Kim et al.

used CFP/YFP and YFP/mCherry pairs obtaining selective excitation of the donor. To unmix the spectral imaging data of the acceptors, a non-negative matrix factorization was applied. This technique eliminated donor bleedthrough and autofluorescence and minimizes calculation artifacts [32].

A red shifted FRET pair, mVenus/mKOκ biosensor, was developed and used in combination with human glutaredoxin-1 and a fluorescent protein Grx1-roGFP2. These spectrally compatible probes had minimal cross-talk and were shown to exhibit great spatiotemporal precision. As proof of concept, simultaneous imaging of Src/Ca_{2+} signaling and glutathione redox potential were measured, revealing that the epidermal growth factor-induced Src signaling is negatively regulated by H_2O_2 [33].

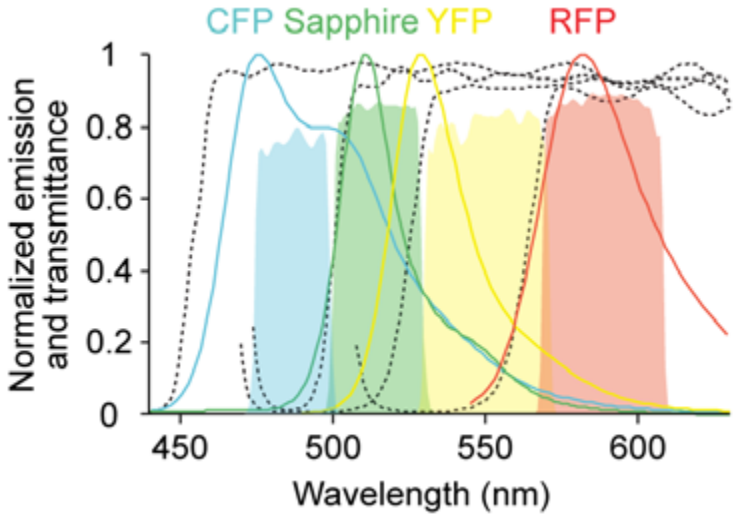

Figure 7: Emission spectra of fluorescent proteins and transmittances of dichroic mirrors and emission filters. Broken lines from left to right indicate the transmission curves of LP455, 500, 530, and 570, and cyan, green, yellow, and red shaded areas represent of BP487/25, 515/30, 550/40, and 590/40 in (LP = long pass, BP = Band pass numbers indicate wavelength and wavelength/half-bandwidth (nm) respectively). (adapted from reference 32)

Fluorescence Quenchers

A non-fluorescent dye, IRDye QC-1, was developed to efficiently quench fluorophores ranging from visible to near-infrared wavelengths in FRET systems. Dye performance was tested by measuring efficiencies in a caspase-3 assay system with various donors all of which showed a 40 to 83-fold increase in fluorescence upon cleavage of the substrates. This effective quenching on a broad range of dyes gives broad applicability in FRET assays [34].

Studies have shown that fluorescence quenching of the acceptor occurs on a bridged organic dyad where triphenyldiamine is the donor and perylenebisimide is the acceptor. This quenching is absent in a solution of free donors and acceptors indicating that it may be due to the presence of the saturated $CH_2O(CH_2)_{12}$ –bridge. This idea was investigated using time-dependent density functional theory (DFT) and molecular dynamics (MD). Calculations comparing a mixture of free donors and acceptors were compared to a bridged molecule in stretched conformation. DFT revealed that the bridge's influence over the donor and acceptor electronic spectra was negligible. However, MD showed that the quenching is caused when the bridge in solution thereby minimizing donor acceptor distances, causing an overlap of spectra [35].

In an effort to improve and develop FRET biosensors, conformational changes in protein folding are modeled using a Fusion Protein Modeler (FPMOD), a computational tool that qualitatively predicts changes in FRET efficiency by sampling the conformational space through rigid-body rotation. Although the correlation between changes in FRET efficiency and emission ratio is difficult to quantify, the values should be directly related. This model was used to evaluate Ca^{2+} biosensor designs and create a new Ca^{2+} biosensor. Models were

shown to have good agreement with experimental results. Incorporation of additional effects has the potential to remove non-optimal conformations and create better quantitative correlation between simulation and experiment [36].

Development of polypeptides to measure changes in oxidation states was achieved by inserting redox sensitive motifs between ECFP and EYFP. The resulting construct showed a 92% increase in FRET efficiency upon oxidation. These constructs can be used to measure intracellular or intraorganellar redox conditions [37].

Optical Switches

Optical switches generate a powerful and precise means to employ phase-selective detection of donor signals associated with the presence or absence of FRET. Nitrobenzospiropyran (NitroBIPS) attached to a GFP-alkylguaninetransferase fusion protein (GFP-AGT) is one such combination used as an optical switch that showed an increase in the sensitivity of detection [38]. Another example uses the small molecule tetramethylrhodamine (TMR) in combination with spironaphthoxazine (NISO), an optical switch that has enhanced quantum yields. NISO transitions between a colorless and colorful state and serves as the acceptor probe in FRET while TMR is the donor. The optical switching of the probe is reversible without additional reactants, making this probe conducive to measurements in cells [39]. Related probes have been identified, but face limitations due to overlapping emission spectra of the fluorescent probe and optical switch. This limitation is overcome due to the fact that the absorption spectrum of NISO is red shifted, maximizing FRET efficiency.

Dissertation Overview

This dissertation utilizes fluorescence microscopy to better understand the dynamics and organization of the cell membrane and how cytoplasmic proteins, extracellular ligand, and cholesterol affect this organization. **Chapter 1** provides a general introduction to fluorescence microscopy and integrins, a transmembrane protein necessary for many cellular processes including adhesion, growth, and differentiation. It also includes a literature review on FRET donor acceptor pairs that have been developed in the last 5 years. **Chapter 2** is a paper published in a special issue of *Analytical and Bioanalytical Chemistry* in 2012: *Young Investigators in Analytical and Bioanalytical Science*, which discusses how the reduced expression of different cytoplasmic proteins affects integrin diffusion. **Chapter 3** focuses on the nanoscale clustering of integrins and mutant integrins in the presence of ligand. **Chapter 4** compares integrin diffusion in the presence of cholesterol and epicholesterol. **Chapter 5** contains general conclusions and possible directions for future wok.

References

1. Molecular Biology of the Cell (2002). 4 edn.,
2. Giancotti FG, Ruoslahti E (1999) Integrin signaling. Science 285 (5430):1028-1032
3. Martin KH, Slack JK, Boerner SA, Martin CC, Parsons JT (2002) Integrin connections map: to infinity and beyond. Science 296 (5573):1652-1653
4. Singer SJ, Nicolson GL (1972) The fluid mosaic model of the structure of cell membranes. Science 175 (4023):720-731
5. Vereb G, Szollosi J, Matko J, Nagy P, Farkas T, Vigh L, Matyus L, Waldmann TA, Damjanovich S (2003) Dynamic, yet structured: The cell membrane three decades after the Singer-Nicolson model. Proc Natl Acad Sci U S A 100 (14):8053-8058
6. Bastiaens PI, Pepperkok R (2000) Observing proteins in their natural habitat: the living cell. Trends Biochem Sci 25 (12):631-637
7. Fanning AS, Anderson JM (1999) Protein modules as organizers of membrane structure. Current opinion in cell biology 11 (4):432-439
8. Chichili GR, Rodgers W (2009) Cytoskeleton-membrane interactions in membrane raft structure. Cell Mol Life Sci 66 (14):2319-2328

9. Plow EF, Haas TA, Zhang L, Loftus J, Smith JW (2000) Ligand binding to integrins. J Biol Chem 275 (29):21785-21788
10. Bunch TA, Helsten TL, Kendall TL, Shirahatti N, Mahadevan D, Shattil SJ, Brower DL (2006) Amino acid changes in Drosophila alphaPS2betaPS integrins that affect ligand affinity. J Biol Chem 281 (8):5050-5057
11. Pampori N, Hato T, Stupack DG, Aidoudi S, Cheresh DA, Nemerow GR, Shattil SJ (1999) Mechanisms and consequences of affinity modulation of integrin alpha(V)beta(3) detected with a novel patch-engineered monovalent ligand. J Biol Chem 274 (31):21609-21616
12. Shattil SJ, Hoxie JA, Cunningham M, Brass LF (1985) Changes in the platelet membrane glycoprotein IIb.IIIa complex during platelet activation. J Biol Chem 260 (20):11107-11114
13. Smith EA, Bunch TA, Brower DL (2007) General in vivo assay for the study of integrin cell membrane receptor microclustering. Anal Chem 79 (8):3142-3147
14. Dibya D, Sander S, Smith EA (2009) Identifying cytoplasmic proteins that affect receptor clustering using fluorescence resonance energy transfer and RNA interference. Anal Bioanal Chem 395 (7):2303-2311
15. Axelrod D, Koppel DE, Schlessinger J, Elson E, Webb WW (1976) Mobility measurement by analysis of fluorescence photobleaching recovery kinetics. Biophys J 16 (9):1055-1069
16. Jacobson K, Ishihara A, Inman R (1987) Lateral diffusion of proteins in membranes. Annu Rev Physiol 49:163-175
17. Zhang CJ, Li L, Chen GY, Xu QH, Yao SQ (2011) One- and two-photon live cell imaging using a mutant SNAP-Tag protein and its FRET substrate pairs. Org Lett 13 (16):4160-4163
18. Shcherbo D, Souslova EA, Goedhart J, Chepurnykh TV, Gaintzeva A, Shemiakina, II, Gadella TW, Lukyanov S, Chudakov DM (2009) Practical and reliable FRET/FLIM pair of fluorescent proteins. BMC Biotechnol 9:24
19. Hsu YY, Liu YN, Wang W, Kao FJ, Kung SH (2007) In vivo dynamics of enterovirus protease revealed by fluorescence resonance emission transfer (FRET) based on a novel FRET pair. Biochem Biophys Res Commun 353 (4):939-945
20. Ganesan S, Ameer-Beg SM, Ng TT, Vojnovic B, Wouters FS (2006) A dark yellow fluorescent protein (YFP)-based Resonance Energy-Accepting Chromoprotein (REACh) for Forster resonance energy transfer with GFP. Proc Natl Acad Sci U S A 103 (11):4089-4094
21. Kumagai Y, Kamioka Y, Yagi S, Matsuda M, Kiyokawa E (2011) A genetically encoded Forster resonance energy transfer biosensor for two-photon excitation microscopy. Anal Biochem 413 (2):192-199
22. Okada S, Ota K, Ito T (2009) Circular permutation of ligand-binding module improves dynamic range of genetically encoded FRET-based nanosensor. Protein Sci 18 (12):2518-2527
23. Prescher JA, Bertozzi CR (2005) Chemistry in living systems. Nat Chem Biol 1 (1):13-21. doi:nchembio0605-13 [pii]
10.1038/nchembio0605-13

24. Hangauer MJ, Bertozzi CR (2008) A FRET-based fluorogenic phosphine for live-cell imaging with the Staudinger ligation. Angew Chem Int Ed Engl 47 (13):2394-2397
25. Zheng G, Guo YM, Li WH (2007) Photoactivatable and water soluble FRET dyes with high uncaging cross section. J Am Chem Soc 129 (35):10616-10617
26. Yu H, Xiao Y, Guo H, Qian X (2011) Convenient and Efficient FRET Platform Featuring a Rigid Biphenyl Spacer between Rhodamine and BODIPY: Transformation of 'Turn-On' Sensors into Ratiometric Ones with Dual Emission. Chemistry
27. Meng F, Sachs F (2011) Visualizing dynamic cytoplasmic forces with a compliance-matched FRET sensor. J Cell Sci 124 (Pt 2):261-269
28. Grant DM, Zhang W, McGhee EJ, Bunney TD, Talbot CB, Kumar S, Munro I, Dunsby C, Neil MA, Katan M, French PM (2008) Multiplexed FRET to image multiple signaling events in live cells. Biophys J 95 (10):L69-71
29. Piljic A, Schultz C (2008) Simultaneous recording of multiple cellular events by FRET. ACS Chem Biol 3 (3):156-160
30. Ai HW, Hazelwood KL, Davidson MW, Campbell RE (2008) Fluorescent protein FRET pairs for ratiometric imaging of dual biosensors. Nat Methods 5 (5):401-403
31. Niino Y, Hotta K, Oka K (2009) Simultaneous live cell imaging using dual FRET sensors with a single excitation light. PLoS One 4 (6):e6036
32. Kim J, Li X, Kang MS, Im KB, Genovesio A, Grailhe R (2011) Quantification of protein interaction in living cells by two-photon spectral imaging with fluorescent protein fluorescence resonance energy transfer pair devoid of acceptor bleed-through. Cytometry A 81 (2):112-119
33. Su T, Zhang Z, Luo Q (2012) Ratiometric fluorescence imaging of dual bio-molecular events in single living cells using a new FRET pair mVenus/mKOkappa-based biosensor and a single fluorescent protein biosensor. Biosens Bioelectron 31 (1):292-298
34. Peng X, Chen H, Draney DR, Volcheck W, Schutz-Geschwender A, Olive DM (2009) A nonfluorescent, broad-range quencher dye for Forster resonance energy transfer assays. Anal Biochem 388 (2):220-228
35. Körzdorfer T, Tretiak S, Kummel S (2009) Fluorescence quenching in an organic donor-acceptor dyad: a first principles study. J Chem Phys 131 (3):034310
36. Pham E, Chiang J, Li I, Shum W, Truong K (2007) A computational tool for designing FRET protein biosensors by rigid-body sampling of their conformational space. Structure 15 (5):515-523
37. Kolossov VL, Spring BQ, Sokolowski A, Conour JE, Clegg RM, Kenis PJ, Gaskins HR (2008) Engineering redox-sensitive linkers for genetically encoded FRET-based biosensors. Exp Biol Med (Maywood) 233 (2):238-248
38. Mao S, Benninger RK, Yan Y, Petchprayoon C, Jackson D, Easley CJ, Piston DW, Marriott G (2008) Optical lock-in detection of FRET using synthetic and genetically encoded optical switches. Biophys J 94 (11):4515-4524
39. Petchprayoon C, Yan Y, Mao S, Marriott G (2011) Rational design, synthesis, and characterization of highly fluorescent optical switches for high-contrast optical lock-in detection (OLID) imaging microscopy in living cells. Bioorg Med Chem 19 (3):1030-1040

CHAPTER 2: ELUCIDATING THE ROLE OF SELECT CYTOPLASMIC PROTEINS IN ALTERING DIFFUSION OF INTEGRIN RECEPTORS

A paper published in the special issue Young Investigators in Analytical and Bioanalytical Science 2012*

*Suzanne Sander, Neha Arora and Emily A. Smith **

Keywords: Fluorescence recovery after photobleaching (FRAP); RNA interference (RNAi); Cell membrane; αPS2CβPS integrin; lateral diffusion; cytoskeleton

ABSTRACT

Cytoplasmic proteins that affect integrin diffusion in the cell membrane are identified using a combination of fluorescence recovery after photobleaching (FRAP) and RNA interference. Integrin receptors are essential for many cellular events, and alterations in lateral diffusion are one mechanism for modulating their function. In cells expressing native cytoplasmic protein concentrations and spread on a slide containing integrin extracellular ligand, 45 ± 2% of the integrin is mobile with a time-dependent 5.2 ± 0.9 x 10^{-9} cm^2/sec diffusion coefficient at 1 second. The time exponent is 0.90 ± 0.07, indicating integrin diffusion moderately slows at longer times. The role of a specific cytoplasmic protein in altering integrin diffusion is revealed through changes in the FRAP curve after reducing the cytoplasmic protein's

expression. Decreased expression of cytoplasmic proteins rhea, focal adhesion kinase (FAK) or steamer duck decreases the integrin mobile fraction. For rhea and FAK there is a concomitant shift to Brownian (i.e., time-independent) diffusion at reduced concentrations of these proteins. In contrast, when the expression of actin 42A, dreadlocks, paxillin, integrin linked kinase (ILK), or vinculin is reduced, integrin diffusion generally becomes more constrained with an increase in the integrin mobile fraction. This same change in integrin diffusion is measured in the absence of integrin extracellular ligand. The results indicate breaking the extracellular ligand-integrin-cytoskeletal linkage alters integrin diffusion properties, and, in most cases there is no correlation between integrin and lipid diffusion properties.

INTRODUCTION

Alterations in the lateral diffusion of lipids, proteins, and small molecules in the cell membrane occur in response to a variety of stimuli, ranging from protein binding [1] to mechanical forces emanating from inside or outside the cell [2,3]. The unrestricted lateral diffusion coefficient of membrane components can be roughly estimated by the Saffman-Delbrück equation [4]. Calculated values are on the order of 10^{-8} cm^2/sec for a typical membrane protein, and lipids have similar diffusion coefficients that are larger only by a factor of ~2 [5,6]. The lateral diffusion of membrane proteins is usually slower than values measured for proteins in model lipid bilayers and values calculated using the Saffman-Delbrück equation [7,8]. This is due to three primary factors: (1) membrane proteins interact with extracellular and cytoskeletal/cytoplasmic proteins; (2) the cell membrane contains a

high concentration of proteins, e.g. 50-80% of the membrane surface area; and (3) membrane components may be confined to domains of varying size, all of which constrain lateral diffusion. In erythrocyte cells lacking key cytoskeletal proteins, the lateral diffusion of a membrane protein increased over 50-fold compared with cells containing all cytoskeletal proteins, indicating that cytoplasmic proteins play a role in altering the lateral diffusion of at least some membrane components [9]. Altered lateral diffusion of mutant membrane proteins with cytoplasmic domains that have been eliminated or shortened can reveal the role of cytoplasmic domains in altering lateral diffusion, but they do not provide information about specific cytoplasmic proteins that may be responsible for altered lateral diffusion.

Several analytical techniques can be used to measure lateral diffusion of membrane components. Single particle tracking [10] and fluorescence correlation spectroscopy [11] can be used to reveal heterogeneous diffusion of membrane components. These techniques require approximately nanomolar concentrations of analyte (e.g., fluorophore labeled protein), which is often significantly below relevant *in vivo* concentrations [12]. Fluorescence recovery after photobleaching (FRAP) can be used to monitor the time required for fluorescent molecules to laterally diffuse into a region of the cell that has previously been photobleached. The photobleached region can be generated by a short, intense laser pulse. FRAP is an ensemble measurement that averages the movement of numerous proteins, which may represent populations with different diffusion characteristics. Possible rare populations may be masked in the ensemble measurement. Fluorescent fusion proteins enable in vivo and ex vivo FRAP measurements of a membrane protein at endogenous expression levels [13]. Several models have been developed to extract diffusion parameters of membrane components from fluorescence recovery curves [14-16]. Combined with techniques to alter

the expression of other proteins, FRAP has the capability for measuring the molecular mechanism of receptor diffusion in the cell membrane.

Integrins are a family of heterodimeric receptors that contain an α and a β subunit with large extracellular domains and comparatively short cytoplasmic domains [2]. Several cytoplasmic proteins interact directly or indirectly with integrins; however, the effects of such interactions in altering their lateral movement in the cell membrane are not well understood. A method utilizing FRAP has been described to elucidate the dynamics of focal adhesions, which are integrin containing macromolecular assemblies that link cells to the extracellular matrix [17]. In this previously published method, the lateral mobility was measured for integrin mutants that disrupt known binding sites to other focal adhesion proteins, and was limited to study proteins that directly bind at known locations on the integrin. The cloning step required to generate integrin mutants also makes the methodology low-throughput. FRAP has also been used to measure changes in integrin diffusion when bound to multimeric ligands compared with monovalent ligands [18]. It was shown that integrin lateral diffusion decreases when bound to a tetrameric ligand compared to a monovalent ligand.

In this current study, RNA interference (RNAi) was used to decrease the expression of select cytoplasmic proteins and the resulting changes in lipid and integrin diffusion were subsequently measured by FRAP in *Drosophila melanogaster* S2 cells (Fig. 1) [19-22]. Whole-genome RNAi studies have primarily measured an easily observed cellular phenotype. When a more complex property such as membrane diffusion is measured, whole-genome studies become less economically and experimentally feasible. However, measuring a chosen subset of target proteins can be insightful. The cytoplasmic proteins included in this

study for RNAi targeting include focal adhesion kinase (FAK), rhea, integrin linked kinase (ILK), paxillin, vinculin, dreadlocks, steamer duck, actin 42A, and akt1. These proteins have a role in integrin signaling, associate with integrins or the cytoskeleton. Focal adhesions incorporate vinculin, paxillin, rhea, and FAK. Akt1 is a kinase that is not located within focal adhesions, but it is known to interact with them via the PI-3 kinase [23]. Steamer duck and ILK are part of a protein complex that is assembled prior to integrin-dependent cell adhesion [24]. Dreadlocks is involved in cytoskeletal reorganization [25], and actin 42A is one of 6 actins expressed in S2 cells. All of the proteins selected in this study are highly conserved across diverse organisms, and information obtained from these experiments will expand the fundamental understanding of integrins function [26,27]. Rhea, dreadlocks, and steamer duck are homologs for the vertebrate proteins talin, Nck-2, and pinch, respectively. The fluorescence recovery curves were modeled to obtain diffusion coefficients, mobile fractions and modes of diffusion, which were compared before and after RNAi treatment. In addition to FRAP measurements, real time polymerase chain reaction (RT PCR) was used to measure a reduction in mRNA concentration after RNAi treatment.

METHODS

Cell Preparation

S2 cells were cultured in Shields and Sang M3 medium (M3, Sigma) with antibiotics and 10% fetal calf serum (FCS) as previously published [28]. Permanently transfected S2 cells expressed wild-type αPS2CβPS integrins (αβ), or αPS2CβPS integrins with a Venus yellow fluorescent protein (αβ-Venus) inserted in the serine rich loop. The serine rich loop is an extracellular domain that has been previously used to insert epitope tags into this integrin

without disrupting the integrin function [29]. The αβ cell line was used to measure lipid diffusion and the αβ-Venus cell line was used to measure integrin diffusion. The αPS2CβPS integrin binds to the extracellular ligand tiggrin. These studies utilized a recombinant version of this protein, [30] whose concentration was determined via gel electrophoresis. Ligand coated microscope slides were prepared as previously described using 0.5 μg mL^{-1} tiggrin [31].

Synthesis of double stranded RNA (dsRNA) and RNAi treatments have previously been described [32,33]. The cells were incubated with dsRNA for 4 days at 22˚C prior to analysis. The expression of all target proteins in S2 cells was confirmed using FLIGHT mRNA microarray expression database [34] and PeptideAtlas mass spectrometry proteomics database [35].

Fluorescence Recovery After Photobleaching

After incubation with dsRNA, the cells were transferred to a 14 mL centrifuge tube and heat shocked in a 36˚C water bath for 30 minutes to induce expression of integrins, which were under the control of the heat shock promoter. The cells were placed in a 22˚C incubator for 3 hours, and then centrifuged at 600xg for 3 minutes. The supernatant was removed and the cells were resuspended in M3 medium without FCS at a final concentration of $3x10^5$ cells mL^{-1}. For lipid diffusion measurements the M3 medium contained carbocyanine dye DiD (Invitrogen, 1,1'-dioctadecyl-3,3,3',3'- tetramethylindodicarbocyanine perchlorate) at a final concentration of 12 μM. For all measurements, 50 μl of cells were plated onto a tiggrin coated slide and allowed to spread for 1 h before rinsing the slide with BES Tyrodes buffer (200 mM BES, 1.37 M NaCl, 29 mM KCl, 1% w/v glucose, 1% w/v bovine serum albumin).

All fluorescence measurements were performed at room temperature utilizing an Eclipse TE2000U microscope (Nikon). A series of fluorescence images were collected before photobleaching the fluorophore and after photobleaching (recovery) using mercury lamp excitation. Example images are shown in Fig. 1. The exposure time for each image was 0.35 seconds, and images were collected every 0.40 seconds. Photobleaching was accomplished with a laser, as outlined below. Lipid diffusion measurements used a x60 magnification, Plan Apo, 0.95 numerical aperture objective and a 635 nm diode laser (~300 μW at sample) was used to photobleach a 37 μm^2 area of the plasma membrane labeled with DiD. Images were collected using a 645/20 nm excitation and a 660/20 nm emission filter. Integrin diffusion measurements used a x100 magnification, Apo TIRF, 1.49 numerical aperture, oil immersion objective and the 488 nm line of an argon ion laser (~250 μW at sample) to photobleach a 41 μm^2 area of the cell membrane containing αβ-Venus. Venus images were collected using a 500/20 nm excitation and a 535/30 nm emission filter. The Venus fluorescence intensity was lower than that for DiD; therefore, for Venus measurements the gain on the Princeton Instrument PhotonMax 512 CCD was set to its maximum value. Integrin diffusion coefficients were measured on ligand/BSA-coated or BSA-coated (10 mg mL^{-1}) glass slides. No cell movement is measured in the time required to collect a complete FRAP data set. All fluorescence measurements included in this study were obtained on spread cells in the region between the perinuclear region and the cell edge (Fig. 1) to ensure that fluorescence contributions from intracellular YFP is minimal, as previously confirmed [31]. The focus was set to the apical surface, and the thickness of the cells ensures that the apical and basolateral surfaces are not probed simultaneously.

Data analysis

Fluorescence images were analyzed using ImageJ version 1.38. Three intensities were measured for every image of the FRAP series: (1) the photobleached area of the plasma membrane corresponding to the area illuminated by the laser spot; (2) an area of the plasma membrane 10 μm away from the photobleached spot (No FRAP); and (3) a background area 30 μm away from the cell (background). All fluorescence intensities were background subtracted. FRAP curves are an average from seven to ten replicate measurements, and were normalized to the pre-photobleach fluorescence intensity. To account for photobleaching from the mercury lamp during the recovery phase, the average recovery curve was divided by the average No FRAP fluorescence intensity at each time point.

The fluorescence recovery curves were fit to models based on Eq. 1[36] with an in-house developed Igor Pro macro (version 4.0).

$$(1)\quad F(t) = \frac{F_0 + F_{in}\left(\frac{t}{\tau}\right)^{\alpha}}{1+\left(\frac{t}{\tau}\right)^{\alpha}}$$

The parameter F_0 is the initial fluorescence intensity after photobleaching; F_{in} is the fluorescence intensity at an infinite recovery time; τ is the time for 50% of the fluorescence to recover; and α is the time exponent providing a measure of how much diffusion is constrained. Every FRAP curve was fit to three models. (1) The Brownian diffusion model sets $\alpha=1$ and allows $F_{in} < 1$, corresponding to an immobile fraction. (2) The constrained, time-dependent diffusion model assumes no immobile fraction by setting $F_{in}=1$. (3) The third model incorporates time-dependent diffusion with an immobile fraction. Fits to the FRAP curve were weighted to the standard error of the pre-bleach fluorescence intensity. The

reduced chi^2 was calculated as chi^2 divided by the experimental degrees of freedom (Table 1). The reduced chi^2 values were compared to determine the most appropriate model for each data set, and a value of 1 indicates a good fit between the model and the experimental data.

The mobile fraction was calculated as: $(F_{in} - F_o)/(1-F_o)$. The immobile fraction is 1 minus the mobile fraction. The diffusion coefficient, D(t), was calculated by inserting τ and α obtained from the fit of the fluorescence recovery curve into Eq. 2.

$$(2)\quad D(t) = \frac{\omega^2}{(4*(\tau/\beta)^{\alpha})} t^{\alpha-1}$$

where ω is the radius of the focused Gaussian laser beam and β is 1.075, 1.13, 1.15, 1.18, 1.22, or 1.26 when the percent photobleach is 30, 45, 50, 55, 60, and 65, respectively. Diffusion parameters obtained for the best-fit model are listed in Tables 2 and 3 while those for the other models are shown in the Electronic supplemental material Tables S1 and S2. Error bars on all reported FRAP fit parameters represent uncertainties at the 95% confidence level.

RT-PCR

Isolation of mRNA from ~4x10^6 cells was achieved using Dynabeads mRNA Direct kit (Invitrogen 610.12) and quantified using the absorbance value at 260 nm. The reverse transcription of mRNA to cDNA (Applied Biosystems #4387406) was carried out at 37°C for 60 minutes and the reaction terminated at 95°C for 5 minutes. The cDNA was combined with master mix (Applied Biosystems #4369016) and gene expression assay for the corresponding gene (Applied Biosystems: rhea Dm01841094_g1, FAK Dm01816810_m1, ILK Dm01843539_g1, actin 42A Dm02362162_s1, vinculin Dm01841855_g1, paxillin Dm02772085_s1, steamer duck Dm02135515_g1, dreadlocks Dm01842270_g1, akt1

Dm02149560_g1, myospheroid Dm01843062_ g1, gamma tubulin at 23C Dm01841764). RT PCR used an initial temperature of 95°C for 10 minutes to activate the enzyme, followed by 40 cycles (95°C for 15 s then 60°C for 60 s). Calibration curves were constructed using genomic DNA that was isolated from S2 cells with a Qiagen Kit (#69504). All steps were performed according to the manufacturers' provided protocols. Statistical significance of the results was determined using the software Rest 2009 [37].

RESULTS AND DISCUSSION

Integrin and lipid diffusion parameters at native cytoplasmic protein concentrations

The main goal of this study was to elucidate the role of select cytoplasmic proteins in altering the lateral diffusion of αPS2CβPS integrins and lipids in the cell membrane of live S2 cells. Integrin diffusion coefficients were measured for cells spread on a mixed extracellular ligand/bovine serum albumin (BSA) coated microscope slide before RNAi treatment to obtain integrin diffusion parameters at native cytoplasmic protein concentrations. The extracellular ligand used in this study was a recombinant version of tiggrin, the native ligand for αPS2CβPS integrins. BSA fills in areas of the slide not occupied by ligand and prevents non-specific interactions between cell membrane components and the glass slide.

The average integrin FRAP curve from replicate measurements (Fig 2A) was fit to models for (1) Brownian diffusion with an immobile fraction, (2) constrained, time-dependent diffusion or (3) time-dependent diffusion with an immobile fraction. For cells spread on a ligand coated slide, the reduced chi^2 value for each model was 1.3, 4.7, and 1.2, respectively (Table 1, control ligand). This indicates that integrin diffusion in the cell

membrane is best-modeled by time-dependent diffusion with a 55 ± 2% immobile fraction. The integrin diffusion coefficient is 5.2 ± 0.9 x 10^{-9} cm^2/sec at 1 s, and slows to 3.6 ± 0.6 x 10^{-9} cm^2/sec at 50 s (Table 2, control ligand). Hereafter short analysis times refer to the diffusion coefficient at 1 s and long analysis times refer to the diffusion coefficient at 50 s. The time-dependent diffusion coefficient may be the result of periodic interactions with intracellular proteins, extracellular ligand, other membrane components; integrins undergoing conformational changes; or integrins partitioning between domains smaller than the probe area of the FRAP experiment and the bulk membrane. Similarly, there are many plausible explanations for the measured integrin immobile fraction. For example, the immobile integrin may be (1) bound to ligand immobilized on the microscope slide, (2) confined to nanoscale domains that do not exchange with the bulk membrane on the time scale of the FRAP experiment, (3) bound to a static cytoplasmic component or (4) a combination of aforementioned factors.

To determine if the immobile fraction or the diffusion properties of the mobile integrin are ligand-dependent, FRAP curves were measured in cells spread on a BSA coated slide in the absence of ligand. The integrin immobile fraction is expected to decrease in the absence of ligand if this fraction represents ligand-bound protein. Comparing integrin FRAP curves in the presence or absence of ligand, the time-dependent diffusion with an immobile fraction model best-fits both curves (Table 1). The immobile fraction decreases from 55 ± 2% to 30 ± 3% in cells spread in the absence of integrin ligand (Table 2). The difference between these two numbers indicates that 25% of the immobile fraction is ligand-dependent, and this fraction likely represents integrin that is bound to immobile ligand. For cells spread on a ligand containing slide, the remaining 30% ligand-independent immobile fraction may

be the result of hindered diffusion due to the presence of the microscope slide or any of the remaining explanations listed above. The percentage of the immobile fraction that is ligand-dependent or ligand-independent may vary with the ligand concentration. The diffusion properties of the mobile integrin fraction are also altered in cells spread in the absence of ligand. Interestingly, the increase in the mobile fraction is accompanied by a 50% slower diffusion coefficient at long analysis times for cells spread in the absence of ligand (Table 2). This indicates that the extracellular matrix (ECM)-integrin linkage reduces diffusion constraints in the mobile fraction and at the same time reduces the fraction of integrins that are mobile.

In contrast to the integrin diffusion properties, the lipid diffusion properties are independent of the presence or absence of extracellular ligand. A combination of reduced chi^2 values for the three diffusion models (Table 1) and time exponents equal to approximately 1 indicate that the lipid diffusion is Brownian (Table 3). The lipid mobile fraction is 35% higher than the integrin mobile fraction, and the lipid diffusion coefficient is approximately an order of magnitude faster (Table 3). The lipid diffusion coefficient is 30 ± 3 (ligand) or 30 ± 2 (no ligand) x 10^{-9} cm^2/sec (Table 3). The lipid diffusion parameters are consistent with several literature reports using different cell lines and experimental conditions [38,39]. The fastest diffusion coefficient that can be measured with the experimental parameters used in this study is 100 x 10^{-9} cm^2/sec as revealed by modeled FRAP curves associated with varying diffusion coefficients (Fig. S1, green Electronic supplementary material).

Reduced mRNA Concentration for RNAi targeted proteins

RNAi requires the lipid-assisted cellular uptake of approximately 500 base pair dsRNA (RNAi probe). Both the efficiency of getting the RNAi probe inside the cell and the RNA sequence can affect the achieved reduction in protein expression, among other factors [19]. In order to limit false positives and false negatives in the fluorescence measurements, RNAi probes for the target proteins were chosen based on their use in previous RNAi screens, thermodynamic binding efficiency and selectivity for the target protein [40]. Based on a trypan blue assay, there is no change in cell viability after any of the RNAi treatments [31,40].

RT PCR confirmed statistically significant reductions in mRNA concentrations after RNAi treatment for all target proteins (Table 1). The largest reduction was measured for actin 42A (90 to 92%) and the smallest reduction was for paxillin (25 to 43%). Reduction of one component of the trimeric protein complex consisting of ILK, pinch (the vertebrate homolog to steamer duck), and parvin may cause partial degradation of the other components within the complex via a proteasome-mediated process, which would not be reflected in the RT PCR data [24]. RNAi selectivity for these proteins may be low.

There were no statistically significant changes in the mRNA concentration for the βPS integrin subunit after RNAi treatment for any of the target cytoplasmic proteins included in this study (data not shown). Supporting the RT-PCR data, the αβ-Venus fluorescence intensity in the cell membrane was statistically similar in cells before and after RNAi treatment for all target proteins (data not shown). Comparable αβ-Venus fluorescence intensities among all treatments indicate that the membrane integrin concentration is not significantly perturbed upon reducing the expression of the target cytoplasmic proteins.

Changes in integrin diffusion at reduced cytoplasmic protein concentrations

Integrin FRAP curves from replicate measurements were collected after RNAi treatment against nine cytoplasmic proteins (Fig. 2). As shown in Table 1, for all curves except rhea, focal adhesion kinase and akt1, the model for time-dependent diffusion with an immobile fraction is the best fit. For rhea, focal adhesion kinase and akt1, the FRAP curves are fit equally well by the Brownian diffusion and time-dependent diffusion model, and similar diffusion parameters are obtained from both models. For these cytoplasmic proteins there are no or fewer diffusion constraints after reducing their expression.

Table 2 shows the measured diffusion parameters obtained from the FRAP curves for cells that were RNAi treated for the indicated cytoplasmic protein. In subsequent discussion all values for the RNAi treated cells are compared to the control value for cells spread on a ligand coated surface. In general, two changes to integrin diffusion occur after reducing the concentration of the targeted cytoplasmic proteins. For a subset of proteins (actin 42A, dreadlocks, paxillin, ILK, vinculin) integrin diffusion generally slows at longer times with an increase in the integrin mobile fraction. This indicates that when these proteins are expressed at native concentrations integrin diffusion is less constrained. For a second subset of proteins (rhea, FAK) the opposite trend is observed. This indicates that these proteins result in more constrained diffusion when they are expressed at endogenous levels. After steamer duck RNAi, there is no statistically significant change in the integrin diffusion coefficient, but the mobile fraction decreases. RNAi against akt1 increases the integrin mobile fraction and results in Brownian diffusion with an overall slower diffusion coefficient.

Cells were spread on a ligand coated microscope slide for all FRAP measurements performed after the RNAi treatments. When the expression of actin 42A is reduced, the

profile of integrin diffusion mimics that measured for cells spread on a microscope slide in the absence of ligand (Table 2). At reduced actin 42A concentrations or in the absence of ligand there is a ~ 25% increase in the integrin mobile fraction and a 50 to 70% decrease in the diffusion coefficient at long analysis times. In human osteosarcoma and mouse embryonic fibroblast cells no direct physical interaction takes place between integrin and actin proteins, as measured with a sub-diffraction fluorescence imaging technique [41]. The integrin cytoplasmic tail and actin are separated by approximately 40 nm. Within the intervening region several adapter proteins are found (e.g. FAK, paxillin, rhea, vinculin). Reduced expression of paxillin or vinculin mimics the changes in integrin diffusion measured when actin 42A expression is reduced. Whereas reducing the expression of rhea and FAK has the opposite effect as reducing the expression of actin 42A.

A key function of rhea is to connect ligand-bound integrin to the actin cytoskeleton, but rhea is not required for integrin binding to ligand. Talin, the vertebrate homolog to rhea, has a role in the avidity regulation of integrins [42]. Increased integrin clustering in the presence of rhea may explain why reduced rhea concentrations result in Brownian diffusion with a faster diffusion coefficient. The αβ-Venus fluorescence images before RNAi treatment do not show integrin clusters that are larger than the diffraction limit of light. The Saffman-Delbrück equation predicts that the integrin clusters would only have to contain a few proteins at endogenous rhea concentrations (i.e., smaller than the diffraction limit of light) to result in the approximately 30% *increase* in integrin diffusion measured after reducing the concentration of rhea. When the expression of ILK is reduced by RNAi there is a two-fold increase in integrin clusters that are smaller than the diffraction limit of light (manuscript in preparation). It is not known if existing clusters increase in size or if more

clusters develop. The Saffman-Delbrück equation predicts a 20 to 40% *decrease* in the diffusion coefficient when integrin clusters double in size, but remain smaller than the diffraction limit of light. The measured change in integrin diffusion after reducing the expression of ILK could be the result of increased integrin clustering.

A recent paper has shown that reducing levels of vertebrate talin in a fibroblast cell line affected FAK signaling during cell spreading on fibronectin [43]. Total FAK levels did not change, but levels of phosphorylated Tyr397 were attenuated in talin depleted cells. Altered FAK signaling may be the mechanism for altered integrin diffusion upon reducing rhea expression. Evidence supporting this hypothesis is the fact that similar changes in integrin diffusion were measured after reducing the expression of rhea or FAK (6.2-7 x 10^{-9} cm^2/sec Brownian diffusion with a reduced mobile fraction).

Correlations measured between integrin diffusion and lipid diffusion

In order to determine if changes in integrin diffusion are the result of overall changes in membrane viscosity, lipid diffusion coefficients were measured after RNAi treatment for the same target proteins. The cell line used for these measurements expressed wild-type integrin and had a fluorescent carbocyanine lipid mimetic incorporated into the cell membrane. For all lipid fluorescence recovery curves (Electronic supplementary material Fig. S2) except actin 42A and dreadlocks, the data were fit by the Brownian diffusion model or the constrained diffusion with an immobile fraction model generated a time exponent close to 1 (Table 1 and 3).

Two significant changes are observed in the diffusion of the fraction of lipid represented by DiD after individually reducing the concentration of nine cytoplasmic proteins. Reducing expression of dreadlocks, paxillin, FAK and ILK results in a 13 to 21%

increase in the lipid mobile fraction. Dreadlocks RNAi is the only one among this list that shows a consistent change between lipid and integrin mobile fractions. Second, lipid diffusion is constrained with an approximately 20% decrease in the time exponent when the expression of actin 42A and dreadlocks are reduced. This increase in constrained diffusion parallels the change measured for integrin diffusion when the expression of these proteins are reduced. This suggests that actin 42A and dreadlocks have a role in overall membrane organization and fluidity. Actin has been shown to affect lipid phase segregation, which indicates a possible functional role in altering lipid nanodomains [44]. Under some conditions lipid nanodomain formation is reduced in the presence of actin. This is consistent with the RNAi results indicating more constrained lipid diffusion in the absence of actin 42A. With these exceptions, altered integrin diffusion after reducing the expression of the other cytoplasmic proteins is not the result of global changes in membrane viscosity.

Theory for the mechanism of altered integrin diffusion

The combined data in the absence of ligand and after reducing the expression of cytoskeletal proteins indicate that breaking the ECM-integrin-cytoskeletal connection has a role in altering integrin dynamics. There are multiple modes of association between integrins and the cytoskeleton. Some of these interactions constrain diffusion while others release diffusion constraints (Fig. 3). Integrins have been shown to partition between nanodomains and the bulk membrane in response to a variety of stimuli including ligand binding [45]. The most likely explanation for how reduced expression of cytoplasmic protein alters the constraints to integrin diffusion is altered partitioning between nanodomains and bulk membrane. In some instances integrin clustering may be a separate mechanism or may be the result of partitioning into (e.g., ILK RNAi) or out of (e.g., rhea RNAi) nanodomains. With

the exception of Akt1, (1) Brownian diffusion is associated with lower mobile fractions while (2) constrained diffusion is associated with higher mobile fractions. (1) If the integrins are confined in nanodomains and do not escape on the time scale of the FRAP experiment, the immobile fraction increases while the remaining integrins in the bulk membrane have fewer restrictions to diffusion. (2) If the integrins partition between nanodomains and the bulk membrane on the time scale of the FRAP experiment and/or the nature of the nanodomains is altered on this time-scale, then the mobile fraction increases but diffusion is constrained. The nature of these nanodomains is not known at this time, but may include heterogeneous populations of lipid and proteins that associate with the cytoskeleton or are formed via interactions with the cytoskeleton. Future studies where the size of the photobleached area is altered may reveal if the mobile integrin is dependent on membrane nanodomains and selective extraction of membrane components may reveal the composition of these domains.

In no case does altering the ECM-integrin-cytoskeletal connection by the means employed herein lead to unrestricted lateral integrin diffusion predicted by the Saffman-Delbrück equation. The ECM-integrin-cytoskeletal linkage is not completely dissociated and high concentrations of membrane protein are present. Simultaneously reducing the expression of multiple cytoplasmic proteins, including proteins that may not have been included in this study, as well as eliminating integrin interactions with other membrane proteins may be required to achieve unrestricted integrin diffusion. Additionally, complete elimination of the target protein expression may have a greater impact on integrin diffusion than reported in Table 3. Complete elimination of protein expression by RNAi is rarely achieved; still the other methods that can be used to alter protein expression are generally time consuming compared to the RNAi approach. Comparing all RNAi targeted proteins,

there is no correlation between the magnitude of mRNA reduction and the magnitude change in integrin diffusion coefficients. However, correlations between protein expression and integrin diffusion may be correlated [46].

SUMMARY

The combination of FRAP and RNAi can be used to elucidate the molecular mechanism of integrin lateral diffusion. The use of RNAi to reduce the expression of a single protein enables the measurement of that protein's contribution to alterations in integrin diffusion. This is in contrast to several other methods where the entire cytoskeletal composition is altered or the target protein must directly bind with the integrin so that the interaction can be disrupted with integrin mutants. Integrins are linked to the cytoskeleton through a network of proteins, which is more than a simple anchor to the membrane. Diverse connections have functional significance in terms of altering integrin dynamics. This in turn affects the ability of integrins to move to different locations on the cell membrane in response to stimuli. For the most part, the mechanism by which the indicated cytoplasmic proteins alter integrin diffusion is more complex than simple changes in lipid viscosity, and partitioning of integrins into nanodomains is hypothesized to be the main factor affecting the mode of integrin diffusion upon altering the ECM-integrin-cytoskeletal connection. The combination of FRAP and RNAi should be suitable to study the diffusion of other fluorescently labeled membrane proteins and will be useful for unraveling the molecular mechanism of membrane dynamics.

ACKNOWLEDGEMENTS

Support for this work was provided by National Science Foundation (CHE-0845236) and the Roy J. Carver Charitable Trust (Muscatine IA). The authors thank A. Miyawaki (Riken, Wako-city, Saitama, Japan) for the original Venus plasmid and Cory Lanker (Iowa State University, Department of Statistics) for help with the statistical analysis.

REFERENCES

1. Hughes PE, O'Toole TE, Ylanne J, Shattil SJ, Ginsberg MH (1995) The Conserved Membrane-proximal Region of an Integrin Cytoplasmic Domain Specifies Ligand Binding Affinity. J Biol Chem 270 (21):12411-12417
2. Giancotti FG, Ruoslahti E (1999) Integrin Signaling. Science 285 (5430):1028-1032
3. Ginsberg MH, Partridge A, Shattil SJ (2005) Integrin Regulation. Curr Opin Cell Biol 17 (5):509-516
4. Saffman PG, Delbrück M (1975) Brownian Motion in Biological Membranes. Proceedings of the National Academy of Sciences of the United States of America 72 (8):3111-3113
5. Jackson MB (2006) Molecular and Cellular Biophysics. Cambridge University Press, New York
6. Peters R, Cherry RJ (1982) Lateral and Rotational Diffusion of Bacteriorhodopsin in Lipid Bilayers: Experimental Test of the Saffman-Delbruck Equations. Proceedings of the National Academy of Sciences of the United States of America 79 (14):4317-4321
7. Jacobson K, Ishihara A, Inman R (1987) Lateral Diffusion of Proteins in Membranes. Annual review of physiology 49:163-175
8. Kucik DF, Elson EL, Sheetz MP (1999) Weak Dependence of Mobility of Membrane Protein Aggregates on Aggregate Size Supports a Viscous Model of Retardation of Diffusion. Biophys J 76 (1 Pt 1):314-322
9. Sheetz MP, Schindler M, Koppel DE (1980) Lateral Mobility of Integral Membrane Proteins is Increased in Spherocytic Erythrocytes. Nature 285 (5765):510-511
10. Koehler DR, Sajjan U, Chow YH, Martin B, Kent G, Tanswell AK, McKerlie C, Forstner JF, Hu J (2003) Protection of Cftr Knockout Mice from Acute Lung Infection by a Helper-dependent Adenoviral Vector Expressing Cftr in Airway Epithelia. Proc Natl Acad Sci USA 100 (26):15364-15369
11. Kahya N, Schwille P (2006) How Phospholipid-cholesterol Interactions Modulate Lipid Lateral Diffusion, as Revealed by Fluorescence Correlation Spectroscopy. J Fluorescence 16 (5):671-678
12. Chen Y, Lagerholm BC, Yang B, Jacobson K (2006) Methods to Measure the Lateral Diffusion of Membrane Lipids and Proteins. Methods 39 (2):147-153
13. Reits EA, Neefjes JJ (2001) From Fixed to FRAP: Measuring Protein Mobility and Activity in Living Cells. Nat Cell Biol 3 (6):E145-147

14. Axelrod D, Koppel DE, Schlessinger J, Elson E, Webb WW (1976) Mobility Measurement by Analysis of Fluorescence Photobleaching Recovery Kinetics. Biophys J 16 (9):1055-1069
15. van Zoelen EJ, Tertoolen LG, de Laat SW (1983) Simple Computer Method for Evaluation of Lateral Diffusion Coefficients from Fluorescence Photobleaching Recovery Kinetics. Biophys J 42 (1):103-108
16. Gordon GW, Chazotte B, Wang XF, Herman B (1995) Analysis of Simulated and Experimental Fluorescence Recovery After Photobleaching Data for Two Diffusing Components. Biophys J 68 (3):766-778
17. Wehrle-Haller B (2007) Analysis of Integrin Dynamics by Fluorescence Recovery After Photobleaching. Methods Mol Biol 370:173-202
18. Sancey L, Garanger E, Foillard S, Schoehn G, Hurbin A, Albiges-Rizo C, Boturyn D, Souchier C, Grichine A, Dumy P, Coll JL (2009) Clustering and Internalization of Integrin alphavbeta3 with a Tetrameric RGD-synthetic Peptide. Mol Ther 17 (5):837-843
19. Kiger AA, Baum B, Jones S, Jones MR, Coulson A, Echeverri C, Perrimon N (2003) A Functional Genomic Analysis of Cell Morphology using RNA Interference. J Biol 2 (4):27
20. Boutros M, Kiger AA, Armknecht S, Kerr K, Hild M, Koch B, Haas SA, Paro R, Perrimon N (2004) Genome-wide RNAi Analysis of Growth and Viability in *Drosophila* Cells. Science 303 (5659):832-835
21. Agaisse H, Burrack LS, Philips JA, Rubin EJ, Perrimon N, Higgins DE (2005) Genome-wide RNAi Screen for Host Factors Required for Intracellular Bacterial Infection. Science 309 (5738):1248-1251
22. Bard F, Casano L, Mallabiabarrena A, Wallace E, Saito K, Kitayama H, Guizzunti G, Hu Y, Wendler F, Dasgupta R, Perrimon N, Malhotra V (2006) Functional Genomics Reveals Genes Involved in Protein Secretion and Golgi Organization. Nature 439 (7076):604-607
23. Zamir E, Geiger B (2001) Molecular Complexity and Dynamics of Cell-matrix Adhesions. J Cell Sci 114 (Pt 20):3583-3590
24. Legate KR, Montanez E, Kudlacek O, Fassler R (2006) ILK, PINCH and Parvin: the tIPP of Integrin Signalling. Nat Rev Mol Cell Biol 7 (1):20-31
25. Wu C (1999) Integrin-linked Kinase and PINCH: Partners in Regulation of Cell-extracellular Matrix Interaction and Signal Transduction. J Cell Sci 112 (Pt 24):4485-4489
26. Takada Y, Ye X, Simon S (2007) The Integrins. Genome Biol 8 (5):215
27. Brower DL (2003) Platelets with Wings: The Maturation of *Drosophila* Integrin Biology. Curr Opin Cell Biol 15 (5):607-613
28. Bunch TA, Grinblat Y, Goldstein LS (1988) Characterization and Use of the *Drosophila* Metallothionein Promoter in Cultured *Drosophila melanogaster* Cells. Nucleic Acids Res 16 (3):1043-1061
29. Bunch TA, Helsten TL, Kendall TL, Shirahatti N, Mahadevan D, Shattil SJ, Brower DL (2006) Amino Acid Changes in *Drosophila* alphaPS2betaPS Integrins that Affect Ligand Affinity. J Biol Chem 281 (8):5050-5057
30. Graner MW, Bunch TA, Baumgartner S, Kerschen A, Brower DL (1998) Splice Variants of the *Drosophila* PS2 Integrins Differentially Interact with RGD-containing Fragments

of the Extracellular Proteins Tiggrin, Ten-m, and D-laminin 2. J Biol Chem 273 (29):18235-18241
31. Dibya D, Sander S, Smith EA (2009) Identifying Cytoplasmic Proteins that Affect Receptor Clustering using Fluorescence Resonance Energy Transfer and RNA Interference. Anal Bioanal Chem 395 (7):2303-2311
32. Clemens JC, Worby CA, Simonson-Leff N, Muda M, Maehama T, Hemmings BA, Dixon JE (2000) Use of Double-stranded RNA Interference in *Drosophila* Cell Lines to Dissect Signal Transduction Pathways. Proc Natl Acad Sci USA 97 (12):6499-6503
33. March JC, Bentley WE (2006) Engineering Eukaryotic Signal Transduction with RNAi: Enhancing *Drosophila* S2 Cell Growth and Recombinant Protein Synthesis via Silencing of TSC1. Biotechnol Bioeng 95 (4):645-652
34. FLIGHT. [http://flightlicrorg/]
35. PeptideAtlas. [wwwmopunizhch/peptideatlas]
36. Feder TJ, Brust-Mascher I, Slattery JP, Baird B, Webb WW (1996) Constrained diffusion or immobile fraction on cell surfaces: a new interpretation. Biophysical journal 70 (6):2767-2773
37. Pfaffl M (2009) Rest 2009. http://www.gene-quantification.de/rest-2009.html.
38. Kusumi A, Nakada C, Ritchie K, Murase K, Suzuki K, Murakoshi H, Kasai RS, Kondo J, Fujiwara T (2005) Paradigm Shift of the Plasma Membrane Concept from the Two-dimensional Continuum Fluid to the Partitioned Fluid: High-speed Single-molecule Tracking of Membrane Molecules. Annu Rev Biophys Biomol Struct 34:351-378
39. Owen DM, Williamson D, Rentero C, Gaus K (2009) Quantitative Microscopy: Protein Dynamics and Membrane Organisation. Traffic 10 (8):962-971
40. Heidelberg. [http://rnai2dkfzde/GenomeRNAi/]
41. Kanchanawong P, Shtengel G, Pasapera AM, Ramko EB, Davidson MW, Hess HF, Waterman CM (2010) Nanoscale Architecture of Integrin-based Cell Adhesions. Nature 468 (7323):580-584
42. Helsten TL, Bunch TA, Kato H, Yamanouchi J, Choi SH, Jannuzi AL, Feral CC, Ginsberg MH, Brower DL, Shattil SJ (2008) Differences in Regulation of *Drosophila* and vertebrate Integrin Affinity by Talin. Molecular biology of the cell 19 (8):3589-3598
43. Zhang X, Jiang G, Cai Y, Monkley SJ, Critchley DR, Sheetz MP (2008) Talin Depletion Reveals Independence of Initial Cell Spreading from Integrin Activation and Traction. Nature cell biology 10 (9):1062-1068
44. Garg S, Tang JX, Ruhe J, Naumann CA (2009) Actin-induced perturbation of PS lipid-cholesterol interaction: A possible mechanism of cytoskeleton-based regulation of membrane organization. Journal of structural biology 168 (1):11-20
45. Decker L, Baron W, Ffrench-Constant C (2004) Lipid rafts: microenvironments for integrin-growth factor interactions in neural development. Biochemical Society transactions 32 (Pt3):426-430
46. Taniguchi Y, Choi PJ, Li GW, Chen H, Babu M, Hearn J, Emili A, Xie XS (2010) Quantifying E. coli proteome and transcriptome with single-molecule sensitivity in single cells. Science 329 (5991):533-538

Table 1. Real-time polymerase chain reaction results and reduced chi^2 values obtained from integrin (top number) or lipid (bottom number) FRAP curves fit to different diffusion models before (control ligand or control no ligand) and after the indicated RNAi treatments

	Constrained Diffusion chi^2	**Brownian Diffusion chi^2**	**Time-dependent diffusion with an immobile fraction chi^2**	**Percent reduction in mRNA after RNAi[a]**
Control ligand	4.7 5.8	1.3 1.1	1.2 1.1	
Control no ligand	3.0 4.1	1.5 1.4	1.0 1.5	
Actin 42A	2.2 3.6	2.5 1.4	1.4 1.0	90-92
Dreadlocks	4.6 3.5	4.7 2.5	4.0 1.0	38-76
Paxillin	4.4 2.1	1.2 1.4	1.0 1.3	25-43
Integrin Linked Kinase	1.5 1.9	1.2 1.8	1.0 1.9	59-73
Vinculin	2.6 1.9	1.6 0.4	1.4 0.4	84-90
Akt1	2.6 3.2	1.3 0.9	1.3 1.0	76-80
Rhea	3.5 3.4	0.9 0.4	0.9 0.4	32-63
Focal Adhesion Kinase	7.8 2.2	2.1 0.9	2.1 1.0	78-92
Steamer Duck	7.1 1.0	2.0 0.5	1.8 0.5	67-82

a Measurements were performed in duplicate (n=2). Real time polymerase chain reaction results are expressed as a range that indicates a 95% confidence interval for expression ratios without normality or symmetrical distribution assumptions as determined using the software REST 2009. The *p* values for all entries in this column are 0.000 which indicates a statistically significant difference in mRNA concentration after RNAi treatment compared to the value measured before RNAi treatment.

Table 2. *Integrin* diffusion parameters obtained from the best-fit model[a] of the FRAP curves for a αβ-Venus cell line before (control ligand or control no ligand) and after the indicated RNAi treatments.

a	**Mobile fraction**	**Time exponent (α)**	**Diffusion coefficient at 1 s (x 10^{-9}cm^2/s)**	**Diffusion coefficient at 50 sec (x 10^{-9}cm^2/s)**
Control Ligand	0.45 ± 0.02	0.90 ± 0.07	5.2 ± 0.9	3.6 ± 0.6
Control No Ligand	0.70 ± 0.03	0.83 ± 0.05	4.1 ± 0.6	2.1 ± 0.2
Actin 42A	0.70 ± 0.04	0.69 ± 0.06	5 ± 1	1.6 ± 0.2
Dreadlocks	0.72 ± 0.05	0.75 ± 0.05	3.0 ± 0.7	1.1 ± 0.2
Paxillin	0.49 ± 0.02	0.85 ± 0.06	4.6 ± 0.8	2.6 ± 0.3
Integrin Linked Kinase	0.49 ± 0.05	0.7 ± 0.1	5 ± 1	1.6 ± 0.4
Vinculin	0.54 ± 0.04	0.79 ± 0.09	7 ± 1	2.9 ± 0.6
Akt1	0.60 ± 0.02		3.1 ± 0.5[b]	
Rhea	0.28 ± 0.01		7 ± 1[b]	
Focal Adhesion Kinase	0.28 ± 0.01		6.2 ± 0.9[b]	
Steamer Duck	0.32 ± 0.01	0.87 ± 0.06	6.3 ± 0.9	3.9 ± 0.6

a Brownian diffusion assumed to be the best-fit model if the reduced chi^2 was the same for time-dependent diffusion with an immobile fraction and Brownian diffusion models
b Brownian diffusion is not time-dependent (alpha = 1); diffusion coefficient will be the same value at all analysis times

Table 3. *Lipid* diffusion parameters obtained from the best-fit model to FRAP curves for a αβ cell line before (control ligand or control no ligand) and after the indicated RNAi treatments

[a]	Mobile fraction	Time exponent (α)	Diffusion coefficient at 1 s (x 10^{-9}cm^2/s)	Diffusion coefficient at 50 s (x 10^{-9}cm^2/s)
Control Ligand	0.80 ± 0.03	1.1 ± 0.1	30 ± 3[b]	
Control No Ligand	0.80 ± 0.01		30 ± 2[b]	
Actin 42A	0.86 ± 0.06	0.8 ± 0.1	22 ± 3	12 ± 2
Dreadlocks	1.01 ± 0.04	0.83 ± 0.07	26 ± 2	13 ± 1
Paxillin	0.94 ± 0.02	0.96 ± 0.06	26 ± 2	22 ± 1
Integrin Linked Kinase	0.96 ± 0.02		36 ± 2[b]	
Vinculin	0.87 ± 0.05	1.1 ± 0.2	34 ± 5	
Akt1	0.74 ± 0.04		28 ± 4[b]	
Rhea	0.87 ± 0.05	1.0 ± 0.1	29 ± 3	
Focal Adhesion Kinase	0.93 ± 0.03		29 ± 2[b]	
Steamer Duck	0.82 ± 0.04	1.0 ± 0.1	31 ± 3	

a Brownian diffusion assumed to be the best-fit model if the reduced chi^2 was the same for time-dependent diffusion with an immobile fraction and Brownian diffusion models
b Brownian diffusion is not time-dependent (alpha = 1); diffusion coefficient will be the same value at all analysis times

Figure 1. Experimental approach. a The cell membrane contains an array of lipids, proteins and small molecules. The αPS2CβPS integrin receptors that are the focus of this work are shown in the cell membrane in the absence of other membrane proteins for simplicity. Integrins are tagged with the Venus fluorescent protein (αβ-Venus). *1* The integrin diffusion properties are measured in cells with endogenous levels of cytoplasmic proteins. Integrins diffusion is described by a time-dependent diffusion coefficient with an immobile fraction. *2* RNAi is used to reduce the expression of one cytoplasmic protein. *3* Changes in the integrin diffusion properties are measured. These studies identify the cytoplasmic proteins that have a role in altering integrin lateral diffusion in the cell membrane as further discussed in the text. **b** Fluorescence images of a cell expressing αβ-Venus integrins at three time points in the FRAP experiment. The *red arrow* highlights the photobleached region of the cell membrane. The *blue arrow* represents the signal that emanates from inside the cell. *Scale bar* 6.7 microns

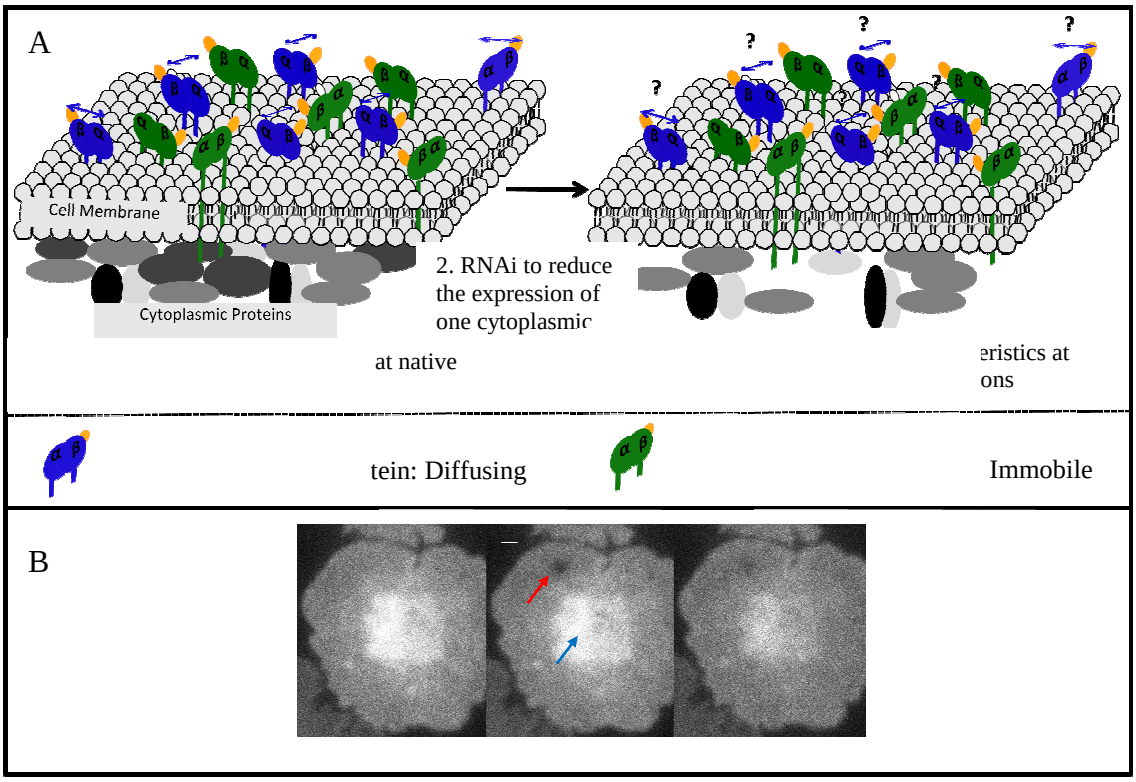

Figure 2. Average fluorescence recovery after photobleaching (FRAP) curves from replicate measurements (*blue circles*) for the S2 cell line expressing αPS2CβPS-Venus integrins at native cytoplasmic protein concentrations: **a** cells spread on ligand coated slide, **b** cells spread in the absence of ligand; and after the following RNAi treatments for cells spread on a ligand coated slide: **c** Actin 42A; **d** Dreadlocks; **e** Paxillin; **f** ILK; **g** Vinculin; **h** Akt1; **i** Rhea; **j** FAK and **k** Steamer duck. The data are either fit to a model that accounts for time-dependent diffusion with an immobile fraction (a-g and k) or a Brownian diffusion model (h-j) (*red line*). All curves have been normalized to the pre-photobleach intensity.

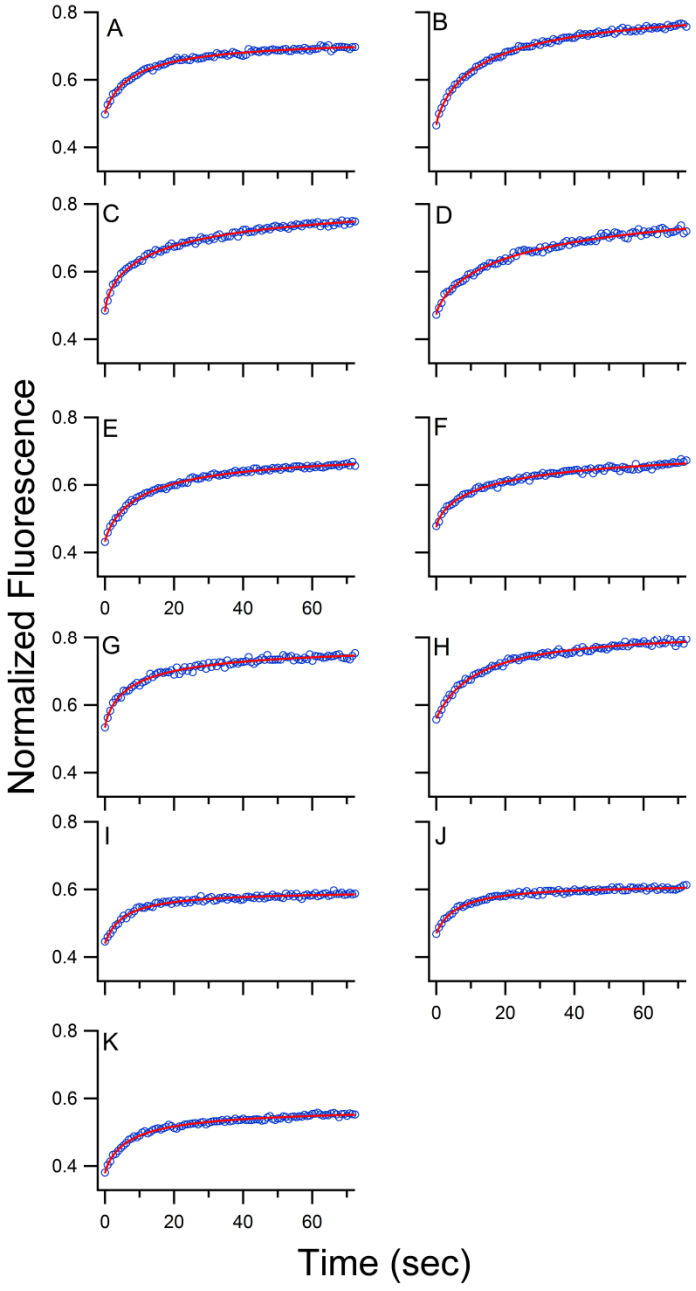

Figure 3. Proposed model for the regulation of integrin dynamics. At endogenous cytoplasmic protein concentrations there is an immobile fraction and equilibrium between mobile integrins in the bulk membrane and in nanodomains. Upon altering the ECM-integrin-cytoskeletal connection this equilibrium is disrupted. In some cases immobile integrins are confined in nanodomains and do not escape. At the same time the remaining integrins in the bulk membrane exhibit Brownian diffusion. In other cases, the integrins partition between nanodomains and the bulk membrane. This increases the mobile fraction, but diffusion is constrained on the time scale of the FRAP experiment.

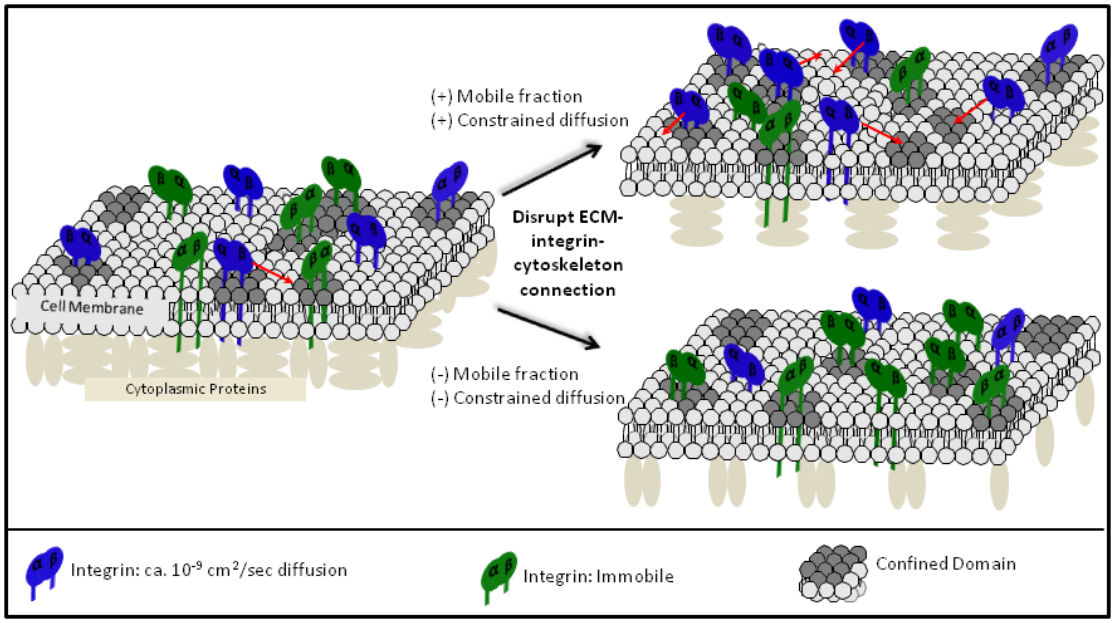

Supporting Information for Chapter 2

Figure S1. **Integrin and lipid FRAP curves.** Average experimental FRAP curve for αβ-Venus cells spread on a ligand containing microscope slide (blue markers). The inset shows the same FRAP curve at longer analysis times. The data are fit to a model with time-dependent diffusion plus an immobile fraction. Experimental FRAP curves for αβ cells labeled with the membrane fluorophore DiD spread on a ligand containing microscope slide (black markers). The data are fit to a model with Brownian diffusion. Theoretical FRAP curve for Brownian diffusion with a 1 x 10^{-7} cm^2/sec diffusion coefficient (green line), the fastest diffusion that can be measured with the experimental method.

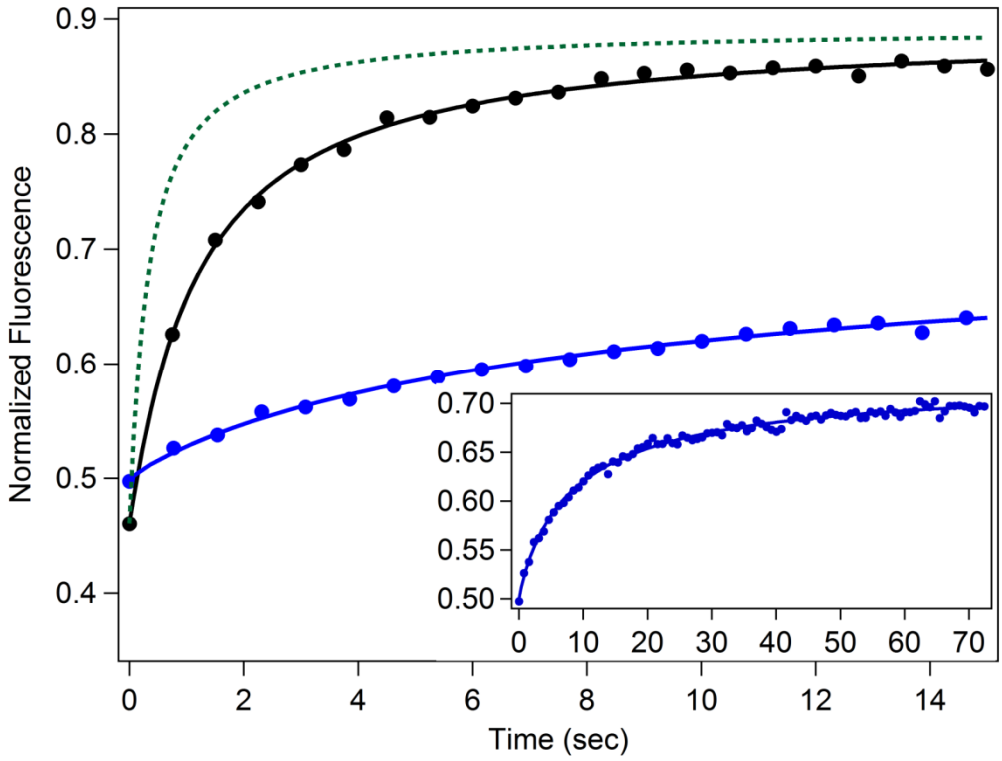

Figure S2. Average FRAP curves from replicate measurements for the S2 cell line expressing wild-type integrins and labeled with the membrane dye DiD (1,1'-dioctadecyl-3,3,3',3'- tetramethylindodicarbocyanine perchlorate) at native cytoplasmic protein concentrations (A) cells spread on ligand coated slide, (B) cell spread in absence of ligand; and after the following RNAi treatments for cells spread on a ligand coated slide: (C) Actin 42A; (D) Dreadlocks; (E) Paxillin; (F) ILK; (G) Vinculin; (H) Akt1; (I) Rhea; (J) FAK and (K) Steamer Duck. The data are either fit to a model that accounts for time-dependent diffusion with an immobile fraction (C-E) or a Brownian diffusion model (A, B,F-K) (red line). The diffusion coefficients and mobile fractions are listed in Table S2. All curves have been normalized to the pre-photobleach intensity.

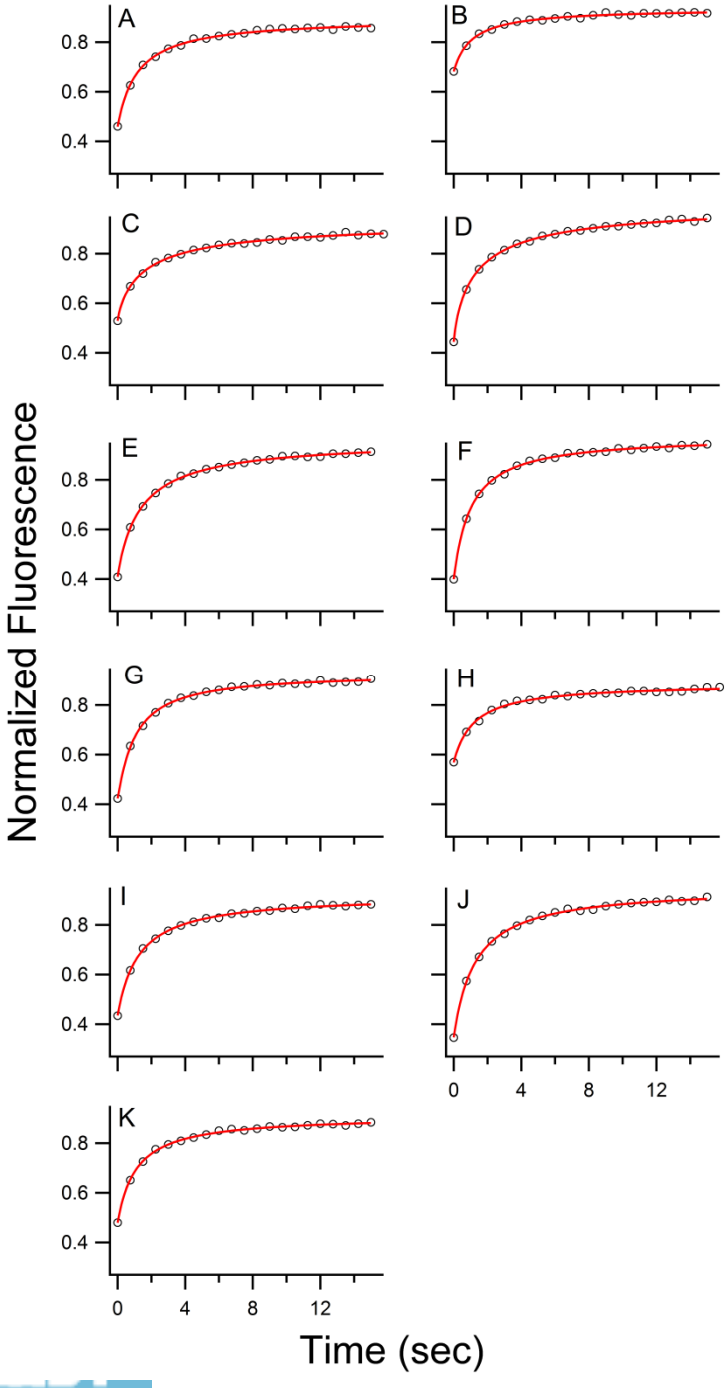

Table S1. Integrin diffusion parameters obtained by fitting FRAP curves to constrained (time dependent) diffusion, Brownian diffusion and time-dependent diffusion with an immobile fraction models for a cell line expressing αPS2CβPS-Venus integrins before (control) and after the indicated RNAi treatment. The fit parameters from the best-fit model, either time dependent diffusion with an immobile fraction or Brownian diffusion, are shown in Table 2 of the manuscript. The control cells were measured for cells spread on an integrin ligand containing microscope slide (ligand) or a slide containing only the protein BSA (no ligand). After RNAi treatment the cells are spread on a ligand coated microscope slide.

	Constrained Diffusion			Brownian Diffusion		Constrained/Brownian Diffusion			
	α	Diffusion Coefficient (1 s) ($x10^{-9}cm^2/s$)	Diffusion Coefficient (50 sec) ($x10^{-9}cm^2/s$)	Mobile fraction	Diffusion Coefficient ($x10^{-9}$ cm^2/s)	Mobile Fraction	α	Diffusion Coefficient (1 s) ($x10^{-9}cm^2/s$)	Diffusion Coefficient (50 sec) ($x10^{-9}cm^2/s$)
Control Ligand	0.38 ± 0.01	5.3 ± 0.4	0.46 ± 0.01	0.43 ± 0.01	4.3 ± 0.6	0.45 ± 0.02	0.90 ± 0.07	5.2 ± 0.9	3.6 ± 0.6
Control No Ligand	0.54 ± 0.01	4.9 ± 0.2	0.81 ± 0.02	0.63 ± 0.01	3.0 ± 0.4	0.70 ± 0.03	0.83 ± 0.05	4.1 ± 0.6	2.1 ± 0.2
Actin 42A	0.48 ± 0.02	5.1 ± 0.3	0.67 ± 0.02	0.56 ± 0.01	3.1 ± 0.4	0.70 ± 0.04	0.69 ± 0.06	5 ± 1	1.6 ± 0.2
Dreadlocks	0.57 ± 0.01	3.1 ± 0.2	0.58 ± 0.01	0.59 ± 0.01	1.9 ± 0.3	0.72 ± 0.05	0.75 ± 0.05	3.0 ± 0.7	1.1 ± 0.2
Paxillin	0.41 ±0.01	4.6 ± 0.3	0.47 ± 0.01	0.45 ± 0.01	3.5 ± 0.5	0.49 ±0.02	0.85 ± 0.06	4.6 ± 0.8	2.6 ± 0.3
ILK	0.42 ± 0.03	3.6 ± 0.6	0.37 ± 0.02	0.40 ±0.02	2.9 ± 0.5	0.49 ±0.05	0.7 ± 0.1	5 ± 2	1.6 ± 0.4
Vinculin	0.39 ± 0.02	6.2 ± 0.6	0.57 ± 0.03	0.48 ± 0.02	4.5 ± 0.7	0.54 ± 0.04	0.79 ± 0.09	7 ± 1	2.9 ± 0.6
Akt1	0.52 ± 0.02	4.8 ± 0.4	0.73 ± 0.03	0.60 ± 0.02	3.1 ± 0.4	0.64 ± 0.04	0.89 ± 0.08	3.8 ± 0.9	2.5 ± 0.4
Rhea	0.28 ± 0.02	4.1 ± 0.7	0.25 ± 0.02	0.28 ± 0.01	7 ± 1	0.27 ± 0.02	1.1 ± 0.1	5.8 ± 2	8.6 ± 3
FAK	0.28 ± 0.01	4.1 ± 0.4	0.25 ± 0.01	0.28 ± 0.01	6.2 ± 0.9	0.28 ± 0.01	0.97 ± 0.08	6.5 ± 1	5.9 ± 1
Steamer Duck	0.31 ± 0.01	4.0 ± 0.3	0.27 ± 0.01	0.30 ± 0.01	5.1 ± 0.7	0.32 ± 0.01	0.87 ± 0.06	6.3 ± 0.9	3.9 ± 0.6

[a] Diffusion parameters were obtained from fitting the average FRAP curve of replicate measurements with the standard deviation representing the uncertainty at the 95% confidence interval of the corresponding coefficients obtained in the fits.

Table S2. Lipid diffusion parameters obtained by fitting FRAP curves to constrained (time dependent) diffusion, Brownian diffusion and time-dependent diffusion with an immobile fraction models for a cell line expressing αPS2CβPS integrins before (control) and after the indicated RNAi treatment. The fit parameters from the best-fit model either Brownian diffusion or time dependent diffusion with an immobile fraction, are shown in Table 3 of the manuscript. The control cells were measured for cells spread on an integrin ligand containing microscope slide (ligand) or a slide containing only the protein BSA (no ligand). After RNAi treatment the cells are spread on a ligand coated microscope slide.

	Constrained Diffusion			Brownian Diffusion		Constrained/Brownian Diffusion			
	α	Diffusion Coefficient (1 s) ($x10^{-9}cm^2/s$)	Diffusion Coefficient (50 sec) ($x10^{-9}cm^2/s$)	Mobile fraction	Diffusion Coefficient ($x10^{-9}cm^2/s$)	Mobile Fraction	α	Diffusion Coefficient (1 s) ($x10^{-9}cm^2/s$)	Diffusion Coefficient (50 sec) ($x10^{-9}cm^2/s$)
Control Ligand	0.60 ± 0.03	22 ± 1	4.6 ± 0.3	0.81 ± 0.03	30 ± 3	0.80 ± 0.03	1.1 ± 0.1	30 ± 3	37 ± 4
Control No Ligand	0.57 ± 0.01	22 ± 1	4.1 ± 0.1	0.80 ± 0.01	30 ± 2	0.80 ± 0.02	1.0 ± 0.1	30 ± 2	30 ± 2
Actin 42A	0.61 ± 0.03	19 ± 1	4.1 ± 0.3	0.81 ± 0.03	23 ± 3	0.86 ± 0.06	0.8 ± 0.1	22 ± 3	12 ± 2
Dreadlocks	0.88 ± 0.02	27 ± 1	17 ± 0.9	0.95 ± 0.02	28 ± 2	1.01 ± 0.04	0.83 ± 0.07	26 ± 2	13 ± 1
Paxillin	0.71 ± 0.04	28 ± 1	8.0 ± 0.3	0.92 ± 0.02	27 ± 1	0.94 ± 0.02	0.96 ± 0.06	26 ± 2	22 ± 1
ILK	0.68 ± 0.03	32 ± 1	9.3 ± 0.3	0.96 ± 0.02	36 ± 2	0.96 ± 0.02	1.01 ± 0.06	36 ± 2	37 ±
Vinculin	0.63 ± 0.03	29 ± 2	6.6 ± 0.6	0.89 ± 0.04	34 ± 5	0.87 ± 0.05	1.1 ± 0.2	35 ± 5	47 ± 6
Akt1	0.81 ± 0.02	15 ± 2	6.9 ± 0.9	0.74 ± 0.04	28 ± 4	0.73 ± 0.05	1.1 ± 0.2	28 ± 5	35 ±
Rhea	0.52 ± 0.04	25 ± 2	3.8 ± 0.2	0.86 ± 0.03	29 ± 3	0.87 ± 0.05	1.0 ± 0.1	29 ± 4	24 ± 3
FAK	0.81 ± 0.03	26 ± 2	12 ± 0.8	0.93 ± 0.03	29 ± 2	0.93 ± 0.03	0.98 ± 0.08	29 ± 3	27 ± 2
Steamer Duck	0.85 ± 0.02	22 ± 2	12 ± 1	0.83 ± 0.03	31 ± 3	0.82 ± 0.04	1.0 ± 0.1	31 ± 4	37 ± 4

[a] Diffusion parameters were obtained from fitting the average FRAP curve of replicate measurements with the standard deviation representing the uncertainty at the 95% confidence interval of the corresponding coefficients obtained in the fits.

CHAPTER 3: NON-INVASIVE LIVE CELL MEASUREMENTS OF RECEPTOR CLUSTERING ALTERED BY INTRACELLULAR PROTEINS

Suzanne Sander, Deepak Dibya, Emily A. Smith

Department of Chemistry, Iowa State University, 1605 Gilman Hall, Ames, Iowa 50011

ABSTRACT

The role of select cytoplasmic proteins in altering integrin receptor clustering on the nanoscale in the presence of extracellular ligand binding is reported. Integrin clustering was measured using fluorescence resonance energy transfer (FRET) combined with RNA interference (RNAi), which is used to reduce the expression of a select cytoplasmic protein. Membrane spanning FRET reporter peptides that cluster with the integrin are used as a non-invasive probe of receptor clustering on the nanoscale. A change in energy transfer after reducing the expression of a cytoplasmic protein provides quantitative information about the protein's role in receptor clustering. Cytoplasmic proteins involved in wild-type and mutant integrin clustering have been identified for cells spread on a surface with 40 ± 10% ligand density. The RNAi targeted proteins in this study include: dreadlock, integrin linked kinase, paxillin, steamer duck, vinculin, rhea, focal adhesion kinase, and Rho1.The RNAi protocol used in these studies targets at least 38% of the cells in a culture, which is sufficient to produce a measurable change in energy transfer for at least a subset of RNAi targeted cytoplasmic proteins due to altered integrin clustering. Experiments were performed with control FRET peptides to ensure that the energy transfer values measured with FRET

reporters correlate with integrin clustering, and are not the result of non-integrin dependent cell membrane properties.

INTRODUCTION

The transmission of information between cells and their environment is necessary for survival, growth, mobility, and other fundamental aspects of development [1]. Receptor cell membrane proteins are intermediaries in the transmission of information across the cell membrane. Membrane spanning integrins are receptors that consist of non-covalently interacting α and β subunits. Integrins bind to both intracellular and extracellular proteins. Outside-in signaling is initiated by ligand binding to the extracellular domain, while inside-out signaling requires the interaction of adapter proteins with the integrins cytoplasmic tails [1,2]. There are dozens of intracellular proteins that have been shown to interact with integrin cytoplasmic domains, including rhea[3], integrin linked kinase [4] and paxillin [5].

Individually, integrins have a low binding affinity for ligand (μM^{-1} to mM^{-1})[6]; however, their high concentration in the membrane and their ability to cluster enables the strong adherence of cells to the extracellular matrix. Characterization of integrin clustering is performed in two different spatial regimes: larger or smaller than the diffraction limit of light, approximately 200 nm. Currently, *non-invasive* methods for measuring clusters smaller in size than 200 nm in *live cells* are limited, and dynamic integrin interactions within the cell membrane are poorly understood. Fluorescence resonance energy transfer (FRET) [7] is a technique that can measure clustering on a scale of 10 nm or less. A non-invasive FRET assay of receptor clustering would not require the direct attachment of donor and acceptor FRET pairs to the receptor.

FRET has been previously applied to study integrin clustering [8-11]. One study used FRET reporter peptides instead of direct fluorophore attachment onto the receptor. The FRET reporter peptides spanned the membrane, clustered with the integrins without altering integrin-ligand binding and were developed by attaching fluorescent proteins to the β subunit's transmembrane and cytoplasmic domain. This FRET assay also eliminated time consuming protein cloning steps for receptor mutant studies [8].

Reported herein is the use of this previously reported FRET assay to identify how intracellular proteins affect integrin clustering. The effects of vinculin, paxillin, focal adhesion kinase, rhea, integrin linked kinase, dreadlock, and steamer duck on the clustering of αPS2CβPS integrins have been measured in S2 cells spread on a surface with 40 ± 10% ligand density, and these effects are compared to results obtained from studies that utilized a lower ligand density [12-15]. Specific amino acid contacts between the transmembrane/cytoplasmic domains are likely to drive the co-clustering of the integrins and FRET reporters [16]. Additionally, the quantitative measurement of integrin and FRET reporter expression levels is reported for the first time.

EXPERIMENTAL

Cells Lines

All experiments were performed using *Drosophila* S2 cells cultured in Shields and Sang M3 medium (M3, Sigma) with antibiotics, streptomycin and penicillin, 10% fetal calf serum (FCS), and methotrexate. Detailed culture protocols have been described elsewhere [17]. Cells were transformed to express wild-type integrins [18], mutant integrins [18], FRET reporters[8], FRET controls [8] or a combination therein.

RNAi treatment

Double stranded RNA (dsRNA) was synthesized as described previously[19,20].Proteomics databases were used to confirm that target proteins are expressed in *Drosophila* S2 cells [21,22]. Cells were plated in a culture dish at a concentration of 1 x 10^6 cell/mL. The cells were rinsed with serum free M3 medium, and then 300 μL serum free M3 medium was added to each well. Ten micrograms of dsRNA was added to each well. The cells were incubated with dsRNA in serum free medium for 60 minutes at 22˚C. Subsequently, 300 μL of M3 medium containing 20% FCS was added to the wells. The cells were incubated for 4 days at 22˚C. Then the cells were placed in a water bath set to 36˚C for 30 minutes to induce the expression of integrins, FRET reporters and FRET controls, which are cloned in heat shock plasmids. The cells were placed in a 22˚C incubator for 3 hours. The cells (200 μL) were centrifuged at 600 g for 3 minutes, re-suspended in 300 μL of M3 medium, counted and diluted to a final concentration of 3 x 10^5 cells/mL. For all measurements, 50 μL of cells were plated into each well of a ligand coated slide. A recombinant version of the αPS2CβPS integrin's ligand (0.025 μg) was used for these studies, as previously described [23]. The cells were allowed to spread in the dark for 1 hour. During this time, the S2 cells spread to their maximum level and no further spreading or cell movement can be measured. The medium was then removed and replaced with 20 mM BES Tyrodes buffer.

Protein Expression Levels

Expression of αPS2CβPS integrin was measured via flow cytometry as previously reported [8]. Expression of extracellular Venus fluorescent protein was similarly measured by flow cytometry. Briefly, 0.5 x 10^6 cells were centrifuged and then resuspended in 50 μl green fluorescent protein (GFP) antibody (Invitrogen) diluted 1:500 (v/v) in M3+FCS, and

placed on ice for 30 minutes. This antibody also binds to yellow fluorescent protein variants. Subsequently, the cells were spun down and resuspended in 50 μL anti-mouse labeled with phycoerythrin (Invitrogen) diluted 1:300 (v/v) in M3+ FCS, and put on ice for an additional 30 minutes. The cells were spun down and resuspended in 2% paraformaldehyde prior to analysis on a BD FACScan flow cytometer.

Fluorescence Measurements

All fluorescence microscopy measurements were made with an Eclipse TE2000U microscope (Nikon) with a 60x, 0.95 numerical aperture objective and a mercury lamp excitation source. Images were captured via a Coolsnap CCD camera (Roper ScienfiticPhotmetrics, Pleasanton, CA) set to bin 8x8 pixels. Image capture was controlled using the program Micromanager, which operates in ImageJ 1.37v software (NIH). Each cell was imaged using three different filters: donor filter set with an excitation of 500/20 nm and an emission of 535/30 nm; acceptor filter set with an excitation of 545/30 nm and an emission of 620/60 nm; and FRET filter set which combines the donor excitation filter with acceptor emission filter. The exposure times for the donor, acceptor, and FRET images were 6, 6, and 12 seconds, respectively.

FRET Data Analysis

In comparison to previous studies using FRET reporters, calculations of energy transfer in this study enable a quantitative measure of the concentration of interacting donor/acceptor pairs on the reporter peptides. Data was analyzed using a plug-in developed for ImageJ. The plug-in subtracts a background value and then calculates a FRET value using equation 1 [24]:

$$E_{app} = \frac{I_{DA} - (a - bd)I_{AA} - (d - ac)I_{DD}}{I_{DA} - (a - bd)I_{AA} - (d - ac - G)I_{DD}} \qquad (1)$$

where I_{DA}, I_{AA}, and I_{DD} are intensities obtained from the images with the FRET, acceptor, and donor filters, respectively. The G term is described below. The equation accounts for bleed-through of acceptor into the FRET filters, acceptor into the donor filters, donor into the acceptor filters, and donor into the FRET filters, using factors *a*, *b*, *c*, and *d*, respectively. For each analyzed cell, a region of interest is defined that excludes pixels corresponding to nuclear and surrounding regions [11]. One FRET value is obtained for each cell by averaging all pixels in the region of interest. Only cells spread to 20 μm in diameter or greater were analyzed.

G Factor

The G factor in equation 2 correlates the decrease in donor fluorescence with an increase in acceptor fluorescence due to energy transfer[25]. The equation for G is:

$$G = \frac{Q_A L_A S_A t_{DA}}{Q_D L_D S_D t_{DD}} \qquad (2)$$

where Q_A and Q_D are the quantum yield of the acceptor and donor; L_A and L_D are the throughput of the acceptor and donor emission light path, S_A and S_D are the quantum sensitivity of the camera for the acceptor and donor emission and t_{DA} and t_{DD} are the exposure times for the FRET and donor filter sets, respectively. G can be measured experimentally using fixed (i.e., static)cells [24];however, formaldehyde fixation significantly alters the photophysical properties of the fluorescent proteins used in these studies. Instead, G was calculated using equation 2 and known system parameters. The quantum efficiency for the acceptor fluorescent protein, Cherry[26], is 0.22 and the quantum

efficiency for the donor fluorescent protein, Venus[27], is 0.57. The acquisition times using the FRET and donor filters are 12 and 6 seconds, respectively. The quantum efficiency of the detector was obtained by integrating the detector's quantum efficiency curve over all wavelengths transmitted in the donor or acceptor's emission filter for S_D or S_A, respectively. Similarly, L_A and L_D were determined by integrating the transmission curves over all emission wavelengths for the dichroic mirror and emission filters in the acceptor filter set (L_A) or donor emission set (L_D). G was calculated to be 1.419 for this experimental configuration.

Statistical Analysis

Statistical analysis was accomplished via the program JMP 7 (SAS Institute Inc, Cary, USA) and statistical consulting from Iowa State University Department of Statistics. All data points represent 100 independent measurements from 3 replicate experiments. In order to statistically compare the raw FRET data, which is not normally distributed, the data was transformed to obtain a normal distribution [28]. This was done by taking the natural log of the raw data. The means were then calculated from the transformed data. The variances of some data sets from this study are not statistically similar as determined by Levene's test so the Welch t-test was used to compare the means. The FRET data is reported in the original data scale by taking the antilog of the mean of the log transformed data, as discussed in statistics text books [29]. A p-value lower than 5% indicates that there is a statistically significant difference between the FRET data from the RNAi treatment and cells that received no RNAi treatment. If the p-value is greater than 5%, there is not enough evidence to conclude that the two groups are different.

RESULTS AND DISCUSSION

FRET Assay

The method for measuring the effects of cytoplasmic proteins in altering the clustering of integrins in live cells is shown in Figure 1. RNAi selectively reduces the expression of a cytoplasmic protein and FRET is subsequently measured via reporter peptides. FRET reporters contain the donor fluorescent protein Venus and the acceptor fluorescent protein Cherry, and are known to cluster when integrins cluster within the cell membrane[8]. Clustering of the FRET reporters results in a decrease in the separation distance between donor and acceptor fluorescent proteins and an increase in measured energy transfer (Figure 1B). Similarly, a decrease in integrin clustering results in an increased separation distance between the FRET reporter peptides, and a decrease in energy transfer (Figure 1C).

FRET Reporter Expression Levels

The expression levels of integrins and FRET reporters in the cell membrane were measured using antibodies and flow cytometry. There is no known antibody that will bind both the FRET reporter and the integrin; therefore, four measurements were required to ensure a direct comparison of expression levels: (i) integrin antibody binding to a cell line expressing wild-type integrin; (ii) integrin antibody binding to a cell line expressing Venus fluorescent protein inserted into the integrin's beta subunit (αβ-Venus); (iii) fluorescent protein antibody binding to the same cell line in (ii); and (iv) fluorescent protein antibody binding to a cell line expressing wild-type integrins and FRET reporter Venus. This multi-step experiment is required since the amount of antibody that binds to its antigen is specific to each antibody, and comparing the binding of integrin antibody to the binding of

fluorescent protein antibody may not reflect true expression levels. The GFP antibody was used to assess Venus expression levels since the molar absorptivity and quantum yield of the Venus fluorescent protein can be differentially altered upon attaching it to the integrin or the FRET reporter, which would not reflect true expression levels.

Table 1 reports the expression ratios obtained from the four measurements described above. The values in rows 1 and 2 are multiplied and then divided by 2 to obtain the relationship listed in row 3. Division by a factor of 2 assumes equal expression of both Cherry and Venus FRET reporters, since the fluorescent protein antibody only binds to Venus (i.e., assumed to be one-half of the FRET reporters).After the expression ratio for the wild-type integrin and FRET reporter was measured, further considerations were made for the differential expression of mutant integrins used in this study (rows 4-5); as well as, for FRET control peptides (row 6). These cell lines will be discussed in further detail below. The expression ratio between FRET reporters and integrins was found to be 1:1.3 to 1:3.9. The ratio varied, not only from cell line to cell line, but also from cell to cell within the same cell line. The integrin:FRET reporter expression ratio cannot be controlled.

The presence of FRET reporters may appear to be problematic since the intracellular domain of the FRET reporter is the same as the beta subunit's intracellular domain, and may compete with a limited concentration of intracellular proteins. This would perturb the measurement of intracellular proteins that affect integrin clustering. However, this is not likely to be the case. A shift in the equilibrium binding of intracellular proteins to the integrins would alter the integrins' conformation and/or affinity for ligand [30]. Previously published results indicate that the integrins' ligand affinity is not altered by the presence of the FRET reporters[8].

It is possible that the intracellular domain of the FRET reporter does not have the required conformation for binding to intracellular proteins. The integrin extracellular domain, which the FRET reporters lack, is required to alter the conformation of the transmembrane and cytoplasmic domains [31].

Integrin Clustering in the Presence of Extracellular Ligand at Native Cytoplasmic Protein Concentrations

Fluorescence microscopy is used to obtain spatially-correlated energy transfer data. This allows certain regions of the cell to be analyzed, as described in the experimental section. In order to measure energy transfer in a microscopy format, the cells must be spread on a bare or ligand coated substrate. In this study, cells were spread on a ligand coated surface. The ligand used was a recombinant protein containing the native ligand's integrin binding domain [32]. Assuming all of the ligand (25 nanograms) that is exposed to the glass slide (30 mm^2) adheres to the glass [32,11], 40 ± 10% of the surface is coated with ligand. The mean FRET values for cells expressing wild-type or mutant integrins and FRET reporters were measured prior to RNAi treatment (Table 2). Protein mutants can be used to elucidate the molecular mechanism of protein function. Two well-studied mutants are included in this study: anα cytoplasmic mutation (αanaβ) and a β extracellular domain mutation (αβV409D). The αanaβ mutation is near a site where cytoplasmic proteins are known to bind [33], and the αβV409D mutation is near the integrin's ligand binding site [34]. Both integrin mutants exhibit increased affinity for ligand relative to wild-type integrin[18]. The energy transfer value calculated using equation 1, which is different than the equation used for previous studies involving the FRET report peptides, for cells expressing wild-type, αanaβ or αβV409D integrins and FRET reporters are statistically

similar, as indicated by a p-value that is above 0.05 (Table 2). This indicates similar amounts of integrin clustering in all cell lines prior to the RNAi treatments, within the assay's detection limit. Histograms of energy transfer measured for cells spread on a surface with no, low, or high ligand concentrations for all four cell lines used in these experiments are shown in Supplemental Information Figure S1.

RNAi Transfection

Drosophila S2 cells were used in this study because of the ease in selectively reducing the expression of a target protein via RNAi [19,35], the high degree of similarity between *Drosophila* and vertebrate integrins[36], and the fact that many of the integrin signaling pathways are conserved between invertebrate and vertebrate integrins[37]. Research has shown that information gained from integrin studies using *Drosophila* cells can translate to vertebrate systems[38].

The process of RNAi requires the cellular internalization of dsRNA corresponding in sequence to the target protein's mRNA. The dsRNA for each target protein is referred to as an RNAi probe. The required information to generate RNAi probes for the entire *Drosophila* genome is available [39]. The RNAi probes utilized in this work have been previously described [11]. The amount a target protein's expression is reduced depends on many variables, including the concentration of the target protein's mRNA, the efficiency of the RNAi probe in crossing the membrane, and the thermodynamics of binding to the target mRNA. The reduced expression of mRNA was measured using real time polymerase chain reaction and showed reduction in mRNA ranging from ~25-90%. (Figure 2) [40].

Antibodies can be used to measure the presence of the target protein in the cell, as well as quantify protein expression [41]. Commercial antibodies are only available for some

of the targeted proteins in this study. Immunohistochemistry measurements were performed before and after RNAi for akt1, dreadlocks, vinculin, and paxillin. The results showed a 26-42% decrease in protein expression (Supplemental Information Figure S2). The reduction in protein expression will differ for each targeted protein and each RNAi probe, but typical reductions in protein expression by RNAi for cultured *Drosophila* cells are between 62-100% [19,42].

Two additional measurements of RNAi responses include quantify an actin fluorescent fusion protein and phenotypic analysis before and after RNAi treatment. An actin green fluorescent protein construct was used to measure a 21% reduction in actin expression in cells [11] (Supplemental Information Figure S2).

RNAi against a cytoplasmic protein that produces a visible phenotype when its expression is reduced, Rho1, was also used to demonstrate the efficient cellular delivery of dsRNA using the experimental protocol used in this study. An insufficient concentration of Rho1 results in cells containing 2 or more nuclei [15]. Four days after Rho1 RNAi, phase contrast microscopy images were taken of untreated (Information Figure S3A) and RNAi treated (Supplemental Information Figure S3B) cells expressing integrins and FRET controls. The percentage of cells that were multinucleate was measured for cells receiving three concentrations of dsRNA (Figure 2C). The results indicate that 10 μg/mL dsRNA, the concentration used for subsequent studies, produces an RNAi effect in at least 38% of the cells. These results should be considered a lower limit since it was not possible to determine if 2 or more nuclei were present in a small population of cells. More cells are affected when higher dsRNA concentration are used; however, deleterious effects occur with higher concentrations of dsRNA [43].Other RNAi probes in this study, which are between 200 and

570 base pairs, should cross the cell membrane with a similar efficiency as the Rho1 RNAi probe.

Integrin Clustering in the Presence of Extracellular Ligand at Reduced Cytoplasmic Protein Concentrations

The average FRET values for S2 cells expressing wild-type integrins and FRET reporters after the indicated RNAi treatment are presented in Table 3. Histograms of the data at different ligand concentrations are provided in Supplemental Information Figure S4. Since the goal of this work is to measure cytoplasmic proteins that alter integrin clustering when their expression levels are reduced, all data are normalized to the data point representing native expression levels (Table 2). A statistical comparison of the data with and without RNAi treatment indicates only ILK inhibition caused a statistically significant change in energy transfer when compared to cells receiving no RNAi treatment. A 2.5-fold increase in energy transfer was measured for the ILK depleted cells, which indicates a 2.5-fold increase in FRET reporter clustering after ILK expression is reduced. The quantitative relationship between FRET reporter and integrin clustering is not known.

Control experiments were performed to ensure that the measured change in energy transfer after ILK RNAi reflects alterations in integrin clustering, and is not a by-product of a change in another cell membrane property. FRET control peptides contain the same donor and acceptor fluorophore, but the membrane spanning and intracellular peptide sequence has no similarity to any protein found in the *Drosophila* proteome. If the change in FRET reporter clustering is integrin dependent, then no change in clustering is expected for the FRET control after the same RNAi treatment. Before RNAi treatment, statistically similar

levels of FRET reporter and FRET control clustering are measured using equation 1 to calculate FRET (Table 2).

Cells expressing wild-type integrins and FRET control peptides showed no statistical difference in energy transfer after any RNAi treatments used in this study (Table 4). Histograms of the data at different ligand concentrations are provided in Supplemental Information S5. This indicates that the increase in energy transfer measured after RNAi treatment for ILK in the cell line expressing the FRET reporters is integrin specific. Under these experimental conditions, it can be concluded that ILK reduces integrin clustering, since reducing ILK expression results is increased integrin clustering. In comparison to previously published results, no statistically significant change in integrin clustering was measured after RNAi treatment for ILK in cells spread on a surface with 4 ± 1% ligand density [11]. This indicates that ILK only plays a role in altering integrin clustering if higher concentrations of extracellular ligand are present. These results highlight that the amount of integrin-ligand binding should be considered when making similar measurements of receptor clustering.

Mutant Integrin Clustering in the Presence of Extracellular Ligand at Reduced Cytoplasmic Protein Concentrations

The average FRET values for S2 cells expressing αβV409D integrins or αanaβ integrins and FRET reporters are shown in Table 4 after the indicated RNAi treatment. Histograms are shown in Figure S6 and S7. A few comparisons can be made between the values for the mutant and wild-type integrins. First, there are four RNAi treatments that result in less energy transfer in the cells expressing the mutant integrins. Vinculin, FAK, and ILK RNAi treatments for αβV409D and rhea RNAi treatment for αanaβ integrins show a 24 to 44% statistically significant decrease in energy transfer compared to the no RNAi data set.

Since there is no statistically significant change in cells expressing the control peptides after these RNAi treatments (Table 3), the FRET reporters are measuring integrin specific changes. Decreased energy transfer values indicate there is less clustering of the FRET reporters and integrins when the expression of these cytoplasmic proteins is reduced. These proteins play a role in increasing integrin clustering in cells expressing these mutants when the cells are spread on a surface with a 40 ± 10% ligand density.

Continuing the comparison between the mutant and wild-type integrins, the αanaβ mutation shows an increase in energy transfer when paxillin and steamer duck expression is reduced, whereas none of the other cell lines shows a change in energy transfer with these RNAi treatments. This indicates there is a difference in the molecular mechanism of action of this protein mutant relative to the other integrins. It is likely that the α cytoplasmic mutation alters the interactions of this integrin with a subset of intracellular proteins [44]. It is not possible to say, at this point, that the alteration is the result of direct interactions with paxillin or steamer duck, or indirectly through other proteins.

A final distinction between the wild-type and mutant integrins is the difference between the increase in energy transfer for cells containing wild-type integrins after RNAi treatment for ILK and the decrease in energy transfer for the αβV409D mutation after the same RNAi treatment. The changes observed for these cell lines may relate to the integrin-ligand affinity, which is from lowest to highest affinity: wild-type, αanaβ, and αβV409D. This trend is reversed for integrin clustering levels after RNAi treatment for ILK. Studies with additional integrin mutants are needed to test this hypothesis.

CONCLUSIONS

When integrins bind to ligand, the result is an assemblage of cytoskeletal proteins that directly or indirectly bind to the integrin cytoplasmic tails [45].The properties of the cytoskeleton, including the identity of the assembled proteins, depend on many factors, including cell type, integrin type, and environmental cues, to name a few. These factors must be considered when measuring the cytoplasmic proteins that affect integrin clustering. It was not previously known that the role cytoplasmic proteins play in altering integrin clustering depends on the extracellular ligand density, and on the integrin's ligand affinity, as measured using integrin mutants. Similar to other RNAi screens that have been performed [42,46], reduced expression levels of the target proteins have not been quantitatively measured for all targeted proteins. It is possible that some of the target cytoplasmic proteins affect integrin clustering, but only when their expression level is reduced below the amount produced in these studies. Additionally, some cytoplasmic proteins may alter integrin clustering only when their expression level is increased. The combination of FRET and RNAi will contribute to a greater understanding of the proteins involved in receptor organization.

ACKNOWLEDGMENTS

This work was supported by the Roy J. Carver Charitable Trust (Muscatine IA), National Science Foundation (CHE-0845236) and Iowa State University Office of the Vice President for Research. The authors thank Roger Tsien (Howard Hughes Medical Institute, La Jolla, CA) for the original mCherry plasmid, Atsushi Miyawaki (Riken, Wako-city, Saitama, Japan) for the original Venus plasmid, Christopher Gonwa-Reeves, Neha Arora, Khushboo Hemnani and Keyna Eilor (Iowa State University) for their assistance with data processing.

REFERENCES

1. Giancotti FG, Ruoslahti E (1999) Integrin signaling. Science (New York, NY 285 (5430):1028-1032
2. Ginsberg MH, Partridge A, Shattil SJ (2005) Integrin regulation. Current opinion in cell biology 17 (5):509-516
3. Tanentzapf G, Brown NH (2006) An interaction between integrin and the talin FERM domain mediates integrin activation but not linkage to the cytoskeleton. Nat Cell Biol 8 (6):601-606
4. Hannigan GE, Leung-Hagesteijn C, Fitz-Gibbon L, Coppolino MG, Radeva G, Filmus J, Bell JC, Dedhar S (1996) Regulation of cell adhesion and anchorage-dependent growth by a new beta 1-integrin-linked protein kinase. Nature 379 (6560):91-96
5. Liu S, Thomas SM, Woodside DG, Rose DM, Kiosses WB, Pfaff M, Ginsberg MH (1999) Binding of paxillin to alpha4 integrins modifies integrin-dependent biological responses. Nature 402 (6762):676-681
6. Plow EF, Haas TA, Zhang L, Loftus J, Smith JW (2000) Ligand binding to integrins. The Journal of biological chemistry 275 (
29):21785-21788
7. Selvin PR (2000) The renaissance of fluorescence resonance energy transfer. Nat StructBiol 7 (9):730-734
8. Smith EA, Bunch TA, Brower DL (2007) General in vivo assay for the study of integrin cell membrane receptor microclustering. Anal Chem 79 (8):3142-3147
9. Kim M, Carman CV, Yang W, Salas A, Springer TA (2004) The primacy of affinity over clustering in regulation of adhesiveness of the integrin {alpha}L{beta}2. J Cell Biol 167 (6):1241-1253
10. Buensuceso C, de Virgilio M, Shattil SJ (2003) Detection of integrin alpha IIbbeta 3 clustering in living cells. The Journal of biological chemistry 278 (17):15217-15224
11. Dibya D, Sander S, Smith E (2009) Identifying cytoplasmic proteins that affect receptor clustering using fluorescence resonance energy transfer and RNA interference. Analytical and Bioanalytical Chemistry
12. Helsten TL, Bunch TA, Kato H, Yamanouchi J, Choi SH, Jannuzi AL, Feral CC, Ginsberg MH, Brower DL, Shattil SJ (2008) Differences in regulation of Drosophila and vertebrate integrin affinity by talin. MolBiol Cell 19 (8):3589-3598
13. Subauste MC, Pertz O, Adamson ED, Turner CE, Junger S, Hahn KM (2004) Vinculin modulation of paxillin-FAK interactions regulates ERK to control survival and motility. J Cell Biol 165 (3):371-381
14. Legate KR, Montañez E, Kudlacek O, Fässler R (2006) ILK, PINCH and parvin: the tIPP of integrin signalling. Nat Rev Mol Cell Biol 7 (1):20-31
15. Prokopenko SN, Brumby A, O'Keefe L, Prior L, He Y, Saint R, Bellen HJ (1999) A putative exchange factor for Rho1 GTPase is required for initiation of cytokinesis in Drosophila. Genes Dev 13 (17):2301-2314
16. Li R, Babu CR, Lear JD, Wand AJ, Bennett JS, DeGrado WF (2001) Oligomerization of the integrin alphaIIbbeta3: roles of the transmembrane and cytoplasmic domains. Proceedings of the National Academy of Sciences of the United States of America 98 (22):12462-12467

17. Bunch TA, Grinblat Y, Goldstein LS (1988) Characterization and use of the Drosophila metallothionein promoter in cultured Drosophila melanogaster cells. Nucleic Acids Res 16 (3):1043-1061
18. Bunch TA, Helsten TL, Kendall TL, Shirahatti N, Mahadevan D, Shattil SJ, Brower DL (2006) Amino acid changes in Drosophila alphaPS2betaPS integrins that affect ligand affinity. The Journal of biological chemistry 281 (8):5050-5057
19. Clemens JC, Worby CA, Simonson-Leff N, Muda M, Maehama T, Hemmings BA, Dixon JE (2000) Use of double-stranded RNA interference in Drosophila cell lines to dissect signal transduction pathways. Proceedings of the National Academy of Sciences of the United States of America 97 (12):6499-6503
20. March JC, Bentley WE (2006) Engineering eukaryotic signal transduction with RNAi: enhancing Drosophila S2 cell growth and recombinant protein synthesis via silencing of TSC1. BiotechnolBioeng 95 (4):645-652
21. FLIGHT. http://flightlicrorg/
22. PeptideAtlas. wwwmopunizhch/peptideatlas
23. Graner MW, Bunch TA, Baumgartner S, Kerschen A, Brower DL (1998) Splice variants of the Drosophila PS2 integrins differentially interact with RGD-containing fragments of the extracellular proteins tiggrin, ten-m, and D-laminin 2. The Journal of biological chemistry 273 (29):18235-18241
24. Zal T, Gascoigne NR (2004) Photobleaching-corrected FRET efficiency imaging of live cells. Biophys J 86 (6):3923-3939
25. Gordon GW, Berry G, Liang XH, Levine B, Herman B (1998) Quantitative fluorescence resonance energy transfer measurements using fluorescence microscopy. Biophys J 74 (5):2702-2713
26. Shaner NC, Campbell RE, Steinbach PA, Giepmans BN, Palmer AE, Tsien RY (2004) Improved monomeric red, orange and yellow fluorescent proteins derived from Discosoma sp. red fluorescent protein. Nat Biotechnol 22 (12):1567-1572
27. Nagai T, Ibata K, Park ES, Kubota M, Mikoshiba K, Miyawaki A (2002) A variant of yellow fluorescent protein with fast and efficient maturation for cell-biological applications. Nat Biotechnol 20 (1):87-90
28. Bland JM, Altman DG (1996) The use of transformation when comparing two means. BMJ 312 (7039):1153
29. Zar J (1999) Biostatistical Analysis. Prentice Hall, Upper Saddle River, NJ
30. Luo BH, Springer TA (2006) Integrin structures and conformational signaling. Current opinion in cell biology 18 (5):579-586
31. Calvete JJ (2004) Structures of integrin domains and concerted conformational changes in the bidirectional signaling mechanism of alphaIIbbeta3. Experimental biology and medicine (Maywood, NJ 229 (8):732-744
32. Fogerty FJ, Fessler LI, Bunch TA, Yaron Y, Parker CG, Nelson RE, Brower DL, Gullberg D, Fessler JH (1994) Tiggrin, a novel Drosophila extracellular matrix protein that functions as a ligand for Drosophila alpha PS2 beta PS integrins. Development 120 (7):1747-1758
33. Jannuzi AL, Bunch TA, Brabant MC, Miller SW, Mukai L, Zavortink M, Brower DL (2002) Disruption of C-terminal cytoplasmic domain of betaPS integrin subunit has dominant negative properties in developing Drosophila. MolBiol Cell 13 (4):1352-1365

34. Jannuzi AL, Bunch TA, West RF, Brower DL (2004) Identification of integrin beta subunit mutations that alter heterodimer function in situ. MolBiol Cell 15 (8):3829-3840
35. Armknecht S, Boutros M, Kiger A, Nybakken K, Mathey-Prevot B, Perrimon N (2005) High-throughput RNA interference screens in Drosophila tissue culture cells. Methods Enzymol 392:55-73
36. Fessler JH, Fessler LI (1989) Drosophila extracellular matrix. Annu Rev Cell Biol 5:309-339
37. Bökel C, Brown NH (2002) Integrins in development: moving on, responding to, and sticking to the extracellular matrix. Dev Cell 3 (3):311-321
38. Brower DL (2003) Platelets with wings: the maturation of Drosophila integrin biology. Current opinion in cell biology 15 (5):607-613
39. FlyBase (http://flybase.bio.indiana.edu).
40. Sander SA, N. Smith, E.A. (2012) Elucidating the role of select cytoplasmic proteins in altering diffusion of integrin receptors. Anal BioanalChem
41. Waters JC (2009) Accuracy and precision in quantitative fluorescence microscopy. The Journal of cell biology 185 (7):1135-1148
42. Kiger AA, Baum B, Jones S, Jones MR, Coulson A, Echeverri C, Perrimon N (2003) A functional genomic analysis of cell morphology using RNA interference. J Biol 2 (4):27
43. Echeverri CJ, Perrimon N (2006) High-throughput RNAi screening in cultured cells: a user's guide. Nat Rev Genet 7 (5):373-384
44. O'Toole TE, Katagiri Y, Faull RJ, Peter K, Tamura R, Quaranta V, Loftus JC, Shattil SJ, Ginsberg MH (1994) Integrin cytoplasmic domains mediate inside-out signal transduction. J Cell Biol 124 (6):1047-1059
45. Delon I, Brown NH (2007) Integrins and the actin cytoskeleton. Current opinion in cell biology 19 (1):43-50
46. Boutros M, Kiger AA, Armknecht S, Kerr K, Hild M, Koch B, Haas SA, Paro R, Perrimon N (2004) Genome-wide RNAi analysis of growth and viability in Drosophila cells. Science (New York, NY 303 (5659):832-835

Table 1. Measured expression ratios for integrins and FRET reporters.

	Measurement (Roman numerals refer to measurements described in the text)	Expression Ratio (All denominators are 1)
1	$\frac{(i)}{(ii)}\ \frac{\alpha\beta}{\alpha\beta - \text{Venus}}$	1.4 ± 0.35
2	$\frac{(iii)}{(iv)}\ \frac{\alpha\beta - \text{Venus}}{\alpha\beta; \text{Venus FRET Reporter}}$	3.3 ± 1.3
3	$\frac{\alpha\beta}{\alpha\beta; \text{Venus and Cherry FRET Reporters}}$	2.3 ± 0.55
4	$\frac{\alpha ana\beta}{\alpha\beta; \text{Venus and Cherry FRET Reporters}}$	1.4 ± 1.3
5	$\frac{\alpha\beta V409D}{\alpha\beta; \text{Venus and Cherry FRET Reporters}}$	3.9 ± 3.6
6	$\frac{\alpha\beta}{\alpha\beta; \text{Venus and Cherry FRET Controls}}$	1.3 ± 0.83

Table 2. Normalized FRET values for cell lines expressing FRET reporters or controls and the indicated integrins. Data is normalized and statistically compared to the value obtained for cells expressing wild-type integrins with FRET reporters.

αβ; Reporters	αanaβ; Reporters	αβV409D; Reporters	αβ; Controls
1.0	1.2 (p=0.61)	1.3 (p=0.27)	1.0 (p=0. 88)

Table 3. Normalized FRET values for S2 cells expressing wild-type integrins and FRET reporters or wild-type integrins and FRET controls after the indicated RNAi treatment.

αβ; Reporters		
RNA [1]	**Normalized[2] Mean FRET**	**P-value**
SD	1.2	0.46
Dock	1.0	0.96
ILK	2.6	0.0014
FAK	1.3	0.34
Rhea	0.80	0.55
Pax	0.84	0.52
Vin	0.63	0.12
αβ; Controls		
SD	1.4	0.11
Dock	1.5	0.06
ILK	1.1	0.74
FAK	1.0	0.46
Rhea	0.59	0.40
Pax	1.1	0.77
Vin	1.1	0.71

1. The abbreviations used in this table are listed in Figure 1.
2. For ease in comparison, all values are normalized to cells expressing wild-type integrins and FRET reporters (αβ; Reporters) or FRET controls (αβ; Controls**)** with no RNAi treatment.

Table 4. Normalized FRET values for S2 cells expressing αβV409D mutant integrins and FRET reporters or αanaβ mutant integrins and FRET reporters after the indicated RNAi treatment.

αanaβ; Reporters		
RNA[1]	**Normalized Mean FRET[2]**	**P-value**
SD	2.2	0.0001
Dock	0.68	0.27
ILK	0.79	0.43
FAK	0.84	0.0011
Rhea	0.43	0.30
Pax	1.9	0.0051
Vin	0.83	0.51
αβV409D; Reporters		
SD	0.82	0.43
Dock	0.83	0.49
ILK	0.24	0.019
FAK	0.43	0.0045
Rhea	0.63	0.54
Pax	0.67	0.11
Vin	0.40	0.0006

1. The abbreviations used in this table are listed in Figure 1.

2. For ease in comparison, all values are normalized to cells expressing αanaβ (αanaβ; Reporters) or αβV409D (αβV409D; Reporters) mutant integrins and FRET reporters with no RNAi treatment.

Figure 1. Schematic depicting FRET assay and proteins known to be involved in integrin signaling complexes. Cytoplasmic proteins targeted in this study to measure how they affect integrin clustering: Rhea, Vinculin (Vin), Integrin Linked Kinase (ILK),Paxillin (Pax), Dreadlock (Dock), Steamer Duck (SD) and Focal Adhesion Kinase (FAK). V: donor fluorescent protein (Venus); C: acceptor fluorescent protein (Cherry). (A) A baseline energy transfer value is measured in cells prior to receiving an RNAi treatment. (B) After removal of a target cytoplasmic protein (e.g. Paxillin), increased integrin clustering results in clustering of the FRET reporters, and an increase in energy transfer is measured. (C) After removal of a target cytoplasmic protein (e.g. Rhea), decreased integrin clustering results in less clustering of the FRET reporters, and a decrease in energy transfer is measured.This is a static picture of a dynamic system.

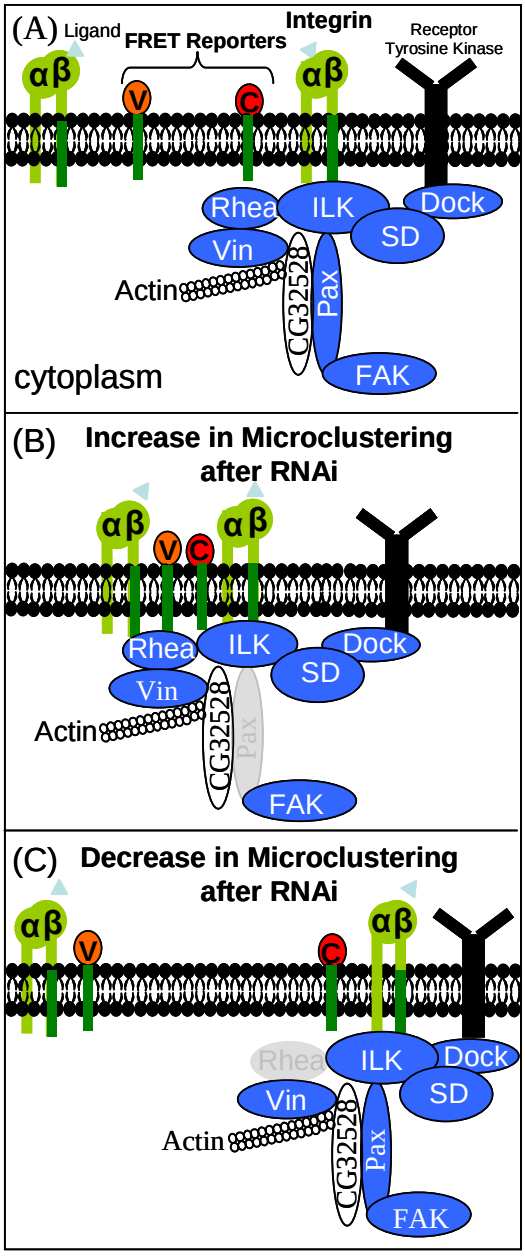

Figure 2. Relative mRNA expression as determined by real time polymerase chain reaction after RNAi treatment for either the indicated gene (white bar) or the Myospheroid gene (gray bar).

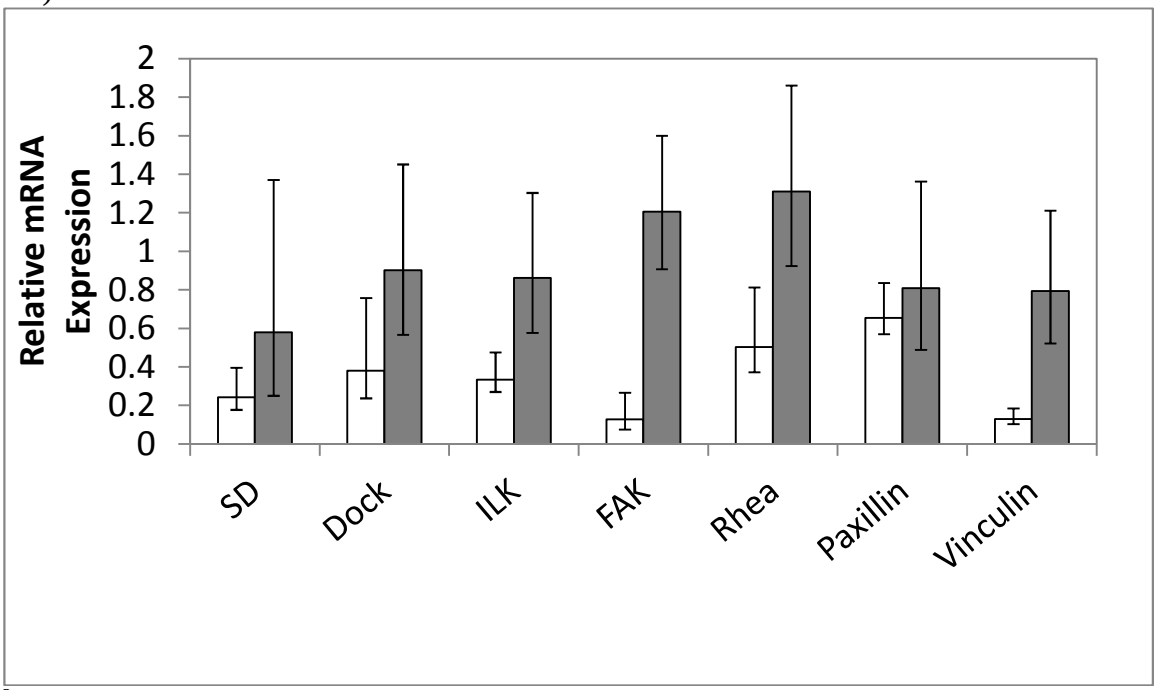

[a] Relative indicates the ratio of mRNA in cells after RNAi treatment to mRNA in cells before RNAi treatment for the indicated gene, endogenous control gene gamma tubulin at 23C. All measurements were performed in duplicate.

Supplemental Information for Chapter 3

Immunocytochemistry

Expression levels of dreadlocks (Jack Dixon, University of Michigan) (), paxillin (Santa Cruz Biotechnology), vinculin (Santa Cruz Biotechnology) and akt1 (Cell Signaling Technology) were measured in αβ cells by immunocytochemistry with antibodies obtained from the referenced suppliers. Cells were spread on a ligand/BSA coated slide for 1 hour, and were then fixed with 4% paraformaldehyde in phosphate buffer for 10 minutes. The cells were thoroughly rinsed with phosphate buffer, and then incubated with primary antibody (Vinculin: 4 μ g mL^{-1}; Paxillin: 4 μ g mL^{-1}; dreadlocks:1:100 dilution; akt1: 1:175 dilution from supplied stock) diluted in M3 medium plus 2 mg mL^{-1} BSA for 2 hours at room temperature in a humid chamber. The cells were rinsed with M3 medium plus 2 mg mL^{-1} BSA and then incubated with secondary antibody purchased from Invitrogen (dreadlocks: 0.002 mg mL^{-1} goat anti-rabbit Alexa Fluor 647;akt1: 0.0027 mg mL^{-1} goat anti-rabbit labeled Alexa Fluor 647; vinculin and paxillin:0.002 mg mL^{-1} chicken anti-goat labeled Alexa Fluor 488) diluted in M3 medium plus 2mg mL^{-1}BSA for 2 hours at room temperature in a humid chamber. To minimize background, the cells were washed thoroughly with phosphate buffer and imaged using a 60x, 0.95 numerical aperture objective with mercury lamp excitation. The following excitation and emission filters for Alexa Fluor 647 (645/20 nm and 660/20 nm) and Alexa Flour 488 (470/50 nm and 545/75 nm) were used. The same exposure time (0.5second) was used to collect all images. To minimize measurement error the excitation intensity was set to ensure less than 5% photobleaching of the fluorophores occurred within 30 minutes (Waters2009).

Figure S1. Histograms showing the distribution of the natural log of the FRET intensities for A) αβ βCV, B) CD2CV, C) αanaβ βCV, D) αβV409D βCV cell lines at different tiggrin concentrations where white is 0 µg/mL, light gray is 0.05 µg/mL, and dark gray is 0.5 µg/mL tiggrin. There are between 85-135 cells for each histogram.

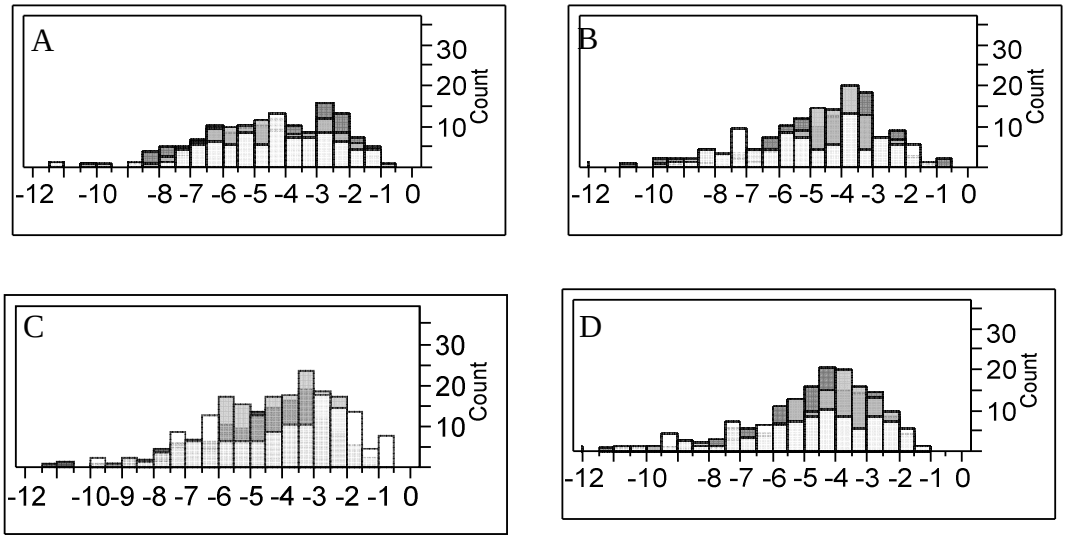

Figure S2. Quantitative immunocytochemistry measurements of protein expression. (A-J) Histograms showing the immunocytochemistry results for the total cellular expression before RNAi treatment (A, C, E, G) and after RNAi treatment (B, D, F, H) for akt1, dreadlocks, vinculin, and paxillin, respectively. The reported percentage value represents the change in the mean fluorescence value after RNAi treatment. An average of 150-300 cells was analyzed in three replicate measurements. Histograms showing the protein expression measurements for the total cellular expression before RNAi treatment (I) and after RNAi treatment (J) for actin 42A.The cells are expressing an actin 42A-GFP fusion protein. The reported percentage value represents the change in the mean fluorescence value after RNAi treatment. (I and J) Reproduced from reference Dibya, D., Sander, S., Smith, E. A. (2009) Identifying Cytoplasmic Proteins that Affect Receptor Clustering using Fluorescence Resonance Energy Transfer and RNA Interference, *Analytical and Bioanalytical Chemistry 395*, 2303-2311.

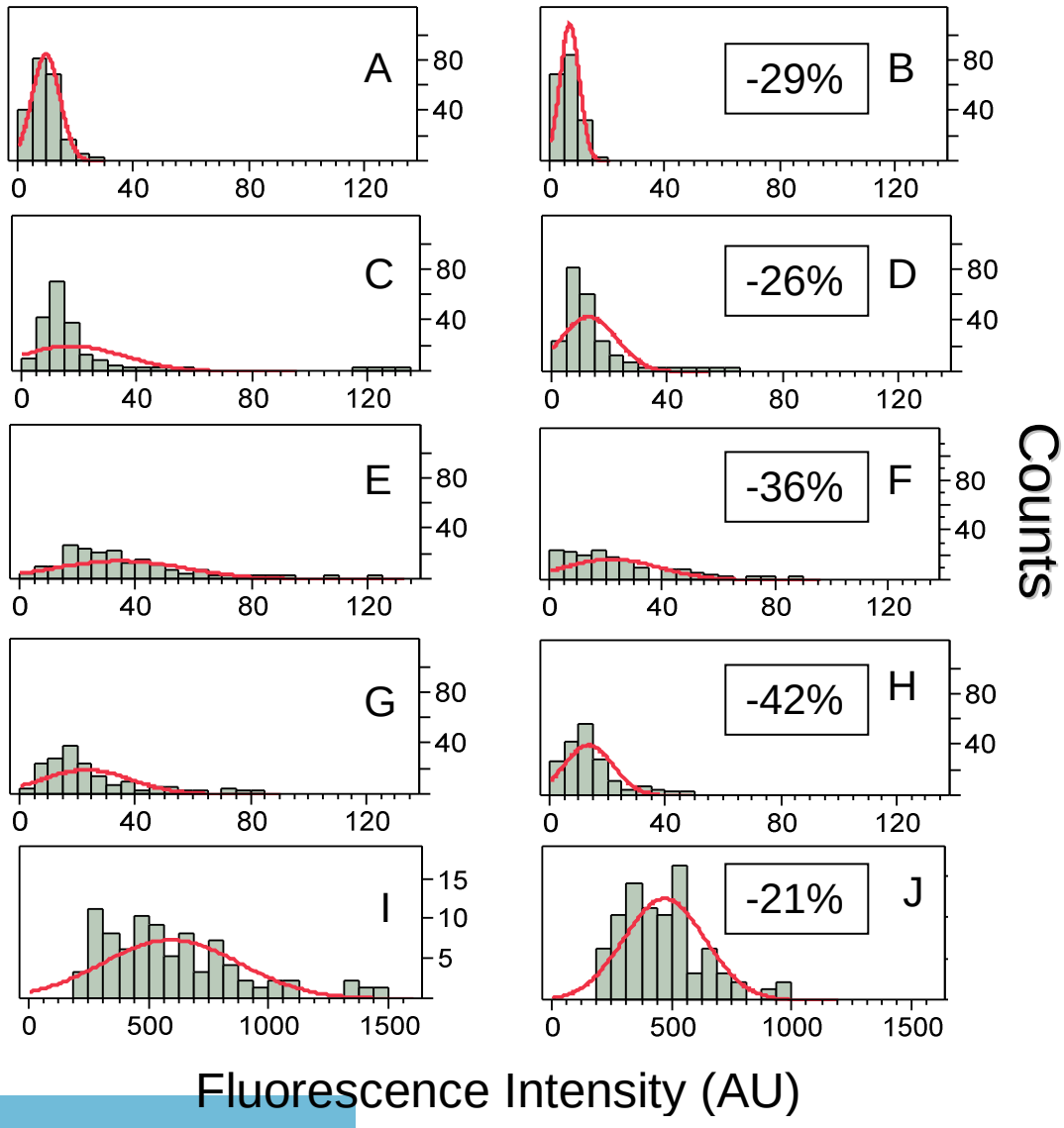

Figure S3. S2 cells containing wild-type integrins and FRET reporters (A) before and (B) 4 days after RNAi treatment using Rho1 dsRNA. Cells that have successfully integrated the dsRNA have two nuclei as depicted by the arrows. (C) The percentage of S2 cells expressing wild-type integrins and FRET reporters that are multinucleate after RNAi treatment for Rho1.

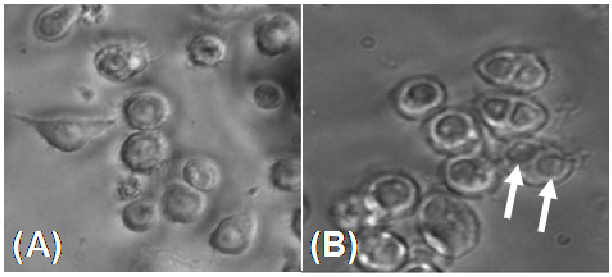

(C)

Rho1 RNAi Treatment (μg)	Multinucleate Cells (%)
0	0.03
10	38
20	43
30	55

Figure S4. Histograms of αβ βCV cells with the indicated RNAi treatment (A-H) control, vinculin, paxillin, rhea, FAK, ILK, dock steamer duck The histograms show the distribution of the natural log of the FRET intensities at low and high tiggrin concentrations (light gray is 0.05 µg/mL, and dark gray is 0.5 µg/mL tiggrin). There are between 85-135 cells for each histogram.

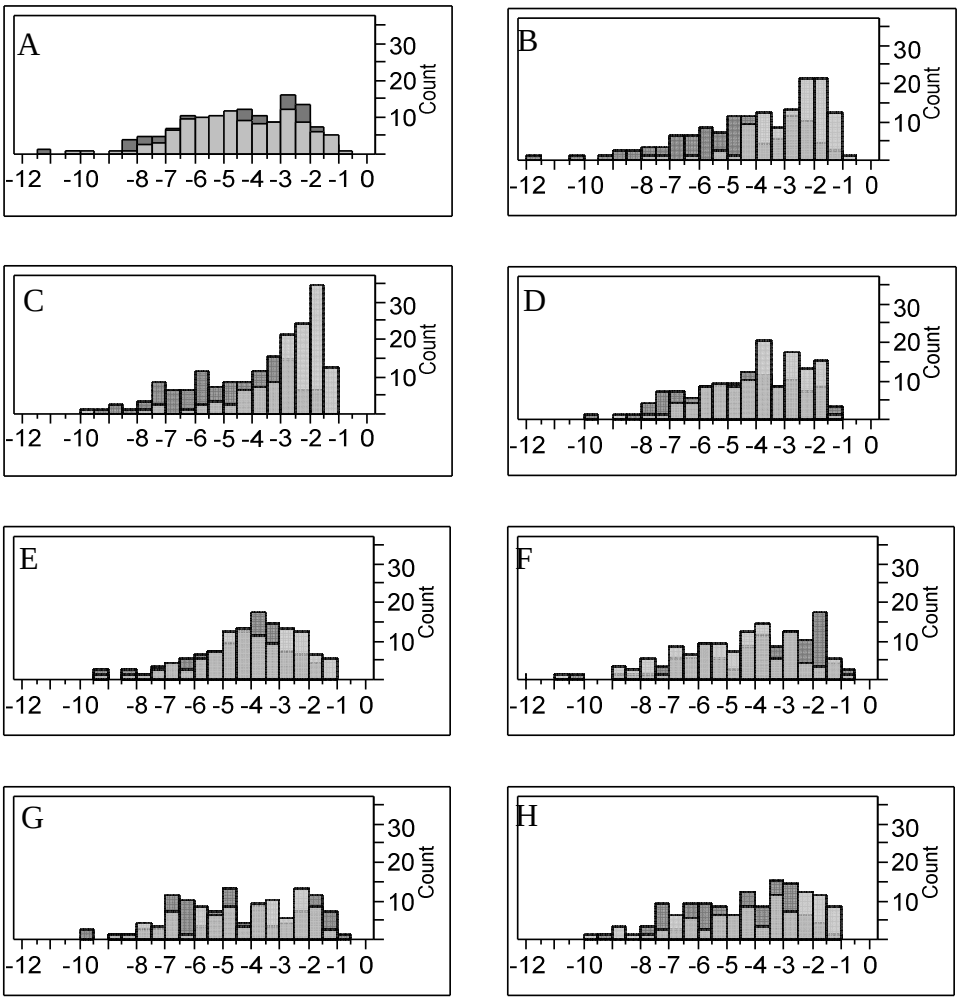

Figure S5. Histograms of CD2CV cells at low and high tiggrin concentrations (light gray is 0.05 µg/mL, and dark gray is 0.5 µg/mL tiggrin) with the corresponding RNAi treatments (A-H) control, vinculin, paxillin, rhea, FAK, ILK, dock, steamer duck. There are between 85-135 cells for each histogram.

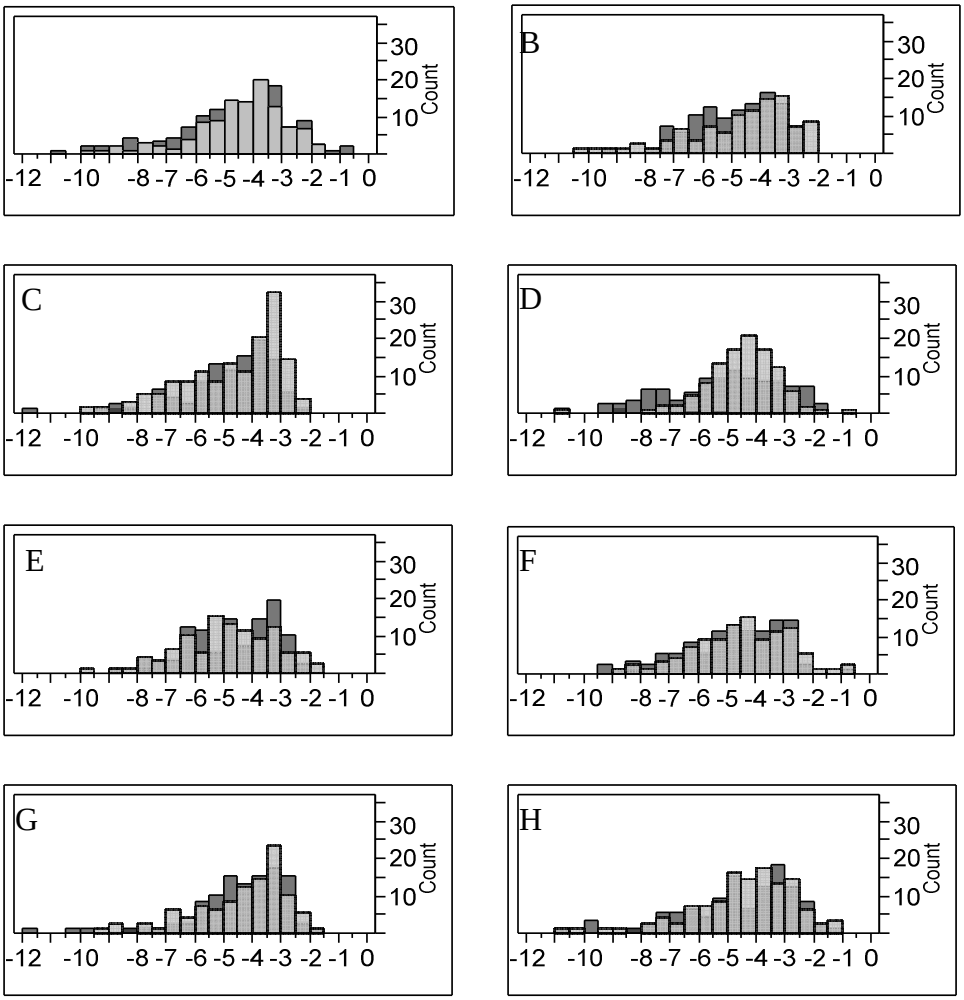

Figure S6. Histograms of αanaβ βCV cells, at low and high tiggrin concentrations (light gray is 0.05 µg/mL, and dark gray is 0.5 µg/mL tiggrin) with the corresponding RNAi treatments (A-H)control, vinculin, paxillin, rhea, FAK, ILK, dock, steamer duck. There are between 85-135 cells for each histogram.

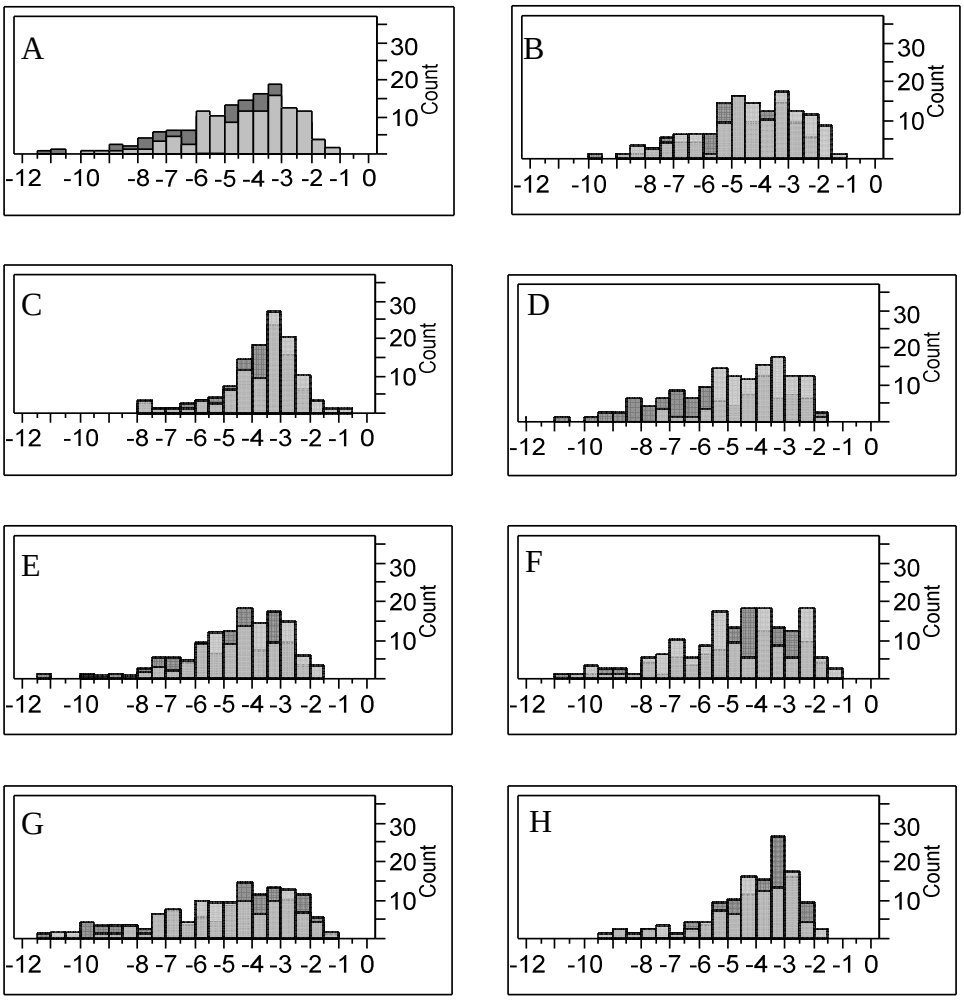

Figure S7. Histograms of αβV409D βCV cells, at low and high tiggrin concentrations (light gray is 0.05 µg/mL, and dark gray is 0.5 µg/mL tiggrin) with the corresponding RNAi treatments (A-H)control, vinculin, paxillin, rhea, FAK, ILK, dock, steamer duck. There are between 85-135 cells for each histogram.

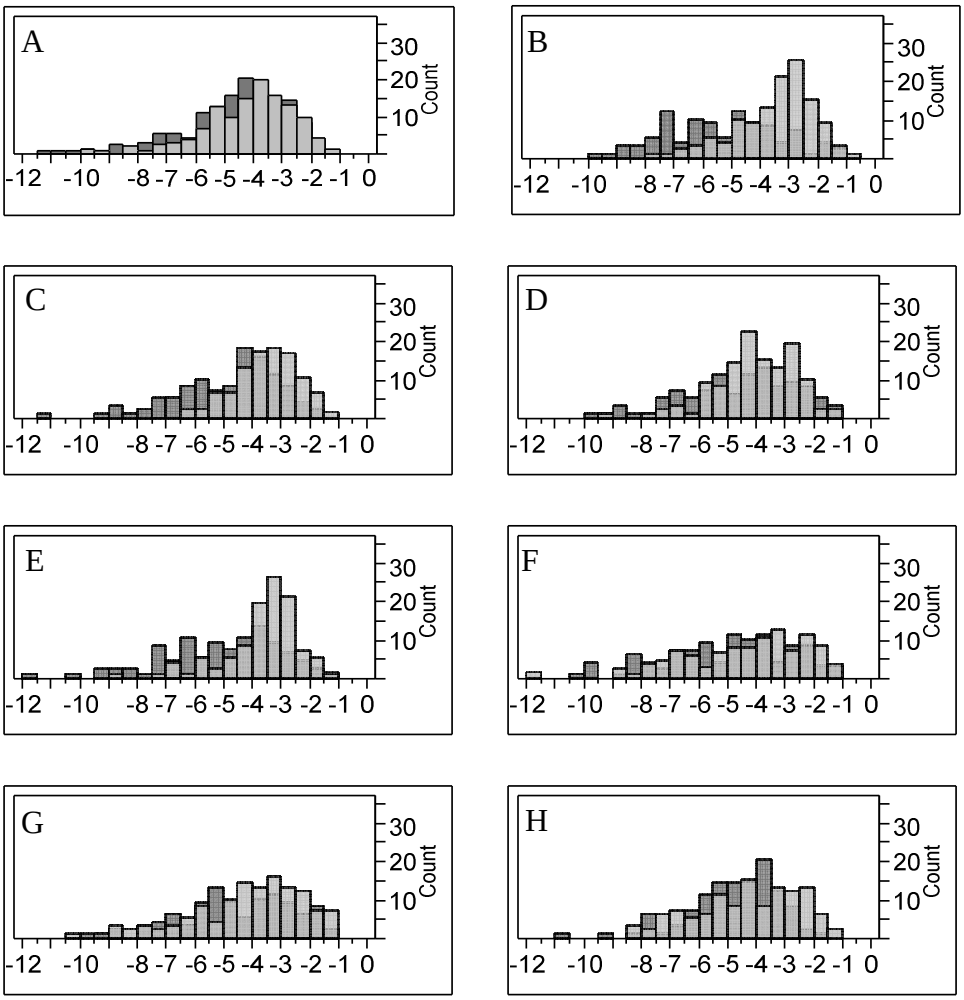

CHAPTER 4: THE BIOPHYSICAL ROLE OF CHOLESTEROL ON INTEGRIN DIFFUSION IN LIVE CELLS

Suzanne Sander and Emily A. Smith

ABSTRACT

Cholesterol is of fundamental importance to the fluidity of the membrane and can influence different cellular connections including signal generation and receptor diffusion. Cholesterol levels were reduced in S2 cells using methyl-β-cyclodextrin (mβCD), and restored using mβCD:cholesterol or mβCD:epicholesterol complexes. Cholesterol concentration from cell extracts was quantified using Amplex Red Cholesterol Assay. Diffusion values were calculated by fitting fluorescence recovery after photobleaching (FRAP) curves to a model for time-dependent diffusion with an immobile fraction. At native cholesterol concentrations, integrin mobility is 77% ± 2% with a time-dependent diffusion of 8.4 ± 0.7 x 10^{-9} cm^2/sec at 1 sec and 5.0±0.5 x 10^{-9} cm^2/sec at 50 sec. At decreased cholesterol concentrations the mobile fraction decreases to 58% ± 0.02 with a faster time-dependent diffusion coefficient of 18 ± 1 x 10^{-9} cm^2/sec at 1 sec and 25 ± 5 x 10^{-9} cm^2/sec at 50 sec. Restoration of cholesterol to the cell membrane confirms that the change in integrin diffusion upon cholesterol extraction was cholesterol specific. In fact, integrin diffusion properties are restored to values measured at native cholesterol concentrations regardless of whether the restored sterol is cholesterol or its stereoisomer epicholesterol. After restoration of epicholesterol to the cell membrane, the mobile fraction is restored to 74% ± 3% and the time-dependent diffusion values slow to near the original values of 9 ± 1 x 10^{-9} cm^2/sec at 1

sec and 3.1 ± 0.4 x 10^{-9} cm^2/sec at 50 sec. Alterations to lipid diffusion are minimal and not correlated to cholesterol concentration.

INTRODUCTION

Cholesterol is a sterol that plays a fundamental role in regulating cell membrane fluidity[1] and helps stabilize and strengthen the membrane. Due to its hydroxyl group and hydrophobic body, cholesterol orients itself in such a way to maximize hydrophobic and hydrophilic interactions. The distribution of cholesterol in the membrane is proposed to be heterogeneous. Research has indicated that cholesterol along with sphingomyelin may be necessary for the formation of lipid nanodomains [2-3], which have higher concentrations of certain membrane proteins and lipids and are more ordered. These domains are more rigid than the rest of the membrane and have been implicated in co-localizing proteins and lipids necessary for transmembrane signaling [4-5]. Specific details concerning size, composition, formation and function of lipid nanodomains remain uncertain. Additionally, the size and composition of lipid nanodomains can change in response to surrounding stimuli [6]. Analysis of influenza virus haemagglutinin with cholesterol suggests that the transmembrane domain is required for participation in lipid nanodomains [7].

Research has shown that lipid bilayers exist in several phases with increasing fluidity: gel, liquid-ordered, and liquid-disordered states [8]. As an integral component of cell membranes, this study helps define cholesterol's function in regulating membrane receptor mobility and diffusion in the membrane. Due to the importance of cholesterol in the plasma membrane of cells, methods have been developed to manipulate cholesterol concentrations. The most common technique is through the use of cyclodextrins. Their hydrophobic cavity

extracts cholesterol from cells. The exact mechanism has not been established and cholesterol may be removed from both nanodomains as well as from other areas of the membrane (i.e. the bulk). Cyclodextrins alter the amount of cholesterol in both the plasma and intracellular membranes. While there is the potential for other hydrophobic molecules to be extracted from the membranes, mβCD preferentially extracts cholesterol [9-10]. Epicholesterol is an optical isomer of cholesterol that is rarely found in nature (Figure 1A). By replacing cholesterol with epicholesterol the specificity of cholesterol's function in altering diffusion in the cell can be isolated and described as either a biophysical or a biochemical process[11].

One group of transmembrane proteins that is known to be involved in the transfer of information into and out of cells is integrins. Integrins consist of an α and β subunit and span the membrane. Integrins have a small intracellular domain that interacts with cytoplasmic proteins and a large extracellular domain that interacts with ligand. Since neither of the subunits have enzymatic activity, these interactions are needed for signal transduction. Integrins have been implicated in many basic cell functions including cell mobility, survival, and growth [12].

This study utilizes methyl-β-cyclodextrin to alter the sterol concentration in *Drosophila* S2 cells transfected to express αPS2CβPS integrin [13]. Fluorescence recovery after photobleaching (FRAP) measures the movement of fluorescent molecules into a region of the membrane that has been previously photobleached [14]. Comparison of the resulting diffusion parameters obtained from fitting the FRAP curves: mobile fraction, time exponent, and diffusion coefficients reveals information regarding the role cholesterol on integrins.

MATERIALS AND METHODS

Cell culture. Experiments utilized permanently transfected S2 cells cultured in Shields and Sang M3 medium (M3, Sigma) with 10% fetal calf serum (FCS) and antibiotics as previously published [15]. S2 cells expressed either wild-type αPS2CβPS integrins (αβ) or αPS2CβPS integrins with a Venus fluorescent protein (αβ-Venus) in the serine-rich loop [16-17]. The αβ cell line was used to quantify cellular and membrane cholesterol or measure lipid diffusion, while the αβ-Venus cell line was used to measure integrin diffusion.

Cholesterol depletion and restoration. To induce integrin expression, cells were heat shocked for 30 min at 36 °C and allowed to recover for 2 h at 22 °C. Cells were centrifuged at 600xg and resuspended at a concentration of 3 x 10^6 cells/mL in either M3 medium (control) or varying concentrations of mβCD solution (0.0625mM, 0.5mM, 2mM) and incubated for 30 min at 22 °C. To remove the mβCD solution, cells were centrifuged at 600xg and resuspended in an equal volume of M3 and incubated for an additional 30 min.

For cholesterol restoration, preparation of cholesterol or epicholesterol-loaded cyclodextrin (mβCD-chol and mβCD-epichol) was prepared as previously published [13]. Briefly, 800 μg of cholesterol/epicholesterol were dried under a stream of nitrogen. The samples were then resuspended in either 1 or 2.5 mM mβCD, vortexed, sonicated, and incubated with shaking overnight at 37 °C. Instead of the final incubation in M3 media, the cells were resuspended in M3 medium containing mβCD-chol or mβCD-epichol complex for 30 min at 22°C, after which time the cells were centrifuged and resuspended in M3 medium.

Extraction of total cellular lipids. After heat shock and incubation, the cellular lipids were extracted using the Bligh-Dyer method [18]. Briefly 3.0 mL methanol/chloroform (2:1 v/v) was added to 10^6 cells. The sample was vortexed for 15 min

and 1.0 mL of 1.0 M NaCl was added and vortexed for 1 min. The solution was allowed to sit for 12 h. The chloroform phase was collected and filtered with Whatman filter paper No. 1 and then evaporated under nitrogen. The cellular lipids were resuspended in phosphate buffer from the Amplex Red Cholesterol Assay kit (0.1M potassium phosphate, pH 7.4, 50mMNaCl, 5 mM cholic acid, and 0.1% Triton X-100) (Life Technologies A12216).

Extraction of membrane lipids. After heat shock and incubation, lipid extraction was performed as previously described [19-20], with the following changes: Plated cells were allowed to spread for 1 h at 22 °C. The membrane lipid was extracted with 5 mL methanol/chloroform (2:1 v/v) with continuous rocking for 1 h. Two mL of 1.0 M NaCl was added to the solution and vortexed for 1 min. Filtration and resuspension was the same as that for that of cellular lipids.

Cholesterol quantification. Cholesterol levels were quantified using an Amplex Red cholesterol assay (Life Technologies, Carlsbad, CA) without cholesterol esterase [21] via a Synergy HT fluorescence microplate reader (BioTek Instruments) with an 530/25 nm excitation filter and a 590/35 nm emission filter. Values were background subtracted. A calibration curve was constructed from five cholesterol standards (measured in triplicate). Since samples showed heteroscedasticity, the standards used a weighted linear fit. [20,22].

Fluorescence recovery after photobleaching and data analysis. After cholesterol depletion or restoration (see above), cells were spread on 0.5 μg mL^{-1}tiggrin coated slides at a concentration of 3E5 cells/mL for 1 hr and then rinsed with BES Tyrodes buffer as previously described [23]. For lipid diffusion measurements, 12 μMcarbocyanine dye DiD (Invitrogen, 1,1'-dioctadecyl-3,3,3',3'-tetramethylindodicarboycyanine perchlorate) was added to the treated cells before plating on the slide.

Fluorescence images were collected on a Princeton Instruments PhotonMax 512 CCD using an Eclipse TE2000U microscope (Nikon), as previously described [24]. The camera gain for the αβ-Venus cell line was set to 3900. Due to the slower recovery time, integrin measurements were collected for 72 seconds, as compared to lipid measurements which were collected for 20 seconds.

Fluorescence images were analyzed as previously described [24] by fitting them to three models based on Eq. 1 [25] with an in-house-developed Igor Pro macro (version 4.0).

$$F(t) = \frac{F_0 + F_{in}\left(\frac{t}{\tau}\right)^{\alpha}}{1 + \left(\frac{t}{\tau}\right)^{\alpha}} \qquad (1)$$

F_0 is the initial fluorescence intensity after photobleaching; F_{in} is the fluorescence intensity at an infinite recovery time; τ is the time for 50% of the fluorescence to recovery, and α is the time exponent providing a measure of how much diffusion is constrained. The most appropriate model set was determined by comparing the reduced chi^2 values obtained for each model. The best fit model generates a reduced chi^2 value of 1. Values obtained from the fit of the fluorescence recovery curve were used to calculate the diffusion coefficient, D(t) (Eq. 2).

$$D(t) = \frac{\omega^2}{4\left(\frac{\tau}{\beta}\right)^{\alpha}} t^{\alpha-1} \qquad (2)$$

where ω is the radius of the focused Gaussian laser beam and β is the photobleach depth [26]. All diffusion parameters are listed in supplementary information Table S1 and S2. Diffusion parameters for the best-fit model of integrins and lipids are listed in Tables 2 and 3. Error bars on all reported FRAP fit parameters represent uncertainty at the 95% confidence level. Most of the curves were best fit to the time-dependent diffusion model. The one exception

was that of the lipid control where Brownian diffusion with an immobile fraction is the best fit showing that the lateral diffusion of lipids is not time dependent in untreated cells.

RESULTS AND DISCUSSION

The goal of this study was to investigate the mechanism for cholesterol's modulation of integrin diffusion. Cholesterol may have either a chemical and/or physical role in altering integrin diffusion. Research has shown different roles of cholesterol as a modulator of receptors by reducing and restoring cholesterol in mammalian cells and monitoring changes in specific receptors. Research showed that the cholecystokinin receptor diffusion correlated with changes in membrane fluidity, while the affinity state for oxytocin receptor had a specific cholesterol requirement suggesting that this receptor is regulated by specific cholesterol-protein interactions [27]. If specific interactions between the cholesterol hydroxyl group and integrins alter integrin diffusion, than a change in cholesterol structure will disrupt these interactions and alter integrin diffusion. If, however, cholesterol plays a biophysical role in integrin diffusion, then replacing cholesterol with its stereoisomer epicholesterol will not result in a change in integrin's diffusion properties.

FRAP measurements (Figure 1C) to determine the diffusion properties of integrins in the cell membrane where cholesterol levels have been reduced and subsequently restored with cholesterol or its stereoisomer epicholesterol will reveal the role cholesterol plays in integrin diffusion.

Cholesterol depletion, restoration and quantification. Cholesterol was extracted from cells using different concentrations of mβCD and both total cellular and membrane cholesterol were quantified. Membrane cholesterol is most relevant to integrin diffusion in

the cell membrane, however, total cellular cholesterol concentration helps establish the effectiveness of the treatments and could reveal information about mβCD's mechanism for extracting cholesterol from the membrane. With increasing concentrations of mβCD, total cellular concentration is decreased by 30, 40 or 55% (Table 1). The percent decrease in membrane cholesterol is lower than the measured decrease for total cellular cholesterol. Using 0.0625 mMmβCD there is no significant change in the membrane cholesterol concentration. However, higher mβCD concentrations reduce the membrane cholesterol concentration by 10 or 20% (Table 1). Cholesterol restoration in cells using 2.5 mM mβCD-chol effectively reverses the cholesterol depletion and actually increases the total cholesterol concentration by 45% as compared to native cholesterol concentrations.

Integrin and lipid diffusion at native cholesterol concentration. The mobile fraction for cells containing normal cholesterol levels is 77 ± 2%, meaning that about a quarter of the integrins are immobile on the timescale of the experiment. The immobile fraction could be attributed to integrin interaction with other components of the cell or its surroundings [24] The integrin diffusion value is $8.4 \pm 0.7 \times 10^{-9}$ cm^2/s at short analysis times and $5.0 \pm 0.5 \times 10^{-9}$ cm^2/s, indicating that diffusion slows which is in part due to ligand integrin interactions [24].

There are no significant changes in either the integrin mobile fraction or the diffusion time constant (hereafter, alpha) after cholesterol is depleted using 0.0625 mM mβCD. This is not surprising since total cellular cholesterol concentration decreased, but membrane cholesterol did not change at this mβCD concentration. At higher mβCD concentrations when 10 to 20% of the membrane cholesterol is extracted, the integrin mobile fraction decreased by 42% or 25% and alpha increased by 13% or 26%, respectively. Interestingly,

the magnitude change in the mobile fraction and alpha are not correlated. Reduced membrane cholesterol results in less mobile integrin, but the fraction that remains mobile has a faster, more Brownian-like diffusion.

Integrin and lipid diffusion at reduced cholesterol concentration. The lateral diffusion of αPS2CβPS integrins was measured in *Drosophila* cells after cholesterol reduction using various concentrations of mβCD (Table 1). The average integrin FRAP curves at a native cholesterol concentration from ten replicate measurements (Figure 2) were fit and was found to be best-fit by a time-dependent diffusion with an immobile fraction model. In order to distinguish the diffusion coefficient at different times in the subsequent discussion, short analysis times refer to diffusion at 1 s while long analysis times refer to diffusion at 50 s. Integrin parameters for the mβCD treatments (Table 2) show that decreased levels of cholesterol decrease the mobile fraction and increase the integrin diffusion at both short and long analysis times.

Integrin and lipid diffusion at restored cholesterol or epicholesterol concentration. Qualitative differences in integrin diffusion at depleted and restored cholesterol concentrations are evident from the FRAP curves (Figure 2). Total cholesterol was restored to a higher concentration than was initially present in the cells. The resulting integrin diffusion in cells containing restored cholesterol returned to their original values at short analysis times, while at longer analysis times, diffusion was slower than measured at native cholesterol concentrations (Table 2). Higher than native cholesterol concentration in the membrane results in a greater number of mobile integrins, however, the movement of the mobile integrin population is slower. Comparable results were observed when similar amounts of epicholesterol were reintroduced into the cells. The combined data of restoring

cholesterol/epicholesterol to the cell membrane indicate that cholesterol plays a biophysical role in influencing integrin diffusion and mobility within the membrane (Figure 3).

Unexpectedly, lipid diffusion parameters did not significantly change when cholesterol was reduced, restored, or replaced with epicholesterol (Table 3). One possible explanation for this observation is that the lipid diffusion parameters represent only a subset of the lipid in the cell membrane, for example the bulk membrane or nanodomain regions. It is also possible that the method to measure lipid diffusion lacks sensitivity to measure small changes in lipid diffusion with statistical confidence. Further studies are underway to explore the unexpected lack of change in lipid diffusion.

CONCLUSIONS

Cholesterol plays a role in integrin diffusion within the cell membrane. By reducing the cholesterol concentrations using mβCD, integrin diffusion values at 1 second (8.4 ± 0.7 $x10^{-9}cm^2/sec$) were increased by a factor of 2, integrin diffusion values at 50 seconds were increased by a factor of 5 and there is a decrease in the mobile fraction as depicted in Figure 3. At 50 seconds the diffusion was 5 times faster changing 5.0 ± 0.5 to a rate of 25 ± 5 However, after epicholesterol was restored to the membrane via a mβCD-epichol complex, diffusion parameters were restored to 9 ± 1 $x10^{-9}cm^2/sec$ at 1 second which are close to the native diffusion. This indicates that the integrin cholesterol interactions are not due to the chemical position of cholesterol's hydroxyl group, but instead cholesterol plays a biophysical role in integrin diffusion.

ACKNOWLEDGEMENTS

Support for this work was provided by the National Science Foundation (CHE-0845236).

The authors thank Atsushi Miyawaki (Riken, Wako City, Saitama, Japan) for the original Venus plasmid.

REFERENCES

1. Oldfield E, Chapman D (1972) Dynamics of lipids in membranes: Heterogeneity and the role of cholesterol. FEBS letters 23 (3):285-297
2. Brown DA, London E (2000) Structure and function of sphingolipid- and cholesterol-rich membrane rafts. The Journal of biological chemistry 275 (23):17221-17224
3. Pankov R, Markovska T, Hazarosova R, Antonov P, Ivanova L, Momchilova A (2005) Cholesterol distribution in plasma membranes of beta1 integrin-expressing and beta1 integrin-deficient fibroblasts. Archives of biochemistry and biophysics 442 (2):160-168
4. Leitinger B, Hogg N (2002) The involvement of lipid rafts in the regulation of integrin function. Journal of cell science 115 (Pt 5):963-972
5. Green JM, Zhelesnyak A, Chung J, Lindberg FP, Sarfati M, Frazier WA, Brown EJ (1999) Role of cholesterol in formation and function of a signaling complex involving alphavbeta3, integrin-associated protein (CD47), and heterotrimeric G proteins. The Journal of cell biology 146 (3):673-682
6. Simons K, Toomre D (2000) Lipid rafts and signal transduction. Nature reviews 1 (1):31-39
7. Scheiffele P, Roth MG, Simons K (1997) Interaction of influenza virus haemagglutinin with sphingolipid-cholesterol membrane domains via its transmembrane domain. The EMBO journal 16 (18):5501-5508
8. Brown DA, London E (1998) Functions of lipid rafts in biological membranes. Annual review of cell and developmental biology 14:111-136
9. Kilsdonk EP, Yancey PG, Stoudt GW, Bangerter FW, Johnson WJ, Phillips MC, Rothblat GH (1995) Cellular cholesterol efflux mediated by cyclodextrins. The Journal of biological chemistry 270 (29):17250-17256
10. Zidovetzki R, Levitan I (2007) Use of cyclodextrins to manipulate plasma membrane cholesterol content: evidence, misconceptions and control strategies. Biochimica et biophysica acta 1768 (6):1311-1324
11. Ge S, White JG, Haynes CL (2010) Critical role of membrane cholesterol in exocytosis revealed by single platelet study. ACS chemical biology 5 (9):819-828
12. Giancotti FG, Ruoslahti E (1999) Integrin signaling. Science (New York, NY 285 (5430):1028-1032
13. Christian AE, Haynes MP, Phillips MC, Rothblat GH (1997) Use of cyclodextrins for manipulating cellular cholesterol content. Journal of lipid research 38 (11):2264-2272

14. Axelrod D, Koppel DE, Schlessinger J, Elson E, Webb WW (1976) Mobility measurement by analysis of fluorescence photobleaching recovery kinetics. Biophysical journal 16 (9):1055-1069
15. Bunch TA, Grinblat Y, Goldstein LS (1988) Characterization and use of the Drosophila metallothionein promoter in cultured Drosophila melanogaster cells. Nucleic acids research 16 (3):1043-1061
16. Bunch TA, Salatino R, Engelsgjerd MC, Mukai L, West RF, Brower DL (1992) Characterization of mutant alleles of myospheroid, the gene encoding the beta subunit of the Drosophila PS integrins. Genetics 132 (2):519-528
17. Bunch TA, Helsten TL, Kendall TL, Shirahatti N, Mahadevan D, Shattil SJ, Brower DL (2006) Amino acid changes in Drosophila alphaPS2betaPS integrins that affect ligand affinity. The Journal of biological chemistry 281 (8):5050-5057
18. Bligh EG, Dyer WJ (1959) A rapid method of total lipid extraction and purification. Canadian journal of biochemistry and physiology 37 (8):911-917
19. Bezrukov L, Blank PS, Polozov IV, Zimmerberg J (2009) An adhesion-based method for plasma membrane isolation: evaluating cholesterol extraction from cells and their membranes. Analytical biochemistry 394 (2):171-176
20. Dibya D, Arora N, Smith EA (2010) Noninvasive measurements of integrin microclustering under altered membrane cholesterol levels. Biophysical journal 99 (3):853-861
21. Amundson DM, Zhou M (1999) Fluorometric method for the enzymatic determination of cholesterol. Journal of biochemical and biophysical methods 38 (1):43-52
22. Almeida AM, Castel-Branco MM, Falcao AC (2002) Linear regression for calibration lines revisited: weighting schemes for bioanalytical methods. Journal of chromatography 774 (2):215-222
23. Dibya D, Sander S, Smith EA (2009) Identifying cytoplasmic proteins that affect receptor clustering using fluorescence resonance energy transfer and RNA interference. Analytical and bioanalytical chemistry 395 (7):2303-2311
24. Sander SA, N. Smith, E.A. (2012) Elucidating the role of select cytoplasmic proteins in altering diffusion of integrin receptors. Analytical and bioanalytical chemistry
25. Feder TJ, Brust-Mascher I, Slattery JP, Baird B, Webb WW (1996) Constrained diffusion or immobile fraction on cell surfaces: a new interpretation. Biophysical journal 70 (6):2767-2773
26. Yguerabide J, Schmidt JA, Yguerabide EE (1982) Lateral mobility in membranes as detected by fluorescence recovery after photobleaching. Biophysical journal 40 (1):69-75
27. Gimpl G, Burger K, Fahrenholz F (1997) Cholesterol as modulator of receptor function. Biochemistry 36 (36):10959-10974

Table 1. Total cellular or membrane cholesterol concentration after the listed depletion or restoration treatment.

	Cholesterol Concentration (femtamoles/cell)	
Cholesterol Depleted		
	Total	Membrane
0 mM mβCD	13 ± 2	3 ± 1
0.0625 mM mβCD	9 ± 1	3.4 ± 0.4
0.5 mM mβCD	8 ± 3	2.7 ± 0.7
2 mM mβCD	6 ± 2	2 ± 1
Cholesterol Depleted/Cholesterol Restored		
2mM mβCD + 2.5 mM mβCD-chol	19 ± 2	1.4 ± 0.4

Table 2. Integrin diffusion parameters as determined from the best-fit model of the FRAP curves for the αβ-Venus cell line before and after treatment with mβCD solutions.

Treatments	Mobile Fraction	Time Exponent (α)	Diffusion Coefficient at 1 s (x10^{-9} cm^2/s)	Diffusion Coefficient at 50 s (x10^{-9} cm^2/s)
0mM mβCD	0.77 ± 0.02	0.87 ± 0.04	8.4 ± 0.7	5.0 ± 0.5
0.0625mM mβCD	0.75 ± 0.02	0.85 ± 0.04	10.2 ± 0.7	5.6 ± 0.5
0.5 mM mβCD	0.45 ± 0.03	0.98 ± 0.11	14 ± 2	13 ± 5
2mM mβCD	0.58 ± 0.02	1.1 ± 0.06	18 ± 1	25 ± 5
2mM mβCD 2.5 mM mβCD-chol	0.90 ± 0.05	0.71 ± 0.07	8 ± 1	2.6 ± 0.4
2mM mβCD 1.0 mM mβCD-epichol	0.89 ± 0.01	0.84 ± 0.01	9.5 ± 0.3	5.0 ± 0.2
2mM mβCD 2.5 mM mβCD-epichol	0.74 ± 0.03	0.72 ± 0.06	9 ± 1	3.1 ± 0.4

Table 3. Lipid diffusion parameters as determined from the best-fit model of the FRAP curves for the αβ cell line before and after treatment with mβCD solutions.

Treatments	Mobile Fraction	Time Exponent (α)	Diffusion Coefficient at 1 s (x 10^{-9} cm^2/s)	Diffusion Coefficient at 50 s (x 10^{-9} cm^2/s)
0mM mβCD	0.87 ± 0.04		15 ± 2[a]	
0.0625mM mβCD	0.83 ± 0.02	0.89 ± 0.05	20 ± 1	13 ± 2
0.5mM mβCD	0.88 ± 0.02	0.94 ± 0.05	17 ± 1	13 ± 2
2mM mβCD	0.94 ± 0.02	0.94 ±0.04	21.9 ± 0.8	18 ± 2
2mM mβCD + 2.5 mM mβCD-chol	0.87 ±0.02	0.89 ± 0.04	19.5 ± 0.9	13 ± 2
2mM mβCD + 1.0 mM mβCD-epichol	0.91 ± 0.02	0.92 ± 0.04	20 ± 1	15 ± 2
2mM mβCD + 2.5 mM mβCD-epichol	0.87 ± 0.02	0.91 ± 0.04	21.4 ± 0.9	15 ± 2

[a]Data fit best to Brownian diffusion (α=1); diffusion coefficient will be the same values at all analysis times

Figure 1.(A) Structure of cholesterol and its stereoisomer (B) epicholesterol. The black arrow denotes the difference in position of the hydroxyl group (C) Images of a spread cell after epicholesterol levels were restored to the cell using 2.5mM mβCD-epichol. Images show the photobleached spot over time as well as a reference image prior to photobleaching. At longer time periods more fluorescent molecules have diffused into the photobleached area. Ninety-nine images were taken at 0.77 sec intervals.

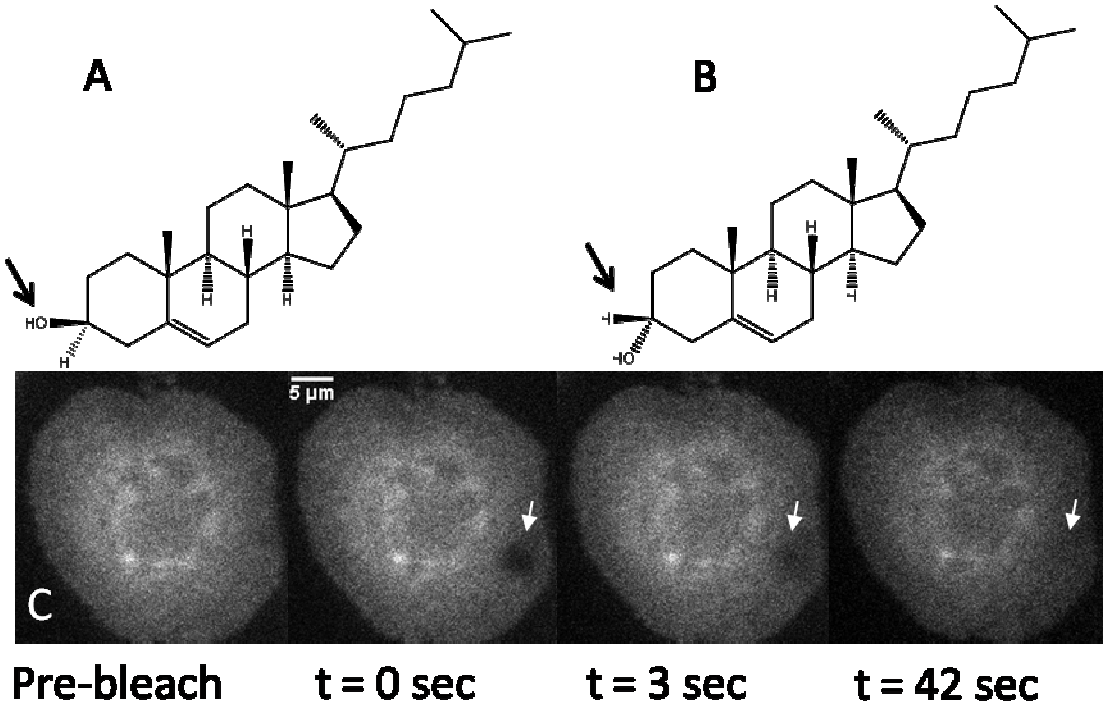

Figure 2.Average fluorescence recovery after photobleaching (FRAP) curves from 10 replicate measurements (circles) of S2 cells expressing αPS2CβPS-Venus integrins (blue) at native cholesterol concentration;(black) reduced cholesterol concentration;(green) restored cholesterol concentration;(red) restored epicholesterol concentration. The data are fit (solid lines following the same color scheme previously described) to a model for time-dependent diffusion with an immobile fraction. Curves have been normalized to the pre-photobleach intensity.

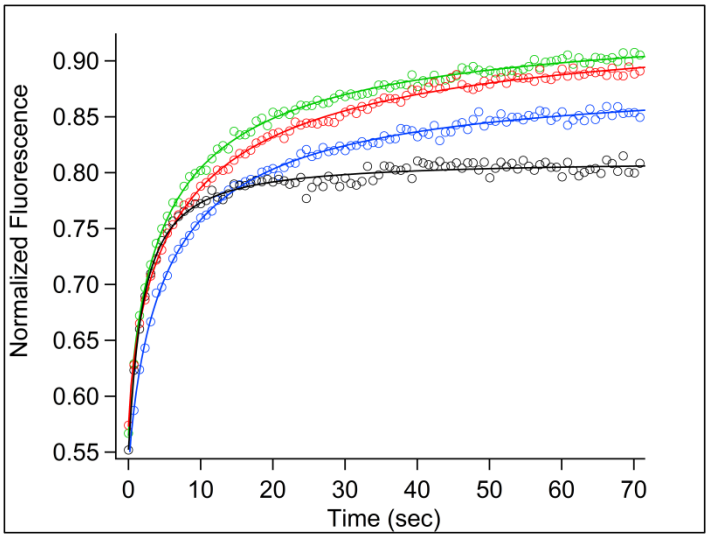

Figure 3.Schematic showing how the presence of cholesterol or epicholesterol in the plasma membrane affects integrin diffusion. Cholesterol intercalates in the lipid bilayer and influences membrane structure and fluidity. Altered integrin diffusion is due to a biophysical role for cholesterol, and is not a result of a biochemical mechanism. Integrin diffusion properties are defined using a time-dependent diffusion model with an immobile fraction.

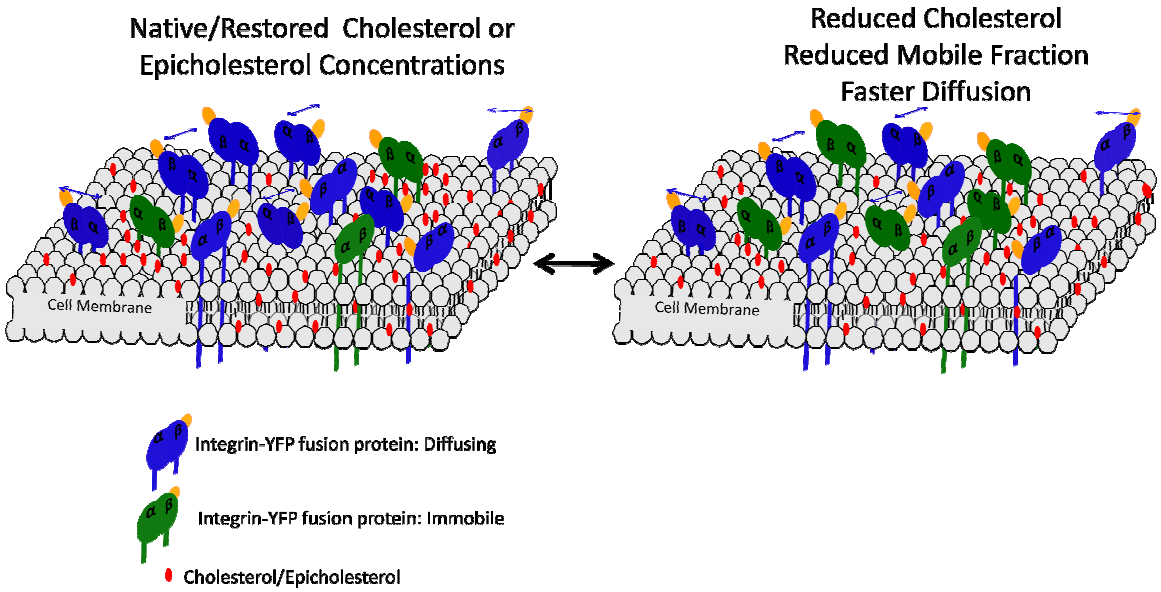

Supplemental Information for Chapter 4

Table S1. Integrindiffusion parameters obtained by fitting FRAP curves to constrained (time dependent) diffusion, Brownian diffusion and time-dependent diffusion with an immobile fraction models for a cell line expressing αPS2CβPS-Venus integrins before (control) and after the indicated cholesterol depletion or restoration. The fit parameters from the best-fit model, either time dependent diffusion with an immobile fraction or Brownian diffusion, are shown in Table 2 of the manuscript. All cells are spread on a ligand coated microscope slide.

	Constrained Diffusion			Brownian Diffusion		Constrained/Brownian Diffusion			
	α	Diffusion Coefficient (1 s) ($x10^{-9}cm^2/s$)	Diffusion Coefficient (50 sec) ($x10^{-9}cm^2/s$)	Mobile fraction	Diffusion Coefficient ($x10^{-9}cm^2/s$)	Mobile Fraction	α	Diffusion Coefficient (1 s) ($x10^{-9}cm^2/s$)	Diffusion Coefficient (50 sec) ($x10^{-9}cm^2/s$)
0 mM mβCD	0.509 ± 0.005	10.3 ± 0.2	1.52±0.02	0.7± 0.1	6.6 ± 0.8	0.77 ± 0.02	0.87 ± 0.04	8.4 ± 0.7	5.0 ± 0.5
0.0625 mM mβCD	0.471 ± 0.008	11.8 ± 0.4	1.49 ± 0.04	0.7 ± 0.1	8 ± 1	0.75 ± 0.02	0.85 ± 0.04	10.2 ± 0.7	5.6 ± 0.5
0.5 mM mβCD	0.24 ± 0.02	10.4 ± 0.9	0.54 ± 0.03	0.4 ± 0.1	14± 3	0.45 ± 0.03	0.98 ± 0.11	14 ± 2	13 ± 5
2 mM mβCD	0.263 ± 0.008	16.6 ± 0.6	0.93 ±0.03	0.6 ± 0.1	19±2	0.58 ± 0.02	1.1 ± 0.06	18 ± 1	25 ± 5
2 mM mβCD 2.5 mM mβCD-chol	0.59 ± 0.02	8.6 ± 0.7	1.7 ±0.1	0.8 ± 0.2	5.0 ±0.7	0.90 ± 0.05	0.71 ± 0.07	8 ± 1	2.6 ± 0.4
2 mM mβCD 1.0 mM mβCD-epichol	0.628 ± 0.004	11.2 ± 0.2	2.63 ± 0.03	0.85± 0.09	3.6 ± 0.8	0.89 ± 0.01	0.84 ± 0.01	9.5 ± 0.3	5.0 ± 0.2
2 mM mβCD 2.5 mM mβCD-epichol	0.46 ± 0.01	9.1 ± 0.5	1.10 ± 0.04	0.7± 0.1	5.8 ±0.8	0.74 ± 0.03	0.72 ± 0.06	9 ± 1	3.1 ± 0.4

[a] Diffusion parameters were obtained from fitting the average FRAP curve of replicate measurements with the standard deviation representing the uncertainty at the 95% confidence interval of the corresponding coefficients obtained in the fits.

Table S2. Lipiddiffusion parameters obtained by fitting FRAP curves to constrained (time dependent) diffusion, Brownian diffusion and time-dependent diffusion with an immobile fraction models for a cell line expressing αPS2CβPS integrins before (control) and after the indicated cholesterol depletion or restoration. The fit parameters from the best-fit model either Brownian diffusion or time dependent diffusion with an immobile fraction, are shown in Table 3 of the manuscript. All cells are spread on a ligand coated microscope slide.

	Constrained Diffusion			Brownian Diffusion		Constrained/Brownian Diffusion			
	α	Diffusion Coefficient (1 s) ($x10^{-9}cm^2/s$)	Diffusion Coefficient (50 sec) ($x10^{-9}cm^2/s$)	Mobile fraction	Diffusion Coefficient ($x10^{-9}$ cm^2/s)	Mobile Fraction	α	Diffusion Coefficient (1 s) ($x10^{-9}cm^2/s$)	Diffusion Coefficient (50 sec) ($x10^{-9}cm^2/s$)
0 mM mβCD	0.75 ± 0.02	13.9 ± 0.7	5.2 ± 0.4	0.86 ± 0.02	15 ± 2	0.87± 0.04	0.96 ± 0.08	15 ± 2	14 ± 4
0.0625 mM mβCD	0.64 ± 0.01	16.3 ± 0.5	3.9 ± 0.2	0.80 ± 0.01	20 ± 3	0.83 ± 0.02	0.89 ± 0.05	20 ± 1	13 ± 2
0.5 mM mβCD	0.74 ± 0.01	14.8 ± 0.4	5.3 ± 0.3	0.86 ± 0.01	17 ± 2	0.88 ± 0.02	0.94 ± 0.05	17 ± 1	13 ± 2
2 mM mβCD	0.81 ± 0.01	20.7 ± 0.5	10.0 ± 0.5	0.92 ± 0.01	22 ± 3	0.94 ± 0.02	0.94 ±0.04	21.9 ± 0.8	18 ± 2
2 mM mβCD 2.5 mM mβCD-chol	0.68 ± 0.02	16.8 ± 0.6	4.7 ± 0.3	0.83 ± 0.01	20 ± 2	0.87 ±0.02	0.89 ± 0.04	19.5 ± 0.9	13 ± 2
2 mM mβCD 1.0 mM mβCD-epichol	0.75 ± 0.01	18.3 ± 0.5	6.9 ± 0.3	0.88 ± 0.01	20 ± 3	0.91 ± 0.02	0.92 ± 0.04	20 ± 1	15 ± 2
2 mM mβCD 2.5 mM mβCD-epichol	0.689 ± 0.01	18.3 ± 0.4	5.3 ± 0.2	0.84 ± 0.01	22 ± 3	0.87 ± 0.02	0.91 ± 0.04	21.4 ± 0.9	15 ± 2

[a] Diffusion parameters were obtained from fitting the average FRAP curve of replicate measurements with the standard deviation representing the uncertainty at the 95% confidence interval of the corresponding coefficients obtained in the fits.

CHAPTER 5: GENERAL CONCLUSIONS AND FUTURE PROSPECTS

General Conclusions

Due to the sensitivity, selectivity, and availability of extrinsic fluorescence sensors, fluorescence has become a prevalent method to study biological systems. Elucidating the molecular mechanism of integrin receptors in the membrane of live cells provides critical insight into a class of membrane proteins involved in basic cellular function, and provides clues about aberrant function that leads to diseases states. The work presented in this thesis uses fluorescence techniques, FRET and FRAP, in combination with RNAi, cholesterol sequestration, and varying ligand concentrations to compare how changes in cytoplasmic proteins, membrane cholesterol, and extracellular matrix concentrations affect integrin diffusion and clustering properties. The techniques discussed can be applied to the study of other membrane receptors.

The techniques in chapter two combine FRAP with different ligand concentrations to show how extracellular matrix interactions are responsible for 25% of the integrin immobile fraction while at the same time reduce diffusion constraints. Additionally, by combining FRAP with RNAi it was observed that interaction with different cytoplasmic proteins either increases or decreases integrins' diffusion constraints, thereby affecting the movement of integrins in response to stimuli.

Chapter 3 combines FRET with RNAi revealing that out of the seven cytoplasmic proteins studied only ILK affected integrin clustering in the presence of high ligand densities. Mutant integrins, αanaβ and αβV409D, were also studied and different changes in clustering were observed as compared to the wild-type integrin. Reduced expression of paxillin and steamer duck caused an increase in energy transfer in the αanaβ mutant integrin. Reduced

expression of ILK in the αβV409D mutation shows the opposite trend as the wild-type, which may be related to integrin-ligand affinity.

Chapter 4 combines FRAP with cholesterol sequestration to show that reduced cholesterol concentration increases integrin diffusion, while decreasing the mobile fraction. Diffusion parameters were restored to near native speeds of $8.4 \pm 0.7 \times 10^{-9}$ cm^2/sec upon restoring membrane sterol levels using epicholesterol, a stereoisomer of cholesterol, indicating cholesterol plays a biophysical role in integrin diffusion.

Future Directions

The FRET technique used to measure clustering in cells can be further developed in different directions, including observing how other membrane proteins, such as receptor tyrosine kinase (RTK), synaptobrevin, and tetraspanins affect integrin clustering.

While FRAP provides important ensemble diffusion information on integrins and their interactions with their surroundings, single particle tracking data will reveal the paths of individual integrins. This will provide additional information to help elucidate the molecular mechanisms of integrins.

Integrin-ligand binding interactions can be further described by monitoring the interactions of fluorescently labeled TWOW-1, a ligand mimetic, with integrins. Single molecule binding can be measured on the different integrin mutants under total internal reflection. Kinetic and thermodynamic effects on equilibrium binding parameters and diffusion coefficients will be identified.

Appropriately designed FRET reporters can be developed to monitor the clustering of other membrane receptors such as glycoproteins or expanded to membrane receptors in

different cell systems i.e. mammalian. There are 24 known vertebrate integrins, whose function may vary depending upon cell type. Conflicting research on how $\alpha_v\beta_3$ integrin affects angiogenesis has been reported [1]. Application of FRET to mammalian cells can help elucidate the mechanism and clarify discrepancies that may exist in the data. Additionally, if similar integrin properties are observed in different cell lines, conservation of molecular function will be recognized. The combined understanding of how intracellular, extracellular, and membrane interactions affect the $\alpha_v\beta_3$integrin network may enhance the current anti-angiogenic therapies based the function of this integrin.

REFERENCE

1. Hodivala-Dilke K (2008) alphavbeta3 integrin and angiogenesis: a moody integrin in a changing environment. Current opinion in cell biology 20 (5):514-519

APPENDIX 1: IDENTIFYING CYTOPLASMIC PROTEINS THAT AFFECT RECEPTOR CLUSTERING USING FLUORESCENCE RESONANCE ENERGY TRANSFER AND RNA INTERFERENCE

A paper published in Analytical and Bioanalytical Chemistry 2009, 395 (7), 2303-2311*

Deepak Dibya, Suzanne Sander and Emily A. Smith

ABSTRACT

Unraveling the complex, dynamic organization of the cell membrane can provide vital information about many aspects of cellular functions. Reported herein is a method for identifying cytoplasmic proteins that affect cell membrane protein organization. RNA interference (RNAi) is used to reduce the expression of select cytoplasmic proteins and a fluorescence resonance energy transfer (FRET) assay is used to measure changes in receptor microclustering. The advantage of this assay is that it does not require attaching fluorescent tags to the receptor. A change in energy transfer after reducing the expression of a cytoplasmic protein provides information about the protein's role in altering receptor organization. As a demonstration of the method, cytoplasmic proteins involved in integrin microclustering have been identified. The cytoplasmic proteins targeted in this study include: dreadlock, integrin-linked kinase, paxillin, steamer duck, vinculin, rhea, focal adhesion kinase, and actin 42A.

Reducing the expression of vinculin, paxillin, rhea, and focal adhesion kinase increased integrin microclustering, as measured by an increase in energy transfer in cells expressing αPS2CβPS integrins. No change in integrin microclustering was measured in a control cell line. Integrin mutants exhibited different microclustering properties compared to the wild-type integrins after reducing the expression of the listed cytoplasmic proteins. The results demonstrate the utility of this assay format, and provide insight into the function of cytoplasmic proteins in integrin microclustering.

INTRODUCTION

A dynamic flow of information between the extracellular and intracellular environments of a cell is required for survival, growth, proliferation, differentiation, and other basic functions (1). The primary signal transducers are receptor cell membrane proteins. Receptors transmit information through three primary mechanisms: (a) binding extracellular ligands; (b) engaging a cascading network of intracellular signaling partners; and (c) clustering within the membrane. Several analytical techniques, such as co-immunoprecipitation, surface plasmon resonance, affinity chromatography, and two-hybrid systems, are used to measure the interactions of receptors with their intracellular and extracellular signaling partners (2).

Observing nanoscale receptor organization in live cells requires a non-invasive detection technique that is not subject to diffraction-limited spatial resolution. Fluorescence resonance energy transfer (FRET) is ideally suited for measuring nanoscale membrane organization (3). FRET studies of receptor microclustering have primarily used the direct attachment of donor and acceptor fluorescent proteins to the extracellular or intracellular

domain of the membrane protein (4, 5). Direct fluorophore attachment could potentially alter the receptor's clustering properties, as well as their interaction with other biomolecules. This experimental approach also requires time-consuming protein cloning steps to attach the donor and acceptor fluorescent proteins to each protein mutant.

A recently reported FRET assay overcomes these problems (6). Shown in Fig. 1 is a schematic of this FRET assay, which is used to measure the microclustering of αPS2CβPS integrins. Integrins are heterodimeric cell membrane receptors that are pivotal to many cellular functions, and mediate signaling through both the cytoplasm and the extracellular matrix (1, 7). The integrin microclustering assay used FRET reporter peptides that were expressed in cells along with integrins. The FRET reporter peptides contain the integrins' β subunit cytoplasmic and transmembrane domain fused to donor or acceptor fluorescent proteins. A previous report showed that the β cytoplasmic and transmembrane region is sufficient for clustering with full-length integrin *in vivo* (8). The donors and acceptors were a monomeric yellow fluorescent protein variant mVenus and a monomeric dsRED variant mCherry, respectively. Hereafter, the term FRET reporters refers to a population of donor transmembrane peptides and a separate population of acceptor transmembrane peptides.

The fusion of fluorescent proteins to the β subunit transmembrane and cytoplasmic domain to generate FRET reporters allows the donor and acceptor fluorophores to take part in integrin clustering. When integrins cluster, so do the FRET reporters. This results in a reduced average donor–acceptor separation distance and an increase in observed FRET. The use of FRET reporters eliminates the need to attach the donor and acceptor directly to the integrin, and does not require numerous steps to clone donor and acceptor fluorescent groups to each integrin mutant. The integrin diffusion and clustering properties are not altered in this

assay format since the fluorescent proteins are not directly attached to the integrins. The reporters: (a) do not contain ligand-binding domains so there is no competition between the integrin and FRET reporters for ligand; (b) do not alter the integrins' ligand binding affinity; and (c) do not produce energy transfer in the absence of integrins (6). A set of FRET control peptides contained the same fluorescent proteins cloned to the transmembrane and cytoplasmic domains of a protein (mouse CD2) with no sequence homology in S2 cells. The assay has been used to measure receptor clustering, but it has not been demonstrated that it can be used to relate intracellular binding events with receptor clustering. This would enable a more detailed molecular understanding of cell membrane organization.

Reported herein is a systematic approach for identifying cytoplasmic proteins that affect receptor microclustering. The method uses the FRET assay described above along with RNA interference (RNAi) to reduce the expression of select proteins. Changes in energy transfer are measured to identify proteins that affect integrin microclustering. The cytoplasmic proteins that have been studied include: rhea (9), vinculin (10), paxillin (10), focal adhesion kinase (10), steamer duck (11), dreadlock (11), integrin-linked kinase (11)and actin42A (12).

EXPERIMENTAL

S2 cell culture

Transformed *Drosophila* S2 cells were cultured in Shields and Sang M3 insect media (M3, Sigma) supplemented with 10% fetal bovine serum (Irvine Scientific), 12.5 mM streptomycin, 36.5 mM penicillin, and 0.2 μM methotrexate (Fisher Scientific) in a 22°C incubator. Cells were co-transfected to express integrin subunits and FRET reporters or

FRET controls. Complete protein sequences for the FRET controls, FRET reporters containing mVenus or mCherry fluorescent proteins (6), wild-type and mutant integrin subunits (6, 13-15)have been published elsewhere. All endogenous proteins contain the heat shock promoter.

dsRNA synthesis

Double-stranded RNA (dsRNA) was generated using published protocols with minor modifications, as noted below (16). Polymerase chain reactions were used to amplify 200 to 700-bp DNA sequences from S2 genomic DNA. The primer sequences can be identified from the information listed in Table 1. Both forward and reverse primers contained the T7 RNA polymerase promoter binding site (TAATACGACTCACTATAGGG). The polymerase chain reaction products were analyzed using 1% agarose gel electrophoresis and were subsequently used as templates for RNA synthesis with the MEGASCRIPT T7 Transcription Kit (Ambion, Austin, TX) to produce single stranded RNA. The single-stranded RNA products were ethanol-precipitated and re-suspended in water. dsRNAs was generated by incubating the solution at 65°C for 30 min followed by slow cooling to room temperature, and analyzed by 1% agarose gel electrophoresis to ensure that only the desired product was obtained. The concentration was measured using the solution absorbance at 280 nm and the solutions were diluted to 1 μg/μL. The dsRNA solution was stored at −20°C until subsequent use.

RNAi treatment

Detailed protocols have been previously published, and were followed with changes noted below (16, 17). Approximately 6×10^5 cells were plated per well in a 12-well cell culture dish. Cells were rinsed with 600 μL of serum-free M3 medium, and 300 μL of serum-free media was added to each well. Ten micrograms of dsRNA was added directly to each well, and the cells were incubated for 60 min in a 22°C incubator followed by addition of 300 μL M3 media containing 20 % fetal bovine serum. The cells were incubated at 22°C for an additional 4 days. Reduced expression of the target protein has been reported up to 5 days after RNAi treatment.

FRET assay

After RNAi treatment and 4 days of incubation, cells were transferred from the cell culture dish to a polypropylene tube and heat-shocked for 30 min at 36°C to induce the expression of integrins and FRET reporters or controls. Cells were then placed in a 22°C incubator for 3 h to achieve maximum protein expression. The cells were centrifuged at approximately 600×g, the pellet was resuspended in serum-free medium and the concentration was adjusted to 3×10^5 cells/mL. The cells were placed on a RBB-tiggrin coated substrate and allowed to spread for 1 h in the serum-free medium. Details about the RBB-tiggrin substrate are provided in the supplemental information. The medium was replaced with 20 mM BES Tyrodes buffer prior to analysis. The analysis was completed within 1.25 h of replacing the medium with BES buffer to ensure cell viability. At least three RNAi treatments were performed for every targeted protein and every cell line. The cells were analyzed using a ×60 magnification, numerical aperture 0.95 objective and a Eclipse

TE2000U microscope (Nikon) with low-intensity mercury lamp illumination. The images were captured with a Coolsnap CCD camera (Roper Scientific Photometrics, Pleasanton, CA) using the program Micromanager, which operates within the ImageJ 1.37v software. The camera was set to bin 8×8 pixels. Images were captured utilizing three different filter sets for each cell analyzed: (a) donor filter set (excitation 500/20 nm, emission 535/30 nm), (b) acceptor filter set (excitation 545/30 nm, emission 620/60 nm), and (c) donor excitation filter with acceptor emission filter (FRET filters). The exposure time for the FRET, acceptor and donor images were 12, 6, and 6 s, respectively. The Drosophila S2 cells did not move in the time it took to capture the three images.

Data and statistical analysis

Data was analyzed using the program ImageJ, and a plugin that was developed with the Java platform. The plug-in calculates a FRET value for each pixel in the image. After the appropriate background value is subtracted from each pixel, a FRET value is calculated using the equation:

$$FRET = \frac{I_{DA} - a(I_{AA} - cI_{DD}) - d(I_{DD} - bI_{AA})}{\sqrt{I_{DD}I_{AA}}} \quad (1)$$

where I_{DA}, I_{AA}, and I_{DD} are intensities obtained from the images with the FRET, acceptor, and donor filters, respectively. The factors a, b, c, and d account for bleedthrough of: acceptor into the FRET filters, acceptor into the donor filters, donor into the acceptor filters, and donor into the FRET filters, respectively. All four bleedthrough factors were non-zero on the microscope system used in these studies. Further discussion of the bleedthrough factors

can be found in the supplemental information. There are numerous alternative FRET equations that can be used in conjunction with this methodology (18-20). Equation 1 is suitable for measuring increases or decreases in FRET efficiency after RNAi treatment.

All statistical analyses were performed using the application JMP 7 (SAS Institute Inc, Cary, USA), with statistical consulting through the Iowa State University Department of Statistics. For every reported value, at least 100 cells from three replicate experiments were analyzed. The raw FRET data are not normally distributed, which means that statistical tests such as the t-test cannot be used on the raw data. The data were transformed to a normal distribution by taking the natural log of the raw data, and the means were calculated from the transformed data. The Welch test was used to compare the means of the log-transformed data since the data sets were determined to have unequal variances by Levene's test. Results of the Welch Test are reported as p values, which are a measure of the significance of the statistical tests. A p value lower than 0.05 provides evidence that the energy transfer measured for the RNAi treatment data set is altered compared to the no RNAi treatment data set. A p value greater than 0.05 does not provide the statistical evidence to say there is a difference between the data sets. In order to report the mean value in the original data scale, the antilog of the mean of the log-transformed data was taken. Further information on these methods can be found in statistics textbooks (21).

RESULTS AND DISCUSSION

FRET assay

Figure 1 shows a schematic of the FRET assay used to study the effect of cytoplasmic proteins on integrin microclustering in live cells. A set of three images is captured for each

cell: donor, acceptor, and FRET. Figure 2 shows a series of images used to calculate energy transfer in cells expressing wild-type integrins and FRET reporters. Using a home-built plug-in for the program ImageJ, an energy transfer value is calculated for each pixel in the image using Eq. 1. A region of interest (ROI) is generated for each cell. Specifically, background regions and regions corresponding to the nuclear and perinuclear regions are excluded from the analysis. Intense fluorescence is observed in these regions, corresponding to FRET reporters inside the cell. The signal from the nuclear and perinuclear regions interferes with the measurement of integrin clustering in the cell membrane. An example ROI is shown in Fig. 2. An average value is calculated from all the pixels in a ROI to generate a single FRET value for each cell. The distribution of FRET values for all pixels in the example ROI is provided in the supplemental information (Supplemental Figure S1).In order to ensure that a suitable ROI can be defined, only spread cells with diameters greater than 20 μm are analyzed. The average diameter of the spread cells analyzed by FRET did not statistically differ for any of the cell lines or RNAi treatments (data not shown).

In order to measure intracellular events that affect integrin clustering, without interference from extracellular ligand binding, minimizing extracellular signaling is desirable. To accomplish this, cells were spread on a surface with low ligand density. The extracellular ligand for the integrins used in these studies (RBB-tiggrin) is a 53 amino acid protein. Assuming RBB-tiggrin's size is 2 nm×3 nm (22), and all the RBB-tiggrin adheres to the glass slide, approximately 3% to 5% of the 30 mm^2 glass slide is covered at the ligand density used in these studies. Bovine serum albumin is used to cover the remaining glass surface to inhibit non-specific cell binding to the glass. A surface with no ligand, coated only with bovine serum albumin, would completely eliminate extracellular signaling events.

However, cell attachment and cell spreading were significantly reduced when no ligand was present. The reduced cell spreading in the absence of ligand precluded FRET measurements on a large-enough number of cells to provide statistically significant results.

Energy transfer was measured in cells expressing integrins and FRET reporter peptides or FRET control peptides. The integrins were either wild-type or mutants. Two well-characterized integrin mutants that are studied have different ligand-binding affinities compared to wild-type integrin. The mutant αanaβ integrins contain a two-point mutation in the cytoplasmic domain of the α subunit. This mutation is considered to mimic signal transduction from inside to outside the cell (23). The mutant αβV409D integrins contain a single-point mutation in the extracellular domain of the β subunit that mimics signal transduction from outside to inside the cell (24).

At 3% to 5% ligand surface densities, statistically similar energy transfer values were measured for three cell lines expressing wild-type or mutant (αanaβ, αβV409D) integrins and FRET reporters (Table 2). This indicates similar levels of FRET reporter microclustering for the three cell lines at these experimental conditions. Similar energy transfer values are also obtained for cells expressing wild type integrins and FRET reporters compared to cells expressing wild-type integrins and FRET controls (Table 2). Three factors must be considered to interpret these results: (1) the energy transfer values are above the detection limit for the microscope system; (2) the total energy transfer measured is a result of integrin-specific FRET reporter clustering and non-integrin-specific FRET reporter clustering from many sources; (3) at high ligand densities, higher energy transfer values are measured for cells expressing FRET reporters compared to cells expressing FRET controls. At 3% to 5% ligand densities, the energy transfer reported in Table 2 (αβ FRET Reporters, αanaβ FRET

Reporters, αβV409D FRET Reporters) is the result of non-integrin-specific microclustering of the FRET reporters. Integrin-specific clustering would be detected as an increase in energy transfer for the cell line expressing FRET reporters relative to the cell line expressing FRET controls, which is observed at high ligand densities (6). It is not possible to say that no integrin microclustering occurs at 3% to 5% ligand density. Integrin microclustering that causes an insignificant increase in FRET reporter microclustering relative to the non-integrin-specific microclustering of the FRET reporter may be present. The data presented in Table 2 is referred to as the no RNAi treatment data in the following discussion.

RNAi transfection

RNAi was used to reduce the expression of select cytoplasmic proteins. The proteins targeted in this work are highlighted gray in Fig. 1. These proteins are known to be involved in integrin-signaling complexes, and are expressed in S2 cells as reported in the FLIGHT mRNA microarray expression database (24) and PeptideAtlas mass spectrometry proteomics database (25). S2 cells are a *Drosophila* cell culture system. Due to substantial structural homology between vertebrate and invertebrate integrins, as well as a similarity between many of the integrin-signaling pathways, information learned about integrin microclustering in *Drosophila* cells can be used to advance the understanding of vertebrate integrins (26).

The choice of *Drosophila* cell culture is optimal for these studies because rapid, simple, and selective reduction in protein expression is possible using RNAi (16, 27). A similar technique used in mammalian cell culture, short-interfering RNA (i.e., siRNA), often suffers from low specificity for the targeted protein and an immune response to the RNA. In RNAi experiments, approximately 500-bp double-stranded RNA corresponding to the

mRNA sequence of the targeted protein is used to reduce protein expression. Whole-genome RNAi studies have been performed, and the sequences used to reduce protein expression in these studies are published and available in several online resources (28, 29). The RNAi probes used in this study were selected from these resources. Two criteria were used in selecting the RNAi probes: thermodynamic binding efficiency and selectivity. The selectivity is a measure of other proteins that may be targeted by the RNAi probe. Since the goal of this work is to identify specific proteins that affect integrin microclustering, only probes with 100% selectivity to the targeted protein were chosen for the FRET studies (other targets, Table 1). The actin42A probe targets the entire class of actin proteins, but does not target other protein classes. Once internalized, the approximately 500- bp dsRNA is reduced to approximately 21-bp fragments.The thermodynamic binding efficiency presented in Table 1 is a measure of how many of the possible 21-mers have thermodynamically favorable binding to the target mRNA. This value is not necessarily reflective of the amount the target protein's expression is reduced. For a given protein, RNAi probes with 100% selectivity and the highest efficiency were selected. Another important consideration is possible changes in cell viability after RNAi treatment. None of the RNAi treatments altered cell viability compared to cells that did not receive RNAi treatment (data not shown).

A cell line expressing green fluorescent protein (GFP) fused to actin 42A was used show that the RNAi protocol used in these studies facilitates the delivery of dsRNA into the cytoplasm. Four days after RNAi treatment against actin 42A, a 21% reduction in the GFP fluorescence was measured compared to cells that did not receive RNAi treatment (Supplemental Figure S2). The reduction in protein expression will vary with each RNAi

probe. Typical RNAi knockdown efficiencies for *Drosophila* cell culture are between 95–99% and 62–100% using Western blotting and cell phenotype analysis, respectively (16, 30).

Cytoplasmic proteins that affect integrin microclustering

Figure 3 (black data bars) shows the average FRET values for at least 100 S2 cells expressing wild-type integrins and FRET reporters after the indicated RNAi treatment. The data were normalized and statistically compared to the value obtained for the no RNAi treatment data.

Four of the RNAi treatments resulted in higher levels of energy transfer compared to the no RNAi treatment data: vinculin, paxillin, rhea, and focal adhesion kinase. The higher energy transfer values indicate an increase in the microclustering of the FRET reporters, which may be due to integrin-specific interactions, non-integrin-specific interactions or a combination of both, as discussed above. This can be determined by measuring the energy transfer in a cell line expressing integrins and FRET control peptides (Fig. 3, gray data bars). If the increase in energy transfer measured after RNAi treatment for cells expressing integrins and FRET reporters is non-integrin-specific, then increased energy transfer is expected in the cell line expressing the FRET controls. However, if the increase in energy transfer is the result of integrin-specific interactions, no change in energy transfer is expected for the cell line expressing the FRET controls. There was no statistically significant change in energy transfer after any of the RNAi treatments for cells expressing the FRET controls. These results indicate that the increase in energy transfer measured in the cell line containing the FRET reporters, after vinculin, paxillin, rhea, and focal adhesion kinase RNAi treatment, is measuring integrin-dependent increases in FRET reporter microclustering. Reducing the

expression of these cytoplasmic proteins increases FRET reporter clustering due to increased integrin microclustering. These proteins prevent integrin microclustering under the conditions used in these studies.

It is not possible to relate the magnitude change in energy transfer to a magnitude change in integrin microclustering using Eq. 1. Furthermore, the change in integrin microclustering may be dependent on how much protein expression is reduced. For each RNAi-targeted protein, the amount its expression is reduced may differ. Different thermodynamic efficiencies (Table 1), the amount of target mRNA within the cell, and differential transport of the dsRNA probe across the cell membrane will influence how efficient the overall RNAi treatment is in reducing expression. The methodology reported here can be used to determine the cytoplasmic proteins that alter integrin microclustering, which has important implications for intracellular signaling events. On-going efforts will enable a quantitative connection between the change in energy transfer and the change in integrin microclustering.

Cytoplasmic proteins that affect the microclustering of integrin mutants

Details about the molecular mechanism of protein clustering can be obtained by studying protein mutants. Figure 4 (black data bars) shows the FRET values for S2 cells expressing αβV409D mutant integrins and FRET reporters after the indicated RNAi treatment. In addition to the four cytoplasmic proteins identified as increasing energy transfer in cells expressing wild-type integrins, an additional RNAi treatment show a statistically significant increase in energy transfer compared to wild-type cells. This protein is dreadlock, which forms a link between integrins and receptor tyrosine kinases. This suggests that

disruption of the cytoplasmic linkage between αβV409D integrins and receptor tyrosine kinases results in higher integrin microclustering.

A previous study revealed the microclustering of the αβV409D integrin mutant is dependent on the presence of other membrane proteins (6). When the extracellular domains of all membrane proteins were digested from the cell surface prior to expressing the integrins and FRET reporters, the microclustering of the αβV409D mutant decreased. In contrast, there was no change in the microclustering of wild-type integrins when the extracellular domains of other membrane proteins were removed from the cell membrane. The previous study did not reveal the identity of the membrane protein(s) responsible for the microclustering of the αβV409D mutant since all membrane proteins were simultaneously targeted for removal. In addition, the transmembrane and cytoplasmic domains of the other membrane proteins remained in the membrane, and key integrin contacts in the cytoplasm may not have been disrupted. The use of FRET reporters and RNAi, as outlined in this report, has the benefit over previous methods for measuring the molecular mechanism of receptor clustering because the entire protein is removed,not just a fragment of the protein, and an individual protein can be targeted. The FRET results for the αβV409D mutant reveal receptor tyrosine kinase is at least one membrane protein responsible for its altered microclustering, via the cytoplasmic protein dreadlock, compared to wild-type integrins.

In comparison to the αβV409D mutation, the αanaβ mutation's microclustering properties were altered only with RNAi treatment for paxillin at 3% to 5% ligand density (Fig. 4, gray data bars). When the same RNAi probe is used to reduce the expression of a cytoplasmic protein in different populations of the same cell type (e.g. S2 cells), the magnitude of the change in energy transfer can be cautiously compared. The FRET data

indicates a 1.6-fold increase in FRET after paxillin RNAi treatment as opposed to six- and four-fold increase with wild-type and αβV409D mutant integrins, respectively. The remaining RNAi treatments that were studied showed no statistically significant differences for the αanaβ mutation compared to the no RNAi treatment data. The lack of change in integrin microclustering for the αanaβ mutation reflects a 'defect' in the ability of the cytoplasmic proteins to participate in the microclustering of this mutation. The lack of change in energy transfer for the αanaβ mutation is not the result of higher microclustering levels prior to the RNAi treatments.The energy transfer value obtained for the αanaβ no RNAi treatment data is similar to the values for cells expressing wild-type and the αβV409D mutation (Table 2). Therefore, αanaβ integrin microclustering levels are similar to other cell lines at 3% to 5% ligand density, prior to RNAi treatment. Additionally, higher energy transfer values have been measured for this cell line in the presence of a high ligand concentration (6), indicating that increased microclustering is possible under some circumstances.

It should not be surprising that decreased energy transfer was not measured after any of the RNAi treatments. As discussed above, at 3% to 5% ligand density the energy transfer measured before treatment is from non-integrin-specific microclustering of the FRET reporters, and the integrin-specific microclustering that may be present is below the detection limit for this assay. The cytoplasmic proteins that prevent integrin microclustering, in the absence of binding to extracellular ligand, have been identified. When the expression of these proteins is reduced, increased energy transfer is measured. When the ligand density is 50% on the glass surface, integrin microclustering levels are higher than what is measured at 3% to 5% ligand densities. Preliminary studies utilizing cells spread on a densely coated ligand

surface have revealed that decreased energy transfer values after RNAi treatment can be obtained (unpublished data).

CONCLUSION

The organization of the cell membrane is important for many basic cell functions, and can lead to pathological conditions when it is altered. Currently, few non-invasive analytical techniques can measure intracellular events that lead to changes in the organization of the cell membrane. The combination of FRET and RNAi has the unique capacity for measuring integrin organization without altering the integrin dynamics. Specific cytoplasmic events leading to integrin microclustering can be identified. When cells are spread on a surface with 3% to 5% ligand density, it was found that four proteins that connect integrins to the cytoskeleton also affect integrin microclustering. The molecular mechanism of integrin microclustering is further understood by analyzing integrin mutants. The microclustering of a mutation (αβV409D) that affects the ligand-binding domain is more sensitive to cytoplasmic interactions that indirectly link integrins to receptor tyrosine kinases compared to wild-type integrins. On 3% to 5% ligand surface densities, an alpha cytoplasmic mutation (αanaβ) loses its sensitivity to microclustering when the expression of all cytoplasmic proteins studied, except paxillin, is reduced. This methodology is not limited to integrins. Similar strategies can be used to study other classes of cell membrane receptors, and will enable a complete understanding of how receptor organization is directed by cytoplasmic binding events.

ACKNOWLEDGMENTS

This work was supported by the Roy J. Carver Charitable Trust (Muscatine IA), National Science Foundation (CHE-0845236) and Iowa State University Office of the Vice President for Research. The authors thank Roger Tsien (Howard Hughes Medical Institute, La Jolla, CA) for the original mCherry plasmid, Atsushi Miyawaki (Riken, Wako-city, Saitama, Japan) for the original Venus plasmid, Man-Yu Yum (Iowa State University) for help with the statistical analysis, Saiju Mathew (Iowa State University) for developing the FRET ImageJ plug-in, and Dilshan Shanaka Harischandra (Iowa State University) for synthesizing the RNA.

REFERENCES

1. Giancotti FG, and Ruoslahti E (1999) Science 285:1028
2. Phizicky EM, and Fields S (1995) Microbiol Rev 59:94
3. Selvin PR (2000) Nat Struct Biol 7:730
4. Buensuceso C, de Virgilio M, and Shattil SJ (2003) J Biol Chem 278:15217
5. Kim M, Carman CV, Yang W, Salas A, and Springer TA (2004) J Cell Biol 167:1241
6. Smith EA, Bunch TA, and Brower DL (2007) Anal Chem 79:3142
7. Ginsberg MH, Partridge A, and Shattil SJ (2005) Current opinion in cell biology 17:509
8. Martin-Bermudo MD, and Brown NH (1996) J Cell Biol 134:217
9. Helsten TL, Bunch TA, Kato H, Yamanouchi J, Choi SH, Jannuzi AL, Feral CC, Ginsberg MH, Brower DL, and Shattil SJ (2008) Mol Biol Cell 19:3589
10. Subauste MC, Pertz O, Adamson ED, Turner CE, Junger S, and Hahn KM (2004) J Cell Biol 165:371
11. Legate KR, Montanez E, Kudlacek O, and Fassler R (2006) Nat Rev Mol Cell Biol 7:20
12. Vicente-Manzanares M, Choi CK, and Horwitz AR (2009) J Cell Sci 122:199
13. Bunch TA, and Brower DL (1992) Development 116:239
14. Bunch TA, Grinblat Y, and Goldstein LS (1988) Nucleic Acids Res 16:1043
15. Jannuzi AL, Bunch TA, Brabant MC, Miller SW, Mukai L, Zavortink M, and Brower DL (2002) Mol Biol Cell 13:1352
16. Clemens JC, Worby CA, Simonson-Leff N, Muda M, Maehama T, Hemmings BA, and Dixon JE (2000) Proc Natl Acad Sci U S A 97:6499
17. March JC, and Bentley WE (2006) Biotechnol Bioeng 95:645

18. Chen H, Puhl HL, 3rd, Koushik SV, Vogel SS, and Ikeda SR (2006) Biophysical journal 91:L39
19. Xia Z, and Liu Y (2001) Biophysical journal 81:2395
20. Zal T, and Gascoigne NR (2004) Biophysical journal 86:3923
21. Zar J (1999) Biostatistical Analysis. Prentice Hall, Upper Saddle, NJ
22. Fogerty FJ, Fessler LI, Bunch TA, Yaron Y, Parker CG, Nelson RE, Brower DL, Gullberg D, and Fessler JH (1994) Development 120:1747
23. Bunch TA, Helsten TL, Kendall TL, Shirahatti N, Mahadevan D, Shattil SJ, and Brower DL (2006) J Biol Chem 281:5050
24. FLIGHT [http://flight.licr.org/]
25. PeptideAtlas [www.mop.unizh.ch/peptideatlas]
26. Brower DL (2003) Current opinion in cell biology 15:607
27. Armknecht S, Boutros M, Kiger A, Nybakken K, Mathey-Prevot B, and Perrimon N (2005) Methods Enzymol 392:55
28. FlyBase. (http://flybase.bio.indiana.edu).
29. Heidelberg [http://www.dkfz.de/signaling2/rnai/ernai_probes.php]
30. Kiger AA, Baum B, Jones S, Jones MR, Coulson A, Echeverri C, and Perrimon N (2003) J Biol 2:27

Table 1 RNAi probes used to reduce protein expression in S2 cells

Cytoplasmic Protein	RNAi probe ID	Thermodynamic binding efficiency[a]	Other protein targets
Vinculin (Vin)	HFA18728	33/493	No
Paxillin (Pax)	BKN29242	72/293	No
Rhea	HFA11300	101/487	No
Focal Adhesion Kinase (FAK)	HFA07426	136/483	No
Integrin Linked Kinase (ILK)	HFA11868	89/469	No
Dreadlock (Dock)	HFA00812	44/220	No
Steamer Duck (SD)	HFA17070	19/249	No
Actin42A	HFA04835	53/480	Yes

The RNAi probe ID, efficiency and other target values are from published and online resources: http://flyrnai.org

[a] The first value in the column is the number of 21 base pair oligonucleotides that have thermodynamically favorable binding to the target mRNA,and the second value in the column is the total number of 21 base pair oligonucleotides generated from the RNAi probe

Table 2 Mean FRET values from at least 100 cells expressing FRET reporters or controls and the indicated integrins: αβ, wild-type; αanaβ, α cytoplasmic mutation; αβV409D, β extracellular domain mutation

αβ FRET Reporters	**αanaβ FRET Reporters**	**αβV409D FRET Reporters**	**αβ FRET Controls**
0.013	0.016 (p=0.33)	0.017 (p=0.23)	0.013 (p=0.96)

Cells are spread on a glass surface coated with a 3% to 5% ligand density, all data are statistically compared to the value obtained for cells expressing wild-type integrins with FRET reporters

Fig. 1 Schematic showing FRET assay and proteins known to be involved in integrin-signaling complexes. Cytoplasmic proteins targeted in this study to measure how they affect integrin micro-clustering: rhea, vinculin, actin, integrin-linked kinase (ILK); CG32528, paxillin, dreadlock (Dock); steamer duck and focal adhesion kinase (FAK). (top) No energy transfer takes place when FRET reporters are separated by greater than 10 nm. (bottom) Reduced expression of a target cytoplasmic protein (e.g., Paxillin) increases integrin clustering and increases energy transfer from donor (D) fluorescent protein to acceptor (A) fluorescent protein. This is a static picture of a dynamic system.

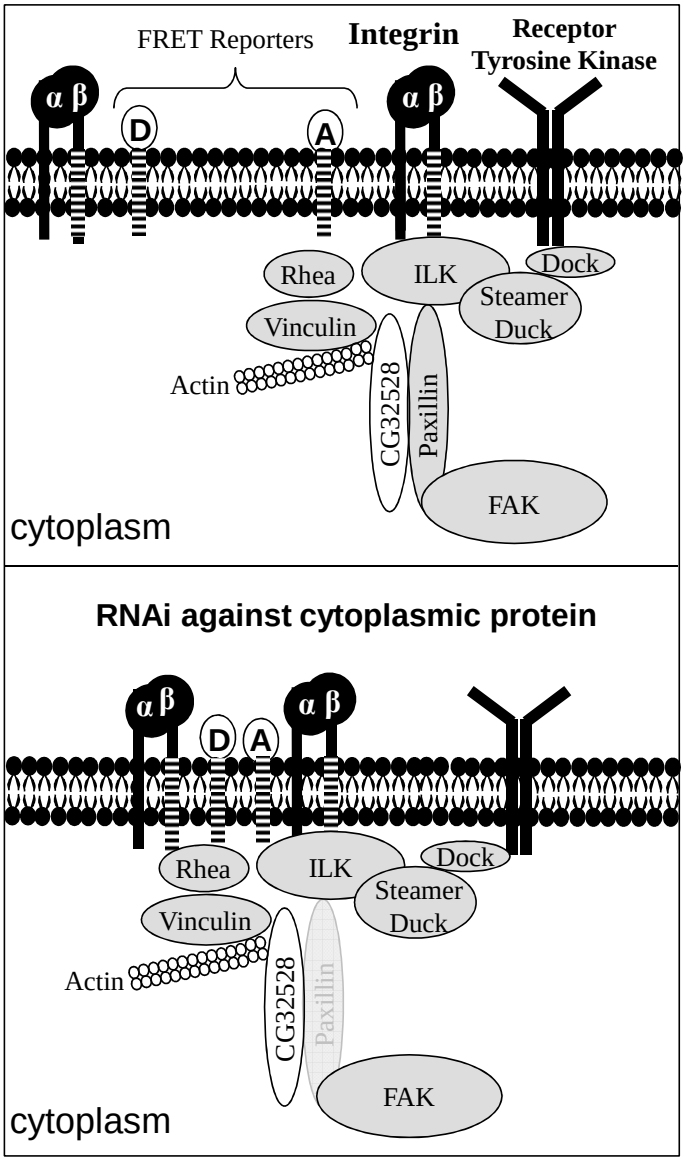

Fig. 2 Fluorescence images of a transformed Drosophila S2 cell, expressing αPS2CβPS integrins and FRET reporters. Image obtained using (top) donor filter set; (middle) acceptor filter set; (bottom) FRET filter set. Color has been added to correspond to the emission filter used to generate each image. FRET values are calculated on a pixel-by-pixel basis according to Eq. 1. A region of interest is generated for each cell that excludes fluorescence emanating from inside the cell. An example region of interest is shown in the top image (green)

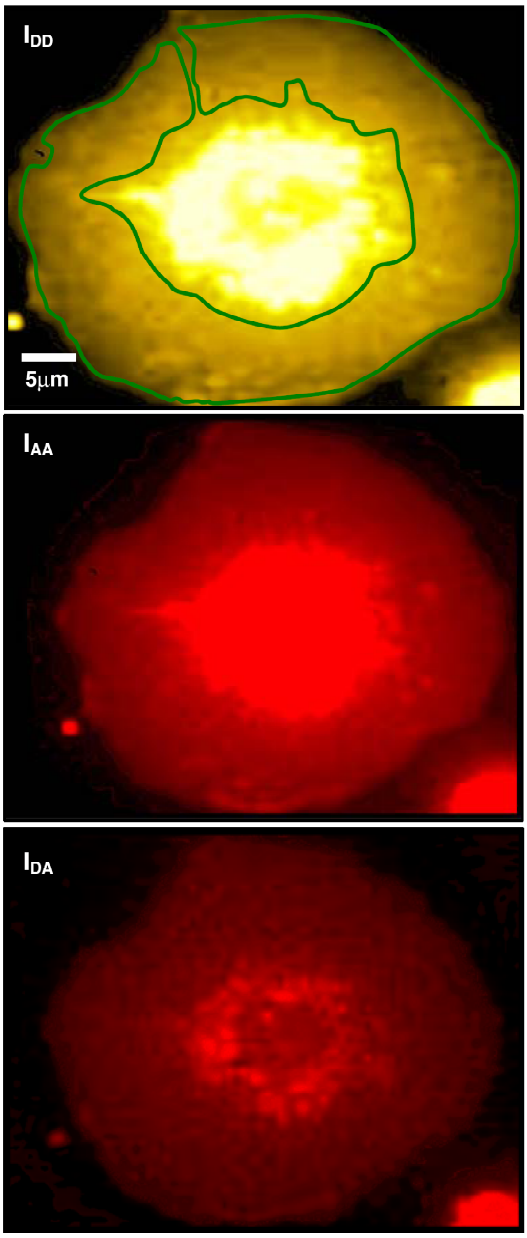

Fig. 3 Normalized FRET values for S2 cells expressing wild-type integrins and FRET reporters (black data bars) or wild-type integrins and FRET controls (gray data bars) after the indicated RNAi treatment. All values are normalized to the no RNAi treatment data (Table 2). A p value below 0.05, shows statistical evidence that the energy transfer measured after RNAi treatment is altered compared to the no RNAi treatment data set. The abbreviations used in this figure are listed in Table 1

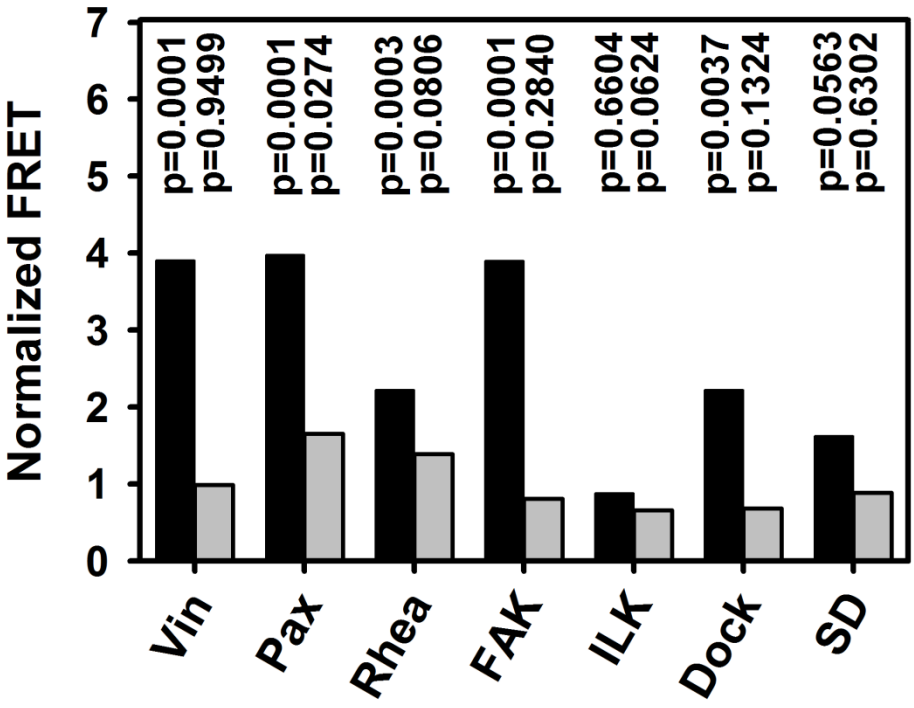

Fig. 4 Normalized FRET values for S2 cells expressing αβV409D mutant integrins and FRET reporters (black data bars) or αanaβ mutant integrins and FRET reporters (gray data bars) after the indicated RNAi treatment. A p value below 0.05 shows statistical evidence that the energy transfer measured after RNAi treatment is altered compare to the no RNAi treatment data set. The abbreviations used in this figure are listed in Table 1

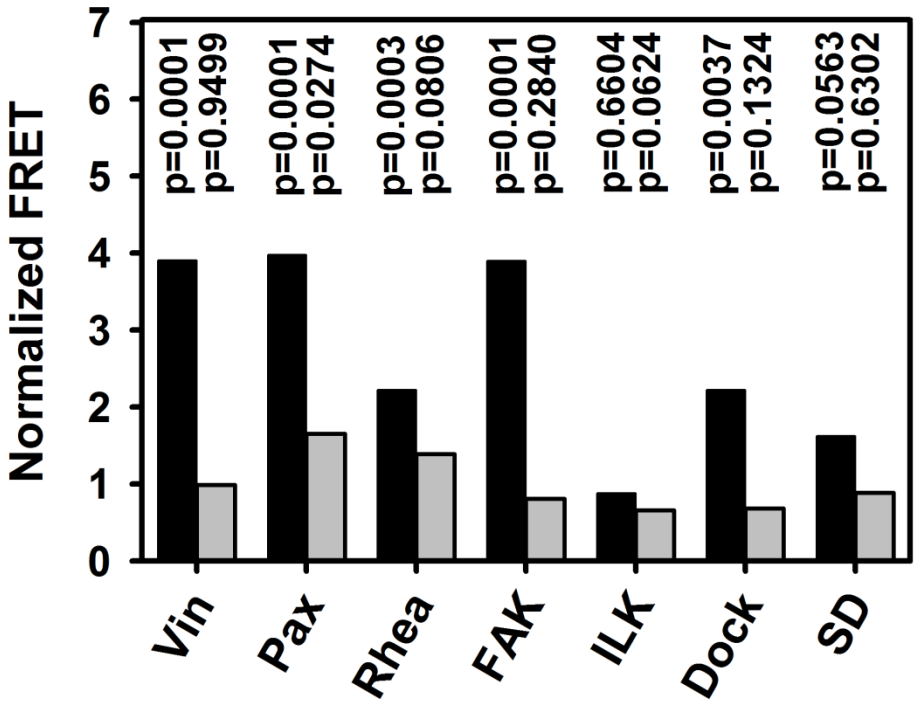

Supplemental Experimental Methods

FRET Bleed-through Factors

The factors *a*, *b*, *c*, and *d* account for bleed-through of: acceptor into the FRET filters, acceptor into the donor filters, donor into the acceptor filters, and donor into the FRET filters, respectively. These values were measured in cell lines that contained only the acceptor FRET control plus wild-type integrins (for a and b) or donor FRET control plus wild-type integrins (for c and d). The data (not shown) for these bleed-through factors reveal a dependence on the amount of donor and acceptor expressed in the cell, and were fit to exponential curves:

$$a = 0.103 + 0.565 \cdot \exp(-0.540 \times 10^{-2} \cdot I_{AA}); \quad (2)$$

$$b = 0.013 + 0.274 \cdot \exp(-0.466 \times 10^{-2} \cdot I_{AA}); \quad (3)$$

$$c = 0.077 + 0.344 \cdot \exp(-0.905 \times 10^{-2} \cdot I_{DD}); \quad (4)$$

$$d = 0.276 - 0.027 \cdot \exp(-0.346 \times 10^{-3} \cdot I_{DD}). \quad (5)$$

For the FRET calculations, if the donor fluorescence intensity was below 50 or the acceptor fluorescence intensity was below 50, the cell was rejected from the analysis. These lower threshold values were used to minimize the residual between the exponential fit and experimental bleed-through factor experimental data. The applied bleed-through factor was determined on a pixel-by-pixel basis during the FRET calculation. Background subtraction was performed on all images using an average intensity from cell-free regions of the image, and zero cellular autofluorescence was observed in the donor, acceptor or FRET images using the stated acquisition parameters.

Preparation of RBB-Tiggrin Surfaces

RBB-tiggrin is a bacterial fusion protein containing the integrin binding domain of the extracellular matrix protein tiggrin. RBB-tiggrin was produced as described previously.[17] Glass microscope slides (Fisherbrand, Fisher Scientific) were sterilized in 70% ethanol for 15 min and dried in a sterile environment. They were coated with a sterile solution containing 0.05 μg/mL RBB-tiggrin in pH 7 phosphate-buffered saline (PBS) for 2 h. The RBB- tiggrin solution was then removed and any remaining exposed glass surface was blocked using a 10 mg/mL solution of bovine serum albumin in pH 7 PBS. Coated slides were stored overnight at 2 °C and used within 24 h.

Actin-GFP Assay

S2 cells expressing integrins, UASpGFP tagged actin42A and pAdhGAL4, were RNAi treated for actin42A. Using these constructs, expression of actin42A-GFP is constitutively active. After RNAi treatment and incubation for 4 days, cells were transferred from the cell culture dish and collected by centrifugation. Cells were prepared for microscopy as described above for the FRET assay. The cells were imaged using a GFP filter set (excitation 470/50 nm and emission 545/75 nm).

Figure S1: Distribution of FRET values for one cell**.** The X-axis represents FRET value and the Y-axis denotes the number of pixels with a given FRET value. All values reported in this image are multiplied by a factor of 100, relative to the FRET values reported in Table 2 of the main text.

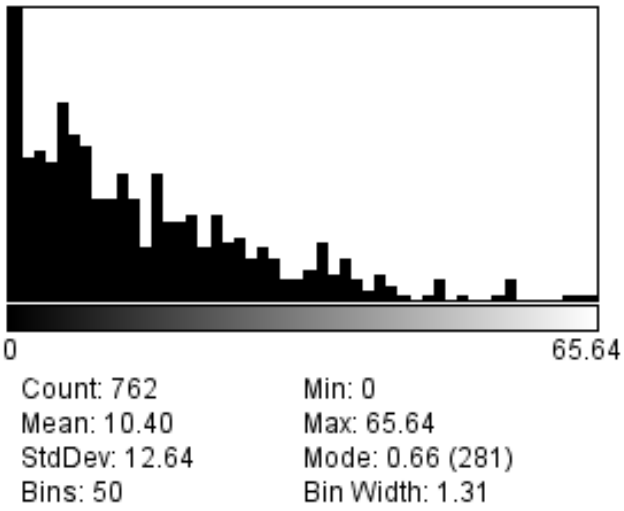

Figure S2: RNA knock-down efficiency. In order to estimate the efficacy of the RNAi treatments in reducing protein expression, a cell line expressing cytoskeletal protein actin42A tagged with green fluorescent protein (GFP) was utilized. The cells were treated with dsRNA for actin42A. This dsRNA also targeted five other actins expressed in S2 cells. Fluorescence intensities were measured after incubating 4 days with dsRNA. Shown in Figure S2A (left) is the fluorescence image of control cells expressing actin42A-GFP and (right) the fluorescence image of the same cell line after actin42A RNAi treatment. Both images are shown in the same intensity scale. The histograms in Figure S2B show the fluorescence of 100 cells (left) for control cells expressing actin42A-GFP and (right) the same cell line after actin42A-average. The mean fluorescence value for the control cell line is 590 and after RNAi treatment the mean value is 466. A statistically significant reduction in fluorescence is measured after RNAi treatment, as determined using the Welch Test (p=0.008).